Solid-State NMR Spectroscopy

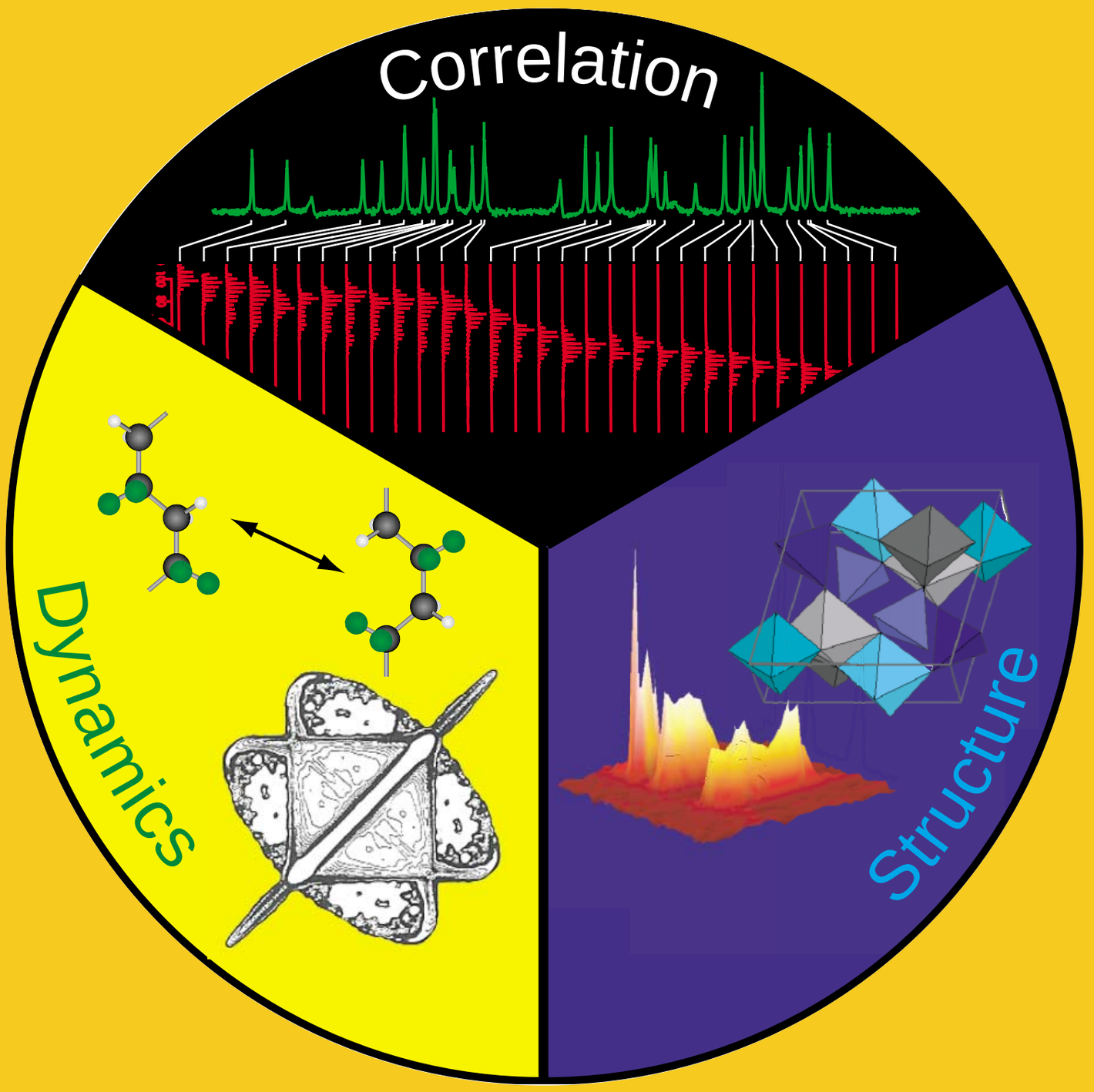

ANGEWANDTE
CHEMIE

Solid-State NMR Spectroscopic Methods in Chemistry

David D. Laws, Hans-Marcus L. Bitter, and Alexej Jerschow*

Over the last decades, NMR spectroscopy has grown into an indispensable tool for chemical analysis, structure determination, and the study of dynamics in organic, inorganic, and biological systems. It is commonly used for a wide range of applications from the characterization of synthetic products to the study of molecular structures of systems such as catalysts, polymers, and proteins. Although most NMR experiments are performed on liquid-state samples, solid-state NMR is rapidly emerging as a powerful method for the study of solid samples and materials. This Review outlines some of the developments of solid-state NMR spectroscopy, including techniques such as cross-polarization, magic-angle spinning, multiple-pulse sequences, homo- and heteronuclear decoupling and recoupling techniques, multiple-quantum spectroscopy, and dynamic angle spinning, as well as their applications to structure determination. Modern solid-state NMR spectroscopic techniques not only produce spectra with a resolution close to that of liquid-state spectra, but also capitalize on anisotropic interactions, which are often unavailable for liquid samples. With this background, the future of solid-state NMR spectroscopy in chemistry appears to be promising, indeed.

Keywords: multipulse techniques · NMR spectroscopy · solid-state structures · spin-spin coupling · structure elucidation

1. Introduction

Since the pioneering demonstration of cross-polarization ^{13}C NMR spectra of solid adamantane and benzene,[1] solid-state NMR spectroscopy has advanced rapidly and is being used to study the structure and dynamics of a variety of solid systems ranging from catalysts and glasses to polymers and proteins. Much of the success of solid-state NMR spectroscopy is due to the evolution of a variety of techniques for studying internuclear distances, anisotropy, torsion angles, atomic orientations, spin diffusion, molecular dynamics, and exchange processes, while maintaining the analytical high resolution and sensitivity that constitute the hallmarks of practically useful NMR experiments in chemistry.

Our goal in this Review is to demonstrate the utility of solid-state NMR spectroscopy for the study of molecular structure and dynamics in solids, and its application as a tool for routine chemical analysis of solid materials. We discuss the interactions between nuclear spins and magnetic fields that give rise to the traditionally broad solid-state NMR signals, as well as the common and less-common methods designed to eliminate this broadening. We review the concepts behind techniques that are routinely used to exploit internuclear interactions (e.g. methods of internuclear distance determination and correlation experiments in solids). We also discuss solid-state NMR spectroscopy of quadrupolar nuclei such as ^{2}H, ^{23}Na, and ^{27}Al and outline how they can be used to probe orientation, dynamics, and structure. Numerous excellent review articles have appeared in the past few years showing how the tools of solid-state NMR spectroscopy can be applied to solving specific problems.[2–31] For the benefit of providing the reader with a more or less complete overview of current solid-state NMR spectroscopic techniques, we refer to those publications and other references given in the text for a presentation of specific applications or specific methods. A detailed mathematical description of solid-state NMR is left out purposely, but, where appropriate, we provide references to books and articles that explain in greater detail the topics presented herein.

2. Solid-state NMR of Low-Abundance Spin ½ Nuclei

The most common NMR experiments performed for solid-state samples are those involving the observation of spin ½ nuclei with low gyromagnetic ratios, for example, ^{13}C, ^{15}N, and ^{29}Si. Thus, we begin with an introduction to the spin interactions that play a role in solid-state NMR spectra of

[*] Prof. Dr. A. Jerschow,[+] Dr. D. D. Laws, Dr. H.-M. L. Bitter
Materials Sciences Division, Lawrence Berkeley National Laboratory
and
Department of Chemistry, University of California at Berkeley
Berkeley, CA 94720 (USA)
E-mail: Alexej.Jerschow@nyu.edu
[+] Present address: Chemistry Department, New York University
New York, NY 10003 (USA)
fax: (+1) 212-260-7905

  1433-7851/02/4117-3097 $ 20.00+.50/0

spin ½ nuclei and discuss common spectroscopic methods that manipulate and even eliminate the effects that these interactions have on solid-state NMR spectra.

If one were to dissolve a sample of 1-^{13}C-labeled (10%) glycine in water and apply a single $\pi/2$ pulse at the appropriate NMR frequency for ^{13}C nuclei, the familiar ^{13}C spectrum shown in Figure 1 would result. Two well-resolved signals appear in the spectrum, corresponding to the ^{13}C-labeled carbonyl carbon atoms and the natural abundance ($\sim$1% for ^{13}C) α carbon atom in the glycine sample. The familiar 1:2:1 splitting pattern of the carbonyl carbon resonance provides information about its J coupling to the two α protons. The splitting of the isotopically dilute α-carbon resonance are a result of J couplings to both the α-protons and the carbonyl carbon atom. In contrast, Figure 2 shows the result of a comparable experiment performed on the same compound in the solid state. The signals for the carbonyl ^{13}C, which were very sharp in the liquid-state spectrum, are now replaced by an extremely broad ($\approx$200 ppm) and generally uninterpretable peak. The broadening of the signal for α-carbon atom renders it barely perceptible. These broad solid-state signals are primarily the result of interactions that are present (but rarely observed) in liquid-state NMR spectra. The three primary interactions are the heteronuclear and homonuclear dipolar couplings, and the chemical-shift anisotropy. In the ensuing sections, we examine

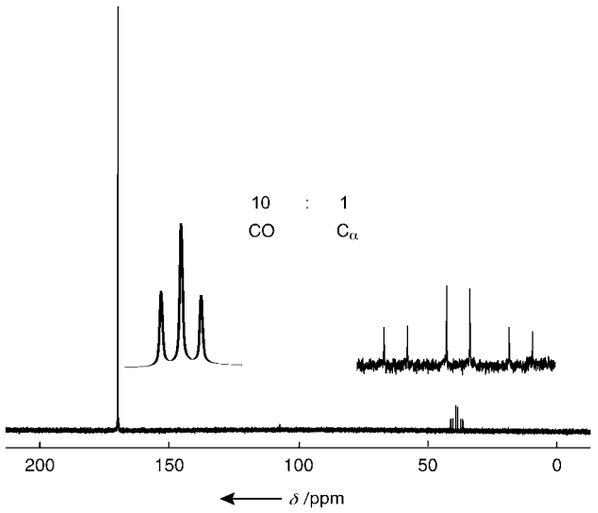

Figure 1. Liquid-state ^{13}C NMR spectrum (75 MHz) of 1-^{13}C labeled (10%) glycine dissolved in H_2O (0.2 mL) to a concentration of $\sim$10 mM.

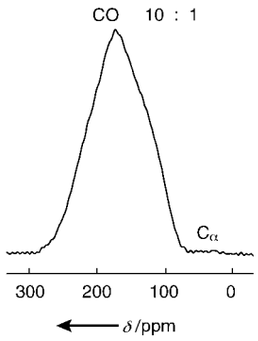

Figure 2. Solid-state ^{13}C NMR spectrum (125 MHz) of 1-^{13}C labeled (10%) glycine powder (90 mg).


D. Laws


H.-M. Bitter


A. Jerschow

David Douglas Laws received his B.S. in chemistry in 1995 from the University of Illinois, Urbana-Champaign where he worked with Professor Eric Oldfield on the calculation of NMR chemical shifts in proteins. He then moved to the University of California, Berkeley, where he received his Ph.D. in chemistry working with Professor Alex Pines on developing techniques to study solid-state proteins by NMR spectroscopy. David now resides with his wife Elizabeth in New Jersey, where he teaches chemistry and coaches swimming at The Lawrenceville School.

Hans-Marcus Bitter obtained his B.S. degree from Princeton University in 1995 and received his Ph.D. in 2000 from the University of California at Berkeley under the supervision of Professor Alexander Pines. Currently, he works as an informatics scientist at Biospect, a South San Francisco biotech company. He resides in San Francisco with his wife Catherine.

Alexej Jerschow received his Ph.D. from the University of Linz (Austria) under the supervision of Professor Norbert Müller for work on the analysis of polymers with multidimensional NMR spectroscopy. He was then a postdoctoral fellow with Professor Geoffrey Bodenhausen and supervisor of the NMR facility of West Switzerland at the University of Lausanne. His research involved the development of novel liquid-state NMR methodology, and the study of complex flow with magnetic resonance imaging methods. As an Erwin Schrödinger fellow with Professor Alexander Pines at the University of California, Berkeley, he developed new solid-state high-resolution NMR techniques for quadrupolar nuclei. He lives with his family in New York and is currently an Assistant Professor of Physical Chemistry at New York University.

the origins of each of these interactions and discuss how their effects on solid-state NMR spectra can be coherently manipulated so as to produce spectra with a resolution closer to that of liquid-state spectra. However, these mechanisms often contain a wealth of structural data and we will also review techniques that aid in obtaining this information.

2.1. Heteronuclear Dipolar Coupling

We begin our analysis of the solid-state ^{13}C NMR spectrum of glycine with an examination of the heteronuclear dipolar coupling. The heteronuclear dipolar coupling arises from an interaction between the nuclear magnetic moments of two different nuclear spins. (By convention, nuclear spins are labeled as I for "abundant" spins, for example, that of the proton, and S for "rare" spins such as that of ^{13}C or ^{15}N nuclei.) In an external magnetic field, the Zeeman interaction describes the energy of the spin I based on its orientation, either parallel ("spin-up") or antiparallel ("spin-down"), with respect to the external field [Eq. (1)], where $\gamma =$ gyromagnetic ratio, $B_0 =$ external magnetic field, and $m_I =$ nuclear spin quantum number (which is either $+\frac{1}{2}$ or $-\frac{1}{2}$ for a spin $\frac{1}{2}$ nucleus).

$$E_{\text{Zeeman}} = -\hbar\gamma B_0 m_I \quad (1)$$

Similarly, spin S will align itself either parallel or antiparallel to B_0. Since each spin represents a nuclear magnetic moment that produces a small magnetic field, the S spin will "feel" the magnetic field produced by the I spin and vice versa when the two spins are within reasonable proximity of each other (< 10 Å). This magnetic field produced by the I spin will either add to or subtract from the external field felt by the S spin, depending on the orientation of the I spin, thereby increasing or decreasing the effective local magnetic field at the site of spin S and thus changing its resonance frequency. The degree to which spin I affects the magnetic field felt by spin S is characterized by the strength of the heteronuclear dipolar coupling, which is represented by the Hamiltonian in Equation (2).

$$H_{IS} = -d(3\cos^2\theta - 1)I_z S_z \quad (2)$$

The parameter d is the dipolar coupling constant [Eq. (3)].

$$d = \left(\frac{\mu_0}{4\pi}\right)\frac{\hbar\gamma_I\gamma_S}{r_{IS}^3} \quad (3)$$

In this case, $r_{IS} =$ internuclear distance, $\mu_0 =$ permeability of free space ($= 4\pi \times 10^7\ \text{N A}^{-2}$), γ_I and $\gamma_S =$ gyromagnetic ratios of the I and S spins, respectively, and I_z and $S_z =$ z components of the nuclear spin angular momentum operators I and S, respectively. The angle θ describes the orientation of the internuclear vector with respect to the orientation of the external magnetic field (Figure 3 shows this for a case in which $I = {}^1H$ and $S = {}^{13}C$). Because the magnitude of the coupling between two nuclear spins depends on the internuclear distance, the dipolar coupling is a *through-space* interaction. In contrast, J coupling requires the presence of chemical bonds. It is transferred through the electrons engaged in these bonds and thus is confined to nuclei within a molecule. Through-space dipolar coupling, however, also occurs between nuclei in *different* molecules. The two coupling mechanisms are therefore complementary in information content.

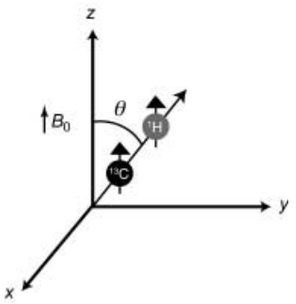

Figure 3. θ is the angle between the $^1H-{}^{13}C$ bond vector and the direction of the external magnetic field B_0.

Three properties of the heteronuclear dipolar coupling Hamiltonian stand out:1) The magnitude of the coupling is proportional to the product of the gyromagnetic ratios. This appears intuitively reasonable because the magnetic moment of a nucleus is proportional to γ, and nuclei with greater magnetic moments produce stronger magnetic fields, which in turn increases the dipolar coupling interaction. 2) The dipolar coupling is inversely proportional to the cube of the internuclear distance, so the interaction falls off rapidly as the nuclei are moved farther apart. 3) The dipolar coupling is dependent on the orientation, which is evident from the $(3\cos^2\theta - 1)$ term in the dipolar Hamiltonian. This means that for two nuclei of spins I and S which are separated by a fixed distance, the magnitude of the dipolar interaction will be greater for certain orientations of the $I-S$ internuclear vector than for others. It is the orientational dependence of the dipolar coupling that limits its role in liquid-state NMR spectroscopy. The reorientation time of a molecule in solution is much faster than the time the dipolar coupling would need to evolve, thus causing the $(3\cos^2\theta - 1)$ term of the heteronuclear dipolar coupling Hamiltonian to average to zero. In a static solid sample comprised of randomly oriented crystallites, however, the internuclear vector remains invariant over time, and the resonance frequency produced by each crystallite depends on its orientation with respect to the external field. In a polycrystalline powder sample in which the crystallites are oriented in all possible directions, the presence of a heteronuclear dipolar coupling produces a spectrum such as that shown in Figure 4 (if no other orientation-dependent interactions are present). The two complementary patterns, termed the "Pake doublet",[32] arise from energy differences determined by H_{IS}, depending on the parallel or antiparallel alignment of the I spin with respect to the S spin (the $I_z S_z$ term gives positive and negative energies, respectively). The intensity of the pattern at a particular frequency reflects the abundance of the crystallites that resonate at that frequency. In a powdered solid, the singular peaks of the Pake pattern correspond to crystallites for which the $I-S$ internuclear vector lies perpendicular to the magnetic field. The two low edges of the Pake pattern correspond to the relatively few crystallites whose $I-S$ internuclear vectors point toward the poles (parallel to the external field). Notably, there is also an orientation of the $I-S$ vector relative to B_0 at which the

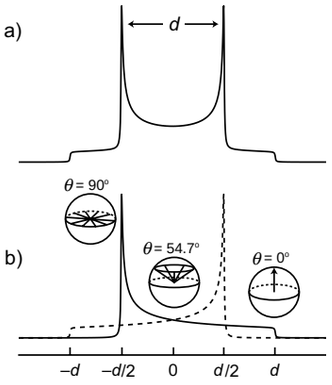

Figure 4. a) Dipolar Pake pattern ("Pake doublet") for two coupled spins in a powder sample; the two signals correspond to a positive (parallel spins) and a negative (antiparallel spins) value of the I_zS_z component. b) The points with maximum intensity corresponds to $\theta = 90°$—a perpendicular orientation to B_0 is adopted by a majority of the crystals. The smallest number of crystals have the internuclear vector parallel to B_0 ($\theta = 0°$). At the magic angle of $\theta = 54.7°$, the dipolar coupling is zero. The spacing between the points of maximum intensity in a) is equal to the dipolar coupling constant d ($d/\hbar$ if expressed in Hz).

resonance frequency of the crystallites is not altered by the heteronuclear dipolar coupling. This is the case at the "magic angle" of $\theta = 54.74°$ ($(3\cos^2\theta - 1) = 0$).

The spectrum in Figure 2 does not resemble a Pake pattern for three reasons: 1) each carbon atom couples to more than one proton; 2) the protons couple with each other; and 3) other anisotropic interactions cause additional broadening of the resonances, as discussed below.

2.2. Heteronuclear Dipolar Decoupling

The heteronuclear coupling that is responsible for much of the broadening in the glycine spectrum in Figure 2 involves the coupling of ^{1}H nuclear spins to the detected ^{13}C nuclear spins, as the ^{1}H – ^{13}C dipolar coupling is typically the dominant interaction experienced by the ^{13}C spin. A typical coupling constant for a bonded ^{1}H – ^{13}C pair (at a distance of about 1 Å) is approximately 30 kHz. However, close inspection of the Hamiltonian in Equation (2) suggests two possible means of eliminating the interaction to give narrower lines. One approach is to take advantage of the fact that the dipolar coupling is zero when the internuclear vector is oriented at the magic angle with respect to the magnetic field. This approach is implemented in a technique known as magic-angle spinning (see Section 2.4). The second method that can be used to eliminate the effect of the ^{1}H nuclei on the ^{13}C spectrum is to manipulate the proton spins in such a way that their effect on the ^{13}C nucleus, when averaged over time, is equal to zero. This is the solid-state dipolar version of spin decoupling, which is used in solution NMR spectroscopy. As can be seen from the signals for the two transitions shown in Figure 4, a proton whose spin is parallel to the external field ("spin-up") produces a shift in the resonance frequency of a ^{13}C nucleus that is opposite to the shift produced by a proton whose spin is antiparallel to the external field ("spin-down"). By constantly applying radio-frequency (RF) pulses that rotate the proton nuclear spins between their "spin-up" and "spin-down" states, the average orientation of the ^{1}H magnetic moments tends to zero, and the dipolar coupling is essentially averaged away (this also applies to the J coupling). This continuous-wave (CW) spin decoupling[33, 34] is widely used to eliminate heteronuclear couplings in solid-state NMR spectroscopy. As can been seen in Figure 5, under CW irradiation at the ^{1}H Larmor frequency, the ^{13}C peak is definitely less broad than that in Figure 2. The resulting spectrum is dominated by the chemical-shift anisotropy (see Section 2.3). Notably, ^{1}H decoupling has a much more dramatic effect on the signal for the α carbon atom (which is now visible in the spectrum) than it does on the signal for the carbonyl carbon atom (Figure 5). This is a result of the distance dependence of the dipolar coupling: with two α protons a distance of ~1 Å away, the α carbon atom experiences a much stronger ^{1}H – ^{13}C coupling than the unprotonated carbonyl carbon atom. In liquid-state NMR spectroscopy, CW decoupling is used much less often as it has been superseded by a number of different multiple-pulse techniques.[35, 36] These techniques are usually not as effective in solid-state NMR spectroscopy for reasons that we will discuss below.

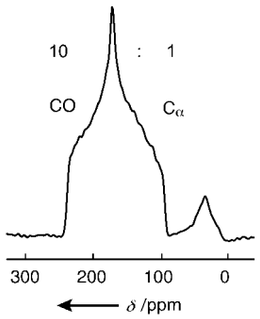

Figure 5. CW ^{1}H decoupled solid-state ^{13}C NMR spectrum (125 MHz) of a 1-^{13}C-labeled (10%) glycine powder.

2.3. Chemical-Shift Anisotropy

The origin of the chemical shift can be understood by examining the effect of B_0 on the electrons around a nucleus. When an external magnetic field is applied to an atom, not only are the nuclear spins perturbed, but the surrounding electrons are also affected since they, too, have magnetic moments. The external field induces circulating currents of electrons that in turn produce small magnetic fields (typically ~1x10^6 times smaller than B_0), which either add to or subtract from the external field felt by the nucleus. Therefore, the effective magnetic field experienced by the nucleus is altered, as is its resonance frequency.

The orientation dependence or *anisotropy* of the chemical shift can be quite dramatic. For a non-sp^3-hybridized ^{13}C atom, the chemical shift anisotropy (CSA) can be as large as 120 – 140 ppm (e.g., see Figure 5). Much larger anisotropies (up to 1000s ppm) can be found for some heavier nuclei. The CSA results from the fact that the atoms in molecules rarely possess spherically symmetric electron distributions; instead, the electron density can be thought of as an ellipsoid, typically elongated along bonds or nonbonding p-orbitals. The degree to which the electron density affects the resonance frequency of a nucleus depends on the orientation of the electron cloud (and hence the orientation of the molecule) with respect to B_0. For example, the resonance frequency of a carbonyl

carbon atom can differ by more than 120 ppm, depending on the orientation of the C=O moiety with respect to the external field, as can be seen in Figure 6. The largest chemical shift (i.e. deshielding effect) in the resonance frequency of the ^{13}C nucleus occurs when the narrowest part of the electron cloud

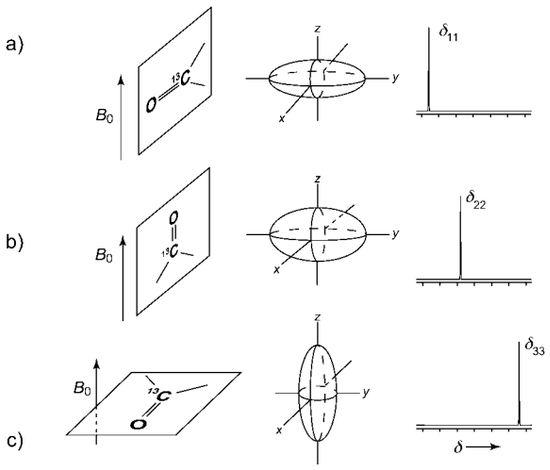

Figure 6. Schematic representation of the principle values of the CSA: δ_{11} (a), δ_{22} (b), and δ_{33} (c). The position of each resonance depends on the orientation of the magnetic field relative to the principal axes of the chemical shift tensor. (Reproduced from ref. [43], with permission.)

is oriented along the B_0 axis (Figure 6a), whereas the smallest shift occurs when the widest part of the electron cloud is oriented along B_0 (Figure 6c). These two chemical shifts, referred to as δ_{11} and δ_{33}, respectively, are two of the three "principal values" of the CSA. The third value δ_{22} is the shift produced by the molecular orientation perpendicular to the axes of δ_{11} and δ_{33} (Figure 6b). These three principal values and the information of the orientation of the ellipsoid (usually specified by the three Euler angles[37]) provide all the information necessary to describe the CSA of a nuclear spin.[38, 39]

In powder samples, in which the vast number of randomly oriented crystallites ensures that all of the possible molecular orientations are sampled, a "powder pattern" such as the one shown in Figure 5 emerges. The left and right edges of the C=O signal correspond to the chemical shifts δ_{11} and δ_{33}, respectively, and the position of the maximum intensity of the pattern corresponds to δ_{22} (for the common convention of $\delta_{11} \geq \delta_{22} \geq \delta_{33}$). The broad CSA signal is the result of an interaction between the detected spins and the external field, and so there is no simple way to remove this interaction by RF pulses (as we did with the heteronuclear dipolar coupling) without affecting the free precession of the spins required for signal detection. However, liquid-state NMR spectroscopy provides a clue as to how the effects of the CSA can be eliminated. In liquids, molecules randomly and rapidly sample the full range of orientations, so that even a strongly asymmetric electron distribution will appear spherical when viewed on the NMR timescale. One can divide the chemical-shift Hamiltonian H_{CS} into an isotropic term and an anisotropic term. For the special case in which $\delta_{11} = \delta_{22}$ (so that the ellipsoids in Figure 6 would be axially symmetric like a cigar), the chemical shift Hamiltonian can be written as shown in Equation (4):

$$H_{cs} = \gamma B_0 I_z [\delta_{iso} + \tfrac{1}{2}\delta_{CSA}(3\cos^2\theta - 1)] \quad (4)$$

δ_{iso} = (isotropic) chemical shielding factor (typically in the order of $10^{-6} \mathrel{\hat{=}}$ ppm) [Eq. (5)].

$$\delta_{iso} = \tfrac{1}{3}(\delta_{11} + \delta_{22} + \delta_{33}) \quad (5)$$

The angle θ relates the orientation of the unique axis of the ellipsoid with respect to B_0, and δ_{csa} dictates the magnitude of the CSA [Eq. (6)]

$$\delta_{CSA} = \delta_{33} - \delta_{iso} \quad (6)$$

In a rapidly tumbling molecule, all possible orientations of the ellipsoid are sampled, causing the orientation-dependent term to average to zero and leaving only the isotropic component of the chemical shift, $\delta_{iso}\gamma B_0 I_z$, which is observed in liquid-state NMR spectra. Imposing a random, liquid-like motion on a solid-state sample is, however, mechanically impractical since it would require motion around multiple axes at speeds that are currently unattainable. By spinning the sample around a unique well-chosen axis (see following Section 2.4), one can also eliminate the anisotropic term of the chemical-shift Hamiltonian.

2.4. Magic-Angle Spinning

We pointed out in Section 2.2 that when the vector between two nuclei makes an angle $\theta = 54.74^\circ$ (the magic angle) with the static magnetic field, the value of the $(3\cos^2\theta - 1)$ term in the heteronuclear dipolar coupling Hamiltonian is zero. The same is true for the axially symmetric CSA, for which an analogous angular dependence is found (in this case, θ is the angle that the long axis of the CSA ellipsoid makes with the static field). This could be accomplished by using a single crystal in which the CSA ellipsoid is oriented so that $\theta = 54.74^\circ$. Single crystals are, however, hard to obtain for many samples, and the orientation of the unique CSA axis with respect to the crystallite frame is not known.

Alternatively, by rapidly spinning a polycrystalline powder sample, one can make the average CSA look like an ellipsoid whose long axis is aligned with the spinning axis. This is also true when the CSA is not axially symmetric. The effect of this average CSA on the spectrum is eliminated if the spinning axis is inclined at 54.74° with respect to the static magnetic field. This technique is known as magic-angle spinning (MAS).[40, 41]

Another qualitative description of the theory that underlies the averaging of the CSA under spinning has been reported:[38, 39, 42] For a static powder sample, the value of the CSA is fixed for a given crystallite orientation. When the sample is spun, the CSA values of all crystallites become time-dependent, since the orientation of the crystallites change. Figure 7 shows that an axis inclined at an angle of 54.74° represents the direction of the space diagonal of a cube. The x, y, and z

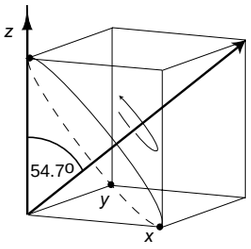

Figure 7. The magic angle (54.7°) is the angle that the space diagonal of a cube makes with the z axis. This is also the direction of the nodal plane in a d_{zz} orbital. Rapid spinning of the sample about this axis removes the dipolar interactions.

coordinate axes appear symmetric when looking down the space diagonal. Over a single rotation period, each crystallite therefore experiences the average of the effective chemical shift $\delta_{iso} = (\delta_{xx} + \delta_{yy} + \delta_{zz})/3 = (\delta_{11} + \delta_{22} + \delta_{33})/3$, the isotropic chemical shift. MAS can therefore be regarded as a dynamic implementation of cubic symmetry,[43] which cancels the anisotropic term.

Figure 8a–d show a series of ^{13}C MAS spectra for uniformly ^{13}C-labeled (10%) glycine at different spinning speeds. As the spinning speed decreases, numerous peaks begin to appear at frequency distances of integer multiples of the spinning speed. These peaks, known as spinning sidebands, result from the incomplete averaging of the revolving CSA ellipsoid at slow spinning speeds.[40, 41] These additional signals always appear in-phase for a perfect

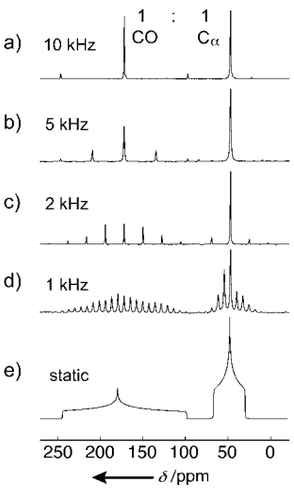

Figure 8. Solid-state ^{13}C NMR spectra (125 MHz) of a uniformly ^{13}C-labeled (10%) glycine powder sample; the spectra were acquired under CW ^{1}H decoupling and MAS at the given spinning speeds. As the spinning speed decreases the envelope of the spinning sidebands begins to resemble the simulated static NMR spectrum e).

powder, but may be anti-phase when a preferential orientation of the crystallites exists in the sample.[44] Although these sidebands are often a nuisance (they can be minimized by spinning at a frequency greater than the width of the CSA pattern), in some instances their presence provides additional information about a sample (see Section 4.4). Figure 8e represents a powder spectrum reconstructed from the CSA parameters obtained by fitting the sideband intensities in Figure 8a–d.[45] This spectrum looks very similar to the experimental spectrum shown in Figure 5, taking into account the difference in the abundance of the ^{13}C labeled α carbon atom.

2.5. Homonuclear Dipolar Coupling

The heteronuclear dipolar coupling is the result of an interaction between the magnetic fields produced by different neighboring nuclear spins (for example ^{1}H and ^{13}C). The same form of coupling exists between like spins, such as two ^{13}C nuclei. However, whereas two unlike nuclear spins (heteronuclei) have very different resonance frequencies (for example, when ^{1}H spins resonate at 500 MHz, ^{13}C spins resonate at 125 MHz), two like spins are able to undergo an energy-conserving "flip-flop" transition in which one spin flips up while the other spin flips down (Figure 9). To account for the

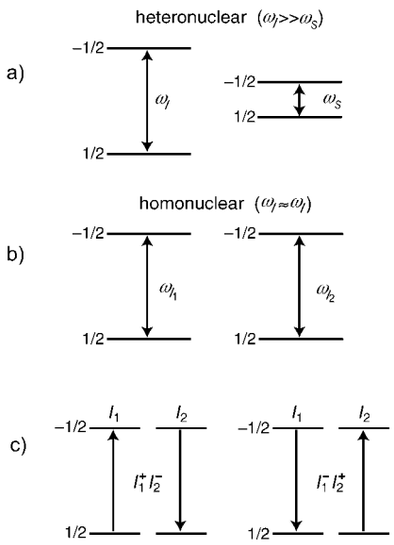

Figure 9. a) At different transition frequencies of two spins ω_I and ω_S, no energy-conserving transition can occur; b) when $\omega_I = \omega_S$, c) the spins can exchange magnetization through an energy-conserving "flip-flop" interaction.

"flip-flop" interaction, an additional term, normally ineffective in the heteronuclear case, is added back in to give the homonuclear dipolar Hamiltonian [Eq. (7)]

$$H_{II} = -d\tfrac{1}{2}(3\cos^2\theta - 1)(3I_{1z}I_{2z} - (\boldsymbol{I}_1 \cdot \boldsymbol{I}_2)) \quad (7)$$

Analogously to Equation (3), $d = (\mu_0/4\pi)(\hbar\gamma_I^2/r_{IS}^3)$. The origin of the term $\boldsymbol{I}_1 \cdot \boldsymbol{I}_2$ $(= I_{1x}I_{2x} + I_{1y}I_{2y} + I_{1z}I_{2z})$ can be better understood by rewriting Equation (7) as Equation (9) in terms of raising and lowering operators [Eq. (8)]

$$I^+ = I_x + iI_y;\ I^- = I_x - iI_y \quad (8)$$

$$H_{IS} = -d\tfrac{1}{2}(3\cos^2\theta - 1)(2I_{1z}I_{2z} - \tfrac{1}{2}(I_1^+ I_2^- + I_1^- I_2^+)) \quad (9)$$

The raising operator I^+ increases the angular momentum of a spin by $\hbar$, which amounts to flipping a spin from the "down" orientation to the "up" orientation (Figure 9). Conversely, the lowering operator I^- lowers the angular momentum of a spin by $\hbar$, causing an "up" spin to flip "down". Together, the $I_1^+ I_2^-$ and $I_1^- I_2^+$ provide for an energy-conserving exchange of spin angular momentum between any two coupled spins whose resonance frequencies overlap. When two like spins have very

different chemical shifts so that there is no overlap between their resonance frequencies, there can be no energy-conserving transition; in the latter case, the homonuclear dipolar Hamiltonian reverts to the form of the heteronuclear dipolar Hamiltonian shown in Equation (2).

For low-γ nuclei such as ^{13}C and ^{15}N, the homonuclear dipolar coupling can often be removed by MAS, as even for directly bonded ^{13}C nuclei, the dipolar coupling constant d does not exceed 5 kHz. However, there still can be "recoupling" effects with certain ratios of spinning speed to chemical-shift difference of the two nuclei (see Section 4). The homonuclear dipolar interaction has perhaps the largest impact on ^{1}H solid-state NMR spectroscopy, as the strength of the homonuclear dipolar coupling between two proton spins can routinely approach 100 kHz because of their large gyromagnetic ratio. The problem of strong $^{1}H-^{1}H$ dipolar coupling is exacerbated by the high abundance of protons in most organic systems, which results in a network of strongly coupled spins that are very difficult to decouple from each other. As a result, solid-state ^{1}H NMR spectra typically consist of a single broad peak, with a line width in the order of 50 kHz. Figure 10a shows a static ^{1}H NMR spectrum of solid glycine, in which the many protons lead to a spectrum that cannot be interpreted. Although MAS does help to reduce the line width (Figure 10b), it is still too broad to be of general use, even at the very high (>30 kHz) MAS speeds now obtainable. Homonuclear decoupling by using RF-pulse sequences are discussed in Section 3.2.

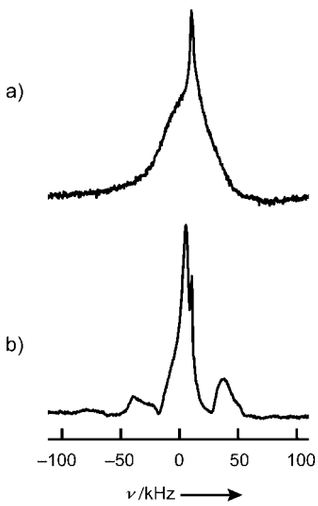

Figure 10. Solid-state ^{1}H NMR spectrum (500 MHz) of glycine powder: a) without spinning, b) with spinning (10 kHz, at the magic angle).

2.6. Cross Polarization

Thus far we have concentrated on the differences between liquid- and solid-state Hamiltonians and spectra, and how these differences can be overcome by utilizing techniques such as spin decoupling and MAS. To complete this section, we turn our attention to an additional difference between liquid- and solid-state NMR experiments. Even in liquid-state experiments that measure ^{13}C or ^{15}N chemical shifts or J couplings, the magnetization is often initially transferred from neighboring protons and then transferred back to the protons for detection to exploit the higher sensitivity. In addition, as relaxation is usually more rapid for protons, one can minimize acquisition times.[46] As a result of the difficulties involved in obtaining high-resolution solid-state ^{1}H NMR spectra, the majority of solid-state NMR experiments detect the magnetization of other nuclei such as ^{13}C, ^{31}P, and ^{15}N. The drawbacks of directly detecting low-γ nuclei such as ^{13}C and ^{15}N are low isotopic abundances, low spin polarization, and low signal intensity. These drawbacks can be circumvented by a solid-state NMR technique that combines both the high polarization and short relaxation time that is typical of ^{1}H NMR spectroscopy with high resolution (e.g. of ^{13}C and ^{15}N nuclei)—this would be the conceptual analogue of the INEPT and DEPT experiments).[47]

To enhance the signals from rare nuclei such as ^{13}C and ^{15}N, many solid-state NMR experiments today routinely involve the transfer of polarization from abundant nuclei (usually ^{1}H nuclei) by using a technique called cross polarization (CP).[1, 38, 39] The process of CP occurs through the tendency of the magnetization to flow from highly polarized nuclei to nuclei with lower polarizations when the two are brought into contact, similar to heat flow from a hot object to a cold object when the two are in thermal contact. For homonuclear spins, the magnetization can be exchanged through mutual energy-conserving spin flips (Figure 9b–c). For heteronuclear pairs such as ^{1}H and ^{13}C, these spin flips are not energy-conserving at high magnetic fields (see Figure 9a). Therefore, the exchange of magnetization must be driven externally by the application of RF fields.

Among the techniques for establishing a dipolar contact between two different spin systems I and S, a particularly effective approach is that of Hartmann and Hahn.[48]

The Hartmann–Hahn method requires the simultaneous application of two continuous RF fields, one at the resonance frequency of the I spin and one at the resonance frequency of the S spin. The effect of any RF field is to rotate the magnetization about the axis of the applied field. The rotation or nutation rate depends on the frequency and amplitude of the RF field. An RF field that oscillates at the I-spin frequency, for example, 500 MHz, would have essentially no effect on S spins with a frequency of 125 MHz and vice versa. By applying two RF fields, one tuned to the I spins the other to the S spins, both the I and S spins can be rotated independently around a particular axis at rates determined by the amplitudes of the two applied fields. When the nutation frequencies of the I and S spins are equal, an energy-conserving dipolar contact between the two spin systems is created. The differences in energy are supplied by the RF fields. It is through this dipolar contact that the polarization is transferred between the I and S spins. One way to describe how this connection is established is by using a reference frame rotating at both the I and the S spin nutation frequencies. In the doubly rotating frame, the spacing between the spin-up and spin-down energy levels is equal for the I and S spins (Figure 11a).

The experimental implementation of this concept to obtain high-resolution NMR spectra of rare or dilute S spins is shown

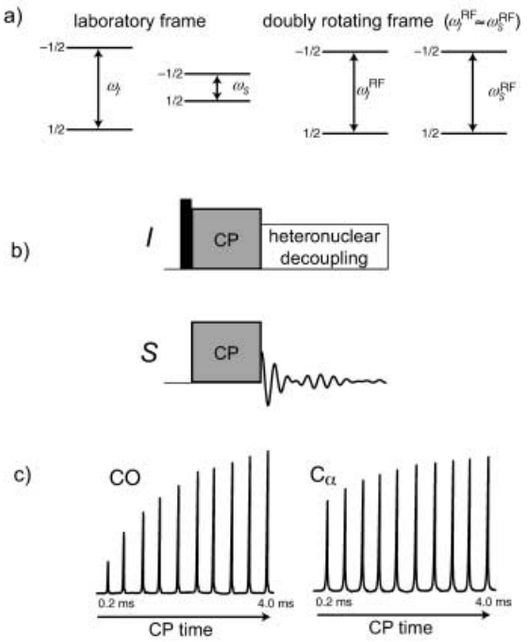

Figure 11. Hartmann–Hahn CP: a) The energy differences between the transitions of the *I* and the *S* spins can be made equal in a doubly rotating frame when the nutation frequencies on both spins are equal. b) Pulse sequence for CP of ^{13}C (*S*) nuclei by protons (*I*) with detection of the ^{13}C magnetization. c) Solid-state ^{13}C NMR spectra (125 MHz) of uniformly ^{13}C-labeled (10%) glycine powder acquired by using the pulse sequence in b) as a function of the CP time. Because of the directly bonded H_α protons, the $^{13}C_\alpha$ nuclei are polarized more rapidly than the unprotonated carbonyl carbon nuclei.

in Figure 11b. First, the proton magnetization is brought into the *xy* plane by a π/2 pulse. RF fields are then applied to the *I* and *S* spins for a period τ_{CP}, causing the magnetization to be exchanged between the *I* spins and the *S* spins in their respective rotating frame. Finally, the *S* spins are detected while the *I* spins are decoupled. This sequence forms the basis of proton-enhanced NMR spectroscopy[1, 49] which, through the combination of CP and MAS,[50, 51] opened the way to routine high-sensitivity, high-resolution, solid-state ^{13}C NMR spectroscopy. The increase in the *S*-spin magnetization during the CP mixing period τ_{CP} depends on the strength of the $I-S$ dipolar coupling (Figure 11c). The polarization buildup in the unprotonated carbonyl carbon atom requires a longer CP time than for the α carbon atom, which is quickly polarized by its bonded protons (Figure 11c). Typical mixing times range from 100 μs to 10 ms. The polarization buildup curve starts to decay beyond a certain mixing time as a result of relaxation and magnetization-transport phenomena. A direct link between integrated signal intensities and stoichiometric abundances is no longer available owing to the many parameters involved, which is also true for liquid-state proton-enhanced or inverse spectroscopy.

The maximum enhancement for a CP contact period under the Hartmann–Hahn conditions $\gamma_I\omega_I = \gamma_S\omega_S$ is γ_I/γ_S (γ_I and γ_S = gyromagnetic ratios of spins *I* and *S*, respectively; ω_I and ω_S = nutation rates imposed by the RF fields).[39] Modifications of the basic CP sequence can give sensitivity improvements beyond this theoretical enhancement through multiple CP contact sequences.[1] In most NMR experiments, the acquisition or sampling rate is dictated by the relaxation time (T_1) of the detected nuclei. Under CP conditions, the sampling rate depends on the relaxation time of the nuclei from which the magnetization is transferred. As the protons in the solid state typically relax more rapidly than most other spin ½ nuclei, many more scans can be acquired in a given amount of time in such an experiment than in a simple single-pulse experiment that detects the rare ^{13}C nucleus directly. This point is illustrated in Figure 12, which shows a solid-state ^{13}C spectrum of (non-^{13}C-enriched) alanyl histidine, both with and

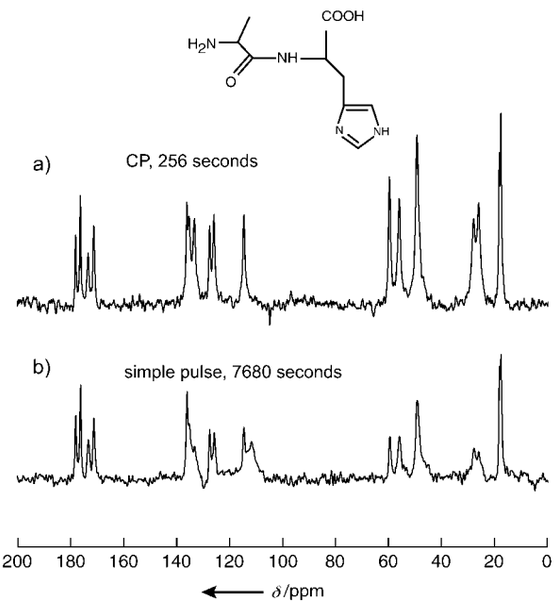

Figure 12. Solid-state ^{13}C NMR spectra (125 MHz) of unlabeled alanyl histidine powder: a) with CP by protons, and b) in a standard single-pulse experiment. Both spectra were recorded under MAS at a speed of 12 kHz and with CW ^{1}H decoupling. The recycle delay for the spectrum in a) was 2 s. The recycle delay for the spectrum in b) was 60 s, owing to the long ^{13}C relaxation time (~18 s for this sample).

without CP from the protons. The signal intensities in the two experiments are not directly proportional for reasons mentioned above. Whereas the overall signal-to-noise ratios of the two spectra in Figure 12a, b are comparable (~1.7:1 for the rightmost peak) the acquisition time of the non-CP spectrum was 45 times longer than for the CP spectrum, owing to the long relaxation time T_1 (~18 s) of the carbon nuclei.

The elegant techniques outlined in this section are powerful and often sufficient tools for many applications in basic chemical analysis and characterization of solid samples. As shown in Figure 12a, a combination of high-power CW decoupling, cross-polarization, and high-speed MAS, can rapidly yield one-dimensional solid-state spectra of compounds containing spin ½ nuclei of low natural abundance such as ^{13}C, ^{15}N, and ^{29}Si, with sufficient spectral sensitivity and resolution. However, as in liquid-state NMR, more advanced multipulse and multidimensional techniques can be utilized to perform a more detailed analysis of the structure and dynamics of a sample. In the following three sections, we provide an overview of such techniques, with primary emphasis on those methods that are easily implemented.

3. Multidimensional NMR and Multipulse Decoupling

The majority of solid-state NMR experiments performed on organic or biological systems involve the detection of low-abundance nuclei such as ^{15}N and ^{13}C. One reason for this is the fact that the homonuclear dipolar coupling can often be neglected because the probability of having two NMR-active nuclei next to each other is very low. In addition, the low gyromagnetic ratios of these nuclei make the strengths of the homonuclear couplings very small, even when the nuclei are directly bonded. MAS at moderate speeds (a few kHz) can eliminate their effects altogether. In contrast, as the homonuclear dipolar coupling between neighboring protons can be strong (in the order of $\sim$100 kHz). Furthermore, because protons have an abundance of almost 100%, MAS does little to narrow the signal, as was shown in Section 2. Reasonably high resolution is achieved in solid-state ^1H NMR spectroscopy through active pulse decoupling of the ^1H spins during signal detection (to be precise: not during the actual sampling of a data point of the signal, but between different data points in the acquisition).[52–54] These experiments are often very demanding on hardware. A simpler and often more reliable way of acquiring high-resolution spectra of protons is to detect the magnetization *indirectly* by using multidimensional NMR spectroscopy. We first review the general acquisition of multidimensional spectra and then we describe methods of multipulse decoupling sequences that can be used in the indirect dimension of these experiments to minimize the effects of the homonuclear coupling between abundant nuclei.

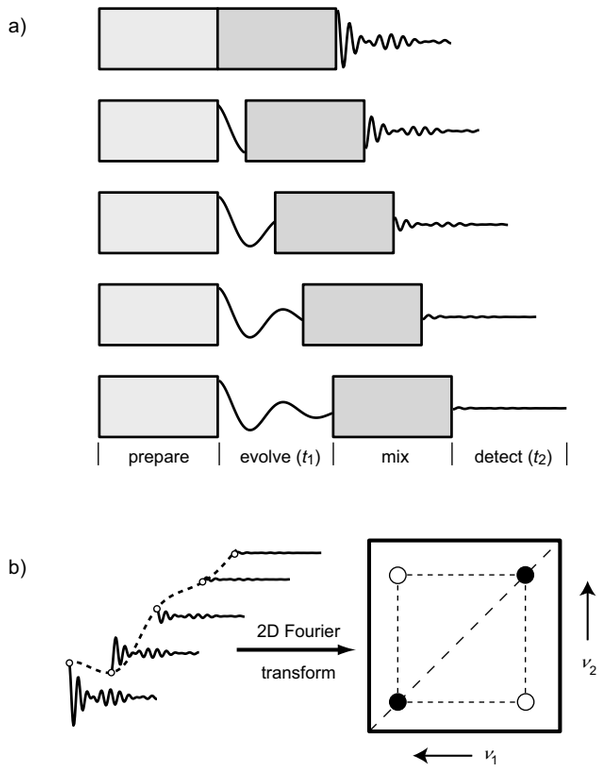

Figure 13. a) Pulse sequence for 2D NMR experiments: The second dimension is obtained by repeating the 1D experiment with sequential time periods t_1 to stroboscopically detect the evolution of the prepared state. b) 2D Fourier transform: First a Fourier transform is performed on each directly detected t_2 signal, followed by a Fourier transform in the t_1 dimension. Since the evolution of the magnetization during t_1 modulates the directly detected t_2 signal, a double Fourier transform produces a spectrum in which the indirectly detected spectrum is correlated with the directly detected spectrum. (Reproduced from ref. [43], with permission.)

3.1. 2D NMR Spectroscopy: The WISE Experiment

Although 2D NMR spectroscopy has many different applications,[54–56] the basic form of all these experiments is essentially the same (Figure 13a). First, the magnetization is prepared in a state appropriate to whatever properties are to be detected in the indirect dimension. For instance, to detect a standard spectrum of the chemical shifts in the indirect dimension, the preparation phase could involve a $\pi/2$ pulse or possibly a CP sequence. Next, the magnetization is allowed to evolve for a time t_1 under a specific NMR Hamiltonian. For instance, if one wishes the I spins in an $I-S$ spin system to evolve only under H_{II} and H_{CS}, then the S spins should be decoupled to remove H_{IS} (a π pulse in the S-spin channel at $t = \frac{1}{2}t_1$ suffices for static samples). To evolve only under H_{II}, a π-pulse or a train of π-pulses can be applied during t_1 to create echoes that refocus H_{CS}.

Following the evolution period t_1, an optional mixing pulse (or a sequence of pulses) is used to prepare the magnetization for the final detection period t_2. As with the initial preparation period, the nature of the mixing period depends largely on the spectrum desired. In heteronuclear experiments, it is often necessary to transfer the magnetization from one set of spins to another. For instance, in an experiment correlating ^1H and ^{13}C chemical shifts, the mixing period might involve CP from the ^1H spins to the ^{13}C spins. Once the mixing period is complete, the resulting magnetization is detected as usual in the direct dimension t_2.

A 2D free-induction decay is acquired by assembling several 1D free-induction decays acquired at increasing times t_1. The different 1D spectra are modulated in t_1 based on the Hamiltonians chosen during this time period. By performing a Fourier transform in both dimensions t_1 and t_2, a 2D spectrum is produced which correlates the interactions detected in the indirect dimension t_1 with the interactions detected in the direct dimension t_2 (Figure 13b).[55]

A simple example of a useful 2D solid-state NMR experiment is the WIdeline SEparation (WISE) experiment (Figure 14a).[57, 58] The ^1H magnetization is initially rotated into the xy plane by a $\pi/2$ pulse. During t_1, the magnetization then evolves under the ^1H chemical shifts, the homonuclear dipolar couplings, and the heteronuclear couplings to ^{13}C nuclei ($H_{CS} + H_{II} + H_{IS}$), after which it is transferred through CP to neighboring ^{13}C nuclei for detection in t_2. A 2D WISE spectrum correlates broad ^1H resonances with the relatively narrow resonances of the neighboring ^{13}C nuclei under MAS (Figure 14b). In this manner, a normally unresolvable 1D ^1H NMR spectrum is separated into the contributions of

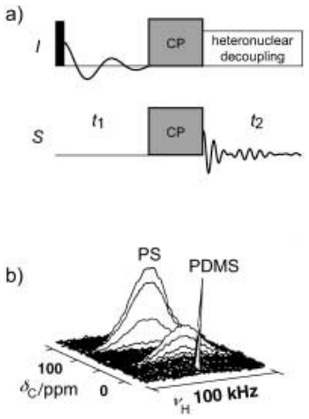

Figure 14. The WISE experiment: a) Pulse sequence for the correlation of ^{1}H and ^{13}C resonances with WISE. b) 2D $^{1}H-^{13}C$ WISE NMR spectrum of a polystyrene-*b*-polydimethylsiloxane (PS-*b*-PDMS) block copolymer (1:1). The broad ^{1}H signals correspond to rigid protons, whereas the narrow ^{1}H signals correspond to mobile protons, in which the homonuclear dipolar coupling is partially averaged out. (Adapted from ref. [57], with permission.)

various ^{1}H sites in proximity to spectroscopically resolved ^{13}C sites. Usually a short CP period assures that mainly nearby (or bonded) nuclear spins are correlated. The spectrum in Figure 14b is taken from a block copolymer of polystyrene and polydimethylsiloxane (1:1). The resonance line widths of the ^{1}H sites in the polymer blend provide information about local molecular mobility of the different polymer components. The greater the mobility of a ^{1}H nucleus, the narrower its ^{1}H NMR signal. Recently, this method has been used to characterize nanostructured inorganic–organic composites.[59, 60]

Although WISE does allow the separation and study of broad ^{1}H resonances based on their coupling to nearby ^{13}C nuclei, the experiment does not achieve the original goal set forth in this section: to remove the ^{1}H homonuclear coupling and to obtain a resolved ^{1}H NMR spectrum of the chemical shifts. In Section 3.2 we show that by using appropriate *homonuclear* decoupling sequences during t_1, the effects of the $^{1}H-^{1}H$ dipolar coupling can indeed be strongly reduced, while the chemical shift evolution is preserved. The application of these RF pulse sequences during t_1 is notably less demanding than in experiments in which pulses and detection periods are interleaved.[52–54]

3.2. Homonuclear Dipolar Decoupling

In the previous sections, we discussed *heteronuclear* dipolar decoupling, in which the dipolar coupling between two sets of spins I and S is removed by a strong RF field applied to the I spins while the S spins evolve. The success of CW decoupling is a result of the form of H_{IS}, which is proportional to I_zS_z. By constantly rotating the I spins around one axis with a continuous RF field, the sign of the energy determined by I_zS_z oscillates between positive and negative, producing a time-averaged value of zero. On the other hand, the *homonuclear* dipolar coupling is proportional to $3I_{1z}I_{2z}-(\boldsymbol{I}_1\cdot\boldsymbol{I}_2)$. As, by definition, the magnetization of the two nuclei cannot be manipulated independently, a CW irradiation of the I spins around one axis will have no effect on the sign of the energies. In a more elaborate approach, one can show that if the direction of the local field exerted by the spins on each other is toggled between *all three* axes, the effect of the coupling vanishes. This has been implemented early on in a multipulse sequence by Waugh et al. (WAHUHA or WHH-4).[61] Although this sequence is not used much any more, it still serves as a good illustrative example of how such techniques work, and how new ones can be designed.

3.2.1. WAHUHA

To understand this and similar sequences, it is helpful to consider a rotation of the reference frame rather that rotations of the spins. Although the rotations of, for example, z magnetization into x magnetization could be considered, the magnetization could also be kept constant and the reference frame rotated in the opposite direction. In this way H_{II} becomes H_{xx}, H_{yy}, or H_{zz}, depending on how the reference frame is rotated by the RF pulses (Figure 15a). H_{xx}, H_{yy}, and H_{zz} are described in Equations (10)—(12)

$$H_{xx} = -d\tfrac{1}{2}(3\cos^2\theta-1)(3I_{1x}I_{2x}-(\boldsymbol{I}_1\cdot\boldsymbol{I}_2)) \quad (10)$$

$$H_{yy} = -d\tfrac{1}{2}(3\cos^2\theta-1)(3I_{1y}I_{2y}-(\boldsymbol{I}_1\cdot\boldsymbol{I}_2)) \quad (11)$$

$$H_{zz} = -d\tfrac{1}{2}(3\cos^2\theta-1)(3I_{1z}I_{2z}-(\boldsymbol{I}_1\cdot\boldsymbol{I}_2)) \quad (12)$$

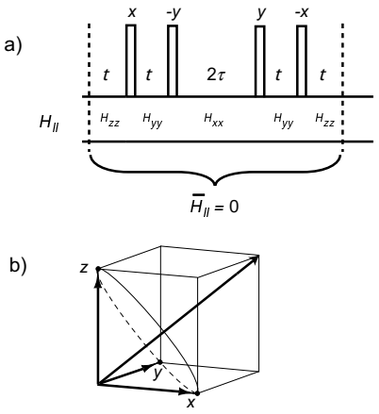

Figure 15. a) Pulse sequence for one cycle of the four-pulse WAHUHA decoupling sequence, in which the magnetization is aligned sequentially along the x, y, and z axes. b) The Lee–Goldburg sequence is the continuous analogue, in which the spins undergo rotation about an axis inclined at the magic angle in spin space (analogous to mechanical magic angle spinning in real space).

Since the scalar product of the two angular momentum operators $\boldsymbol{I}_1\cdot\boldsymbol{I}_2$ can be defined as in Equation (13), the sum $H_{xx}+H_{yy}+H_{zz}=0$.

$$\boldsymbol{I}_1\cdot\boldsymbol{I}_2 = I_{1x}I_{2x}+I_{1y}I_{2y}+I_{1z}I_{2z} \quad (13)$$

Therefore, any pulse sequence that shifts the reference frame along the x, y, and z axes (and with it the "direction" of

the local dipolar fields) for equal periods of time should successfully eliminate the homonuclear dipolar coupling. On the other hand, the chemical shift in the usual laboratory frame is proportional to I_z alone. When the reference frame is rotated sequentially along all three axes (during three consecutive time periods) the chemical shift will be proportional to $(I_x + I_y + I_z)/3$. The overall average chemical shift evolution is then scaled by a factor of $1/\sqrt{3}$ relative to the evolution without the decoupling sequence.[61] Thus, the WAHUHA sequence accomplishes our goal of eliminating the $^1H-{}^1H$ homonuclear dipolar coupling while still allowing the magnetization to evolve under H_{CS}.

We could also consider allowing the reference frame to continuously change from the x to the y and the z direction. This has been implemented in an early windowless sequence called Lee–Goldburg decoupling.[62] The magnetization (or the reference frame) is rotated about an effective magnetic field in the rotating frame that can be created by applying an off-resonance RF irradiation. If the RF strength ω_{RF} is adjusted so that $\omega_{RF} = \sqrt{2}\Delta\omega$ ($\Delta\omega$ = frequency offset), an effective RF field is produced in the rotating frame and is inclined at the magic angle with respect to z. The magnetization (or the reference frame) follows a conical path, crossing the z, y, and x axes at equal angles (Figure 15b). In MAS, the spatial averaging analogue of the above techniques, one would have exactly the same effect if sufficiently rapid sample reorientation were possible. There is one exception, though: the chemical shift is not scaled in MAS.

3.2.2. Decoupling Supercycles

Although the WAHUHA sequence is theoretically very effective in removing the homonuclear dipolar interaction, complications are often encountered in practice. Pulse imperfections and chemical-shift-offset effects can interfere with ^1H homonuclear decoupling when using WAHUHA. These problems can be circumvented to a large extent by the use of decoupling supercycles, which are repetitive implementations of simple sequences such as WAHUHA, with specific phase shifts of the RF pulses.[63, 64] For example, the supercycle MREV-8[65, 66] is a composite sequence of two WAHUHA pulse trains, with a 180° phase shift in two of the last four pulses (Figure 16a). This sequence has been shown to be much more robust against various pulse imperfections and frequency-offset effects.[38] In addition to MREV-8, there exist more complex decoupling supercycles, including BR-24,[67] BLEW-12,[68] CORY-24,[69] TREV-8,[70] and MSHOT.[71]

Often, symmetrization principles are used to improve the performance of different sequences. In the continuous Lee–Goldburg decoupling sequence mentioned above, the symmetrization is implemented by switching the offset between $+\Delta\omega$ and $-\Delta\omega$ and simultaneously changing the phase of the RF irradiation by 180° (Figure 16b). Errors in the averaging trajectories are removed by this procedure (Figure 16c). This method is called the frequency-switched Lee–Goldburg (FS-LG) sequence and has been extremely useful in many applications.[72–79]

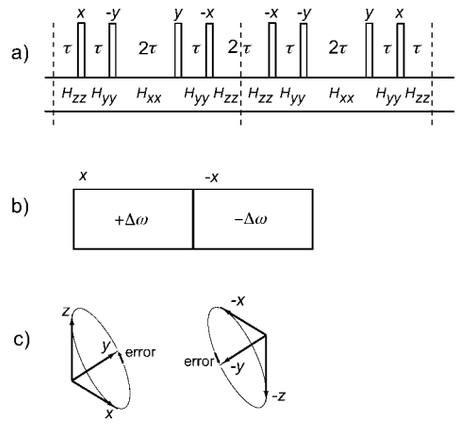

Figure 16. a) Pulse sequence for one cycle of the MREV-8 decoupling sequence; b) FS-LG decoupling; c) compensation for errors in the magnetization trajectories with the FS-LG sequence.

A complication that must be considered when using a homonuclear decoupling sequence under MAS conditions is the possible interference between sample spinning and multipulse decoupling. This affects the time-averaging of H_{II} in different ways, in particular when the spinning speed is very high.[75] Since this interference often degrades the effectiveness of multipulse decoupling sequences, it is advantageous to optimize the multipulse sequence for MAS. First, the pulse cycles should be rotor-synchronized; that is, an integer number of pulse trains should be applied per rotor cycle. Second, as many pulse cycles should be applied per rotor period as possible. However, these guidelines make the implementation of long sequences (especially the 24-pulse BR-24 sequence) very difficult under fast MAS, in which the rotor cycle can be as short as 30 μs. A powerful alternative involves FS-LG:[72, 73] the full cycle time is typically of the order of 10–20 μs, which is still significantly shorter than the rotor period at routine speeds (10–20 kHz). In practice, FS-LG has proven to be a very effective decoupling sequence at different spinning speeds. Lee–Goldburg irradiation can also be used instead of a continuous-wave field during CP. This leads to homonuclear decoupling during the heteronuclear magnetization transfer, which makes the transfer more selective to directly bonded atoms. This has been exploited to measure the distance between heteronuclei.[80, 81]

Promising new homonuclear decoupling schemes are being developed that are based on a new class of symmetry rules, allowing for a minimization of the RF–rotation interference.[82]

3.2.3. Multiple-Quantum Spectroscopy

Although it is possible to remove the effects of the homonuclear dipolar interaction by multipulse sequences, it is also possible to tailor the interaction Hamiltonian to a specific form. The appropriate multipulse sequence can be applied to create an effective double-quantum dipolar Hamiltonian [Eq. (14)].[83]

$$H_{dq} = -d\tfrac{1}{2}(3\cos^2\theta - 1)(I_{1+}I_{2+} + I_{1-}I_{2-})$$

In the presence of many coupled spins, this Hamiltonian creates high multiple-quantum coherences, which are limited only by the size of the spin system. One can therefore use this method for spin counting and for determining cluster sizes and the dimensions of coupling networks in solids and in liquid crystals.[84–86] Since multiple-quantum coherences cannot be detected directly, 2D NMR spectroscopy is required to observe the evolution of multiple-quantum coherences in the indirect dimension t_1. Selective excitation of certain multiple-quantum coherences has been achieved by using appropriate supercycles.[87] For molecules oriented by the magnetic field or other means, these methods have led to the simplification of spectra,[88] which aided in resonance assignment and structure determination. Recently, the alignment of β strands in amyloid fibrils has been investigated by using multiple-quantum NMR spectroscopy.[89]

3.3. Heteronuclear Correlation

We complete our discussion of homonuclear dipolar decoupling by describing the solid-state heteronuclear correlation (HETCOR) experiment.[90, 91] Similar to heteronuclear single-quantum (HSQC) and multiple-quantum (HMQC) correlation experiments in liquid-state NMR spectroscopy,[46] the HETCOR experiment in solids correlates ^{1}H chemical shifts with the chemical shifts of another nucleus, such as ^{13}C or ^{15}N. One possible HETCOR sequence for ^{1}H–^{13}C correlations is shown in Figure 17. As in the WISE sequence, the ^{1}H magnetization is first excited by a π/2 pulse.

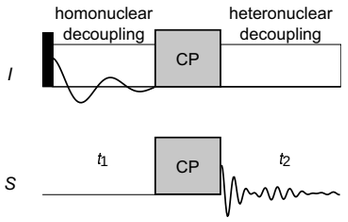

Figure 17. Principle of the HETCOR experiment: The pulse sequence is identical to that of the WISE experiment, except for the incorporation of homonuclear dipolar decoupling in the indirect dimension. Heteronuclear decoupling of the *S* spins can also be incorporated into the indirect dimension.

During the t_1 period, the protons are decoupled from each other by using one of the decoupling techniques mentioned in Section 3.2. An optional CW-decoupling field can be applied to the ^{13}C nuclei so that H_{IS} is also removed and the protons evolve only under their chemical-shift Hamiltonian H_{CS}. Following the t_1 period, the magnetization is transferred to the ^{13}C nuclei by CP, and is then detected during t_2. Figure 18 shows a ^{1}H–^{13}C HETCOR spectrum of a ^{13}C-labeled chlorophyll *a* aggregate obtained by using FS-LG homonuclear dipolar decoupling during t_1.[92] Although the ^{1}H resonances are still somewhat broad (~1–2 ppm), they are sufficiently narrow to observe and measure the variety of ^{1}H chemical shifts in the sample.

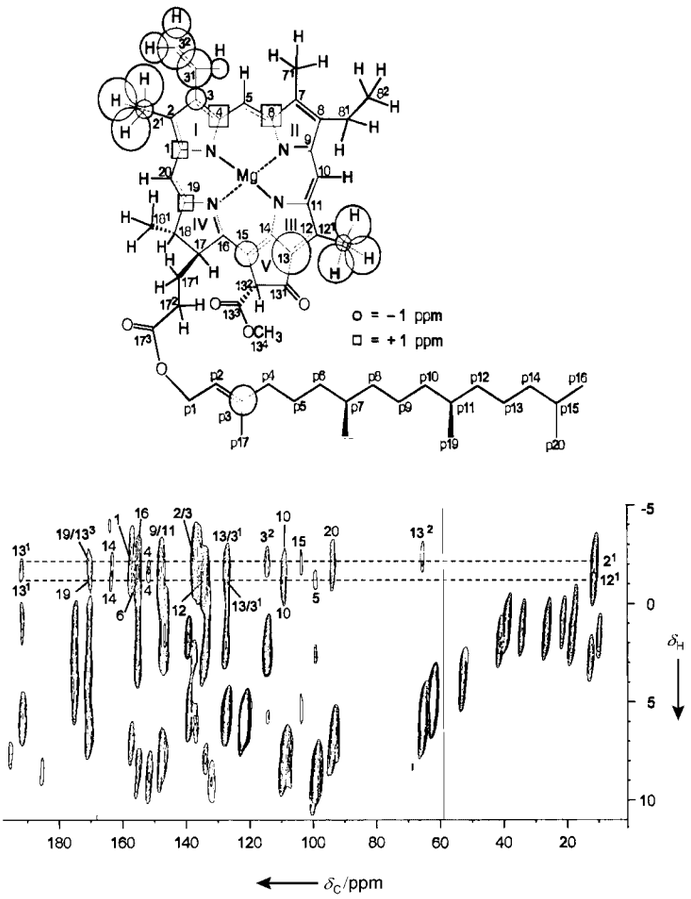

Figure 18. ^{1}H–^{13}C HETCOR spectrum of uniformly ^{13}C-enriched chlorophyll *a* aggregates in water obtained at a field strength of 14.1 T and with a spinning speed of 13 kHz. A pulse sequence similar to that shown in Figure 17 was used. The high resolution in the proton dimension is a result of the FS-LG decoupling during the t_1 period. δ_C and δ_H are the chemical shifts of the carbon atoms and the protons, respectively. (Reproduced from ref. [92], with permission.)

Unlike HSQC or HMQC in liquids, which both utilize through-bond *J* couplings to transfer polarization, HETCOR relies on dipolar interactions and thus correlates spatially close bonded and nonbonded nuclei. As was shown in Figure 11c, strongly coupled spins transfer polarization more rapidly than weakly coupled spins. The distance of magnetization transport during CP can therefore be controlled to some extent by varying the CP mixing time. For long CP mixing times, the magnetization will be transported farther away, even to carbon atoms that are not directly bonded. By comparing HETCOR spectra taken at different mixing times, it is possible to gain insight into the local structure and atomic distribution in the sample.

Closely related to the HETCOR experiment is the separated local field experiment, which allows one to correlate the heteronuclear *I*–*S* dipolar coupling constants to the frequency of the chemical shift of the *S* spin in single crystals or oriented molecules (similar to *J* spectroscopy in liquids).[93–95]

In this experiment, a π pulse acting on both the I and the S spins at $t = \frac{1}{2}t_1$ refocuses the chemical shift as well as the CSA, while the homonuclear coupling is removed by one of the homonuclear decoupling sequences. Therefore, only the heteronuclear $I-S$ coupling will be in effect during t_1. A variant of this technique, called PISEMA (polarization inversion spin exchange at magic angle), has successfully been used to determine the secondary structures of solid proteins.[96–98] The concerted variations in the ^{13}C and ^{15}N chemical shifts and the $^{1}H-^{13}C$ and $^{1}H-^{15}N$ dipolar couplings cause the signals that arise from different residues to lie along circular paths, the form of which is characteristic of the secondary structure.

3.4. Multipulse Heteronuclear Dipolar Decoupling

Before leaving the discussion of multipulse NMR spectroscopy, we return once again to the topic of heteronuclear dipolar decoupling. We have limited our discussion of heteronuclear decoupling to CW irradiation. However, the beauty and efficiency of multipulse decoupling in the homonuclear case raises the question as to whether an efficient multipulse sequence can be employed for heteronuclear decoupling. In liquids, a wealth of multipulse sequences are available, including MLEV-16, WALTZ-16, and GARP.[35, 99–101] In the solid state, however, because of the magnitude of the coupling constants and interference effects between heteronuclear and homonuclear couplings (see Section 2.2), these sequences can be inferior to CW decoupling. In addition, sign changes of the dipolar coupling constants under MAS result in a partial cancellation of the effects of these multipulse sequences.[43] The heteronuclear decoupling technique called two-pulse phase modulation (TPPM)[102] was shown to produce results superior to simple CW decoupling, particularly under MAS. As shown in Figure 19 the TPPM sequence breaks the CW irradiation into

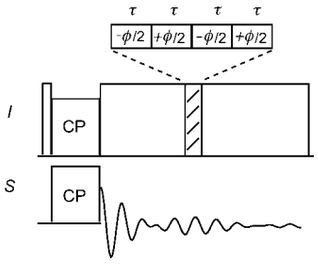

Figure 19. TPPM decoupling sequence: RF irradiation is applied continuously, with an alternating phase shift of $+\phi/2$ and $-\phi/2$, for every time period τ. The values of ϕ and τ are optimized before the experiment to achieve maximum decoupling efficiency.

a series of discrete time periods τ (in the order of 3–20 μs) during which the phase of the irradiation alternates between $+\phi/2$ and $-\phi/2$. Typically, the values of ϕ and τ must be optimized for a particular sample in order to produce the smallest possible line widths. Figure 20 shows the spectra of ^{13}C-labeled calcium formate acquired under proton TPPM

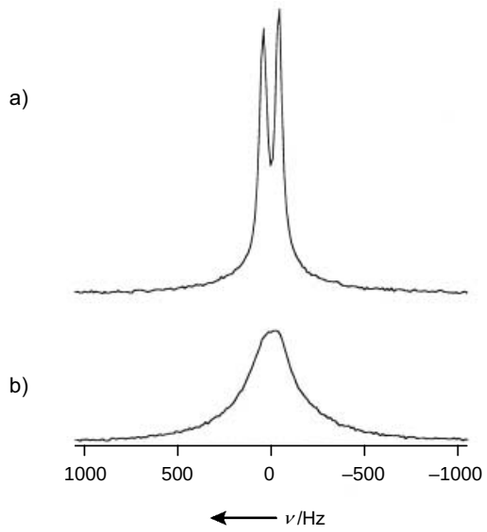

Figure 20. ^{13}C CP MAS NMR spectrum of calcium formate: a) with TPPM decoupling, and b) with CW decoupling. In both cases, the spinning speed was 10.7 kHz. The splitting observed in a) is a result of the chemical shift difference of 80 Hz between the two crystallographically different ^{13}C sites in calcium formate. (Reproduced from ref. [102], with permission.)

decoupling (Figure 20a) and under CW decoupling (Figure 20b). A typical ϕ value is about 50°, and τ is often adjusted to give a flip angle of approximately 150°. With the improved resolution that results from TPPM decoupling, the difference in chemical shifts (80 Hz) between the two crystallographically non-equivalent ^{13}C sites in calcium formate is resolved, which is not possible with standard CW decoupling under the same conditions. Although a rigorous study of why this procedure improves heteronuclear decoupling is still missing, it is believed that the favorable properties of the TPPM sequence are related to a facilitation of flip-flop transitions among the abundant proton nuclei, which assist the heteronuclear decoupling in a process called "self-decoupling".[103–106] The less stringent requirements for the decoupling power of the TPPM sequence are particularly apparent with high-speed MAS. As can be seen in the ^{13}C NMR spectrum of (non-^{13}C-enriched) cyclosporin A (Figure 21), line widths of 10 to 50 Hz can be obtained and the vast majority of the resonances in the spectrum are resolved. Although alternative decoupling methods have been proposed,[107, 108] TPPM is still the most widely used sequence.

In this section, we showed that it is possible, through a combination of multipulse homonuclear decoupling and 2D NMR spectroscopy, to obtain high-resolution solid-state ^{1}H NMR spectra. Phase modulation of heteronuclear decoupling sequences can produce CP MAS spectra of rare spins with a resolution close to that of liquid-state spectra. The concept of using a series of pulses to manipulate a Hamiltonian has applications far beyond hetero- and homonuclear decoupling. As will be seen in Section 4, multipulse sequences and 2D NMR spectroscopy can be used to derive information from interactions (e.g. CSA or dipolar coupling) that are normally removed under MAS.

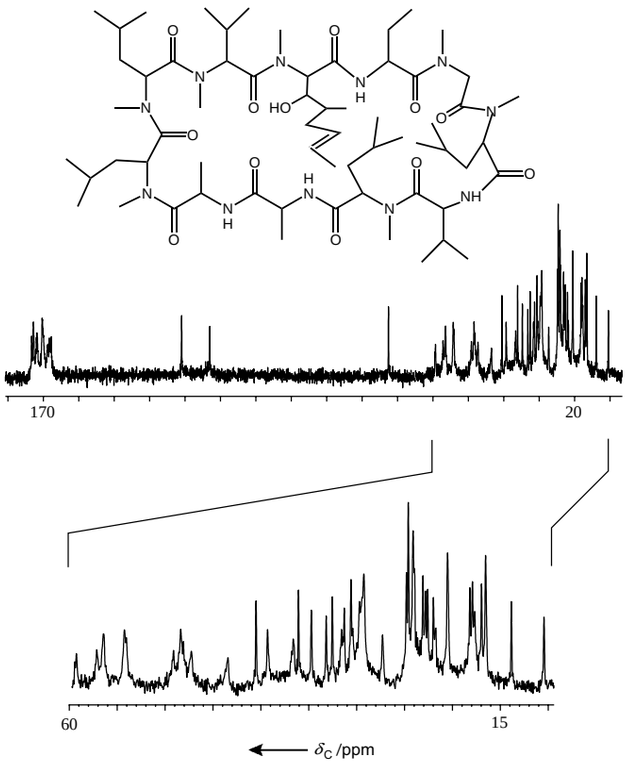

Figure 21. ^{13}C CP MAS NMR spectrum (125 MHz) of cyclosporin A (see structure). The spectrum was measured with a spinning frequency of 33.3 kHz using TPPM decoupling ($\phi = 20^\circ$). With the combination of high spinning speeds and TPPM decoupling, the ^{13}C line widths are 10–50 Hz. (Courtesy of A. Lesage and L. Emsley).

4. Reintroducing Lost Hamiltonians

Section 2 of this review addressed the question of how to remove some of the undesirable effects of interactions that are found in solid-state NMR spectroscopy, for example, dipolar coupling and CSA, by utilizing techniques such as MAS and high-power spin decoupling. The resulting spectrum has a resolution close to that of a liquid-state NMR spectrum (e.g., see Figures 12a and 21). However, the signals produced by dipolar coupling and CSA provide information about the environment of the nuclei, and this information is lost by removing these interactions through spinning and decoupling. In the following section, we discuss techniques that selectively reintroduce dipolar couplings and CSA under MAS to measure distances or establish correlations based on proximity. Although a vast number of methods can be used to reintroduce the dipolar coupling and the CSA, we discuss in detail only a limited number of techniques that serve both as representative examples and as basic building blocks for more complicated experiments.

4.1. Distance Measurements in Solids

An integral part of structure determination in molecular systems is the measurement of distances between atoms. In liquid-state NMR spectroscopy, this is usually accomplished through the measurement of cross-relaxation rates by nuclear Overhauser effect spectroscopy (NOESY).[46, 109] These relaxation mechanisms can usually be neglected in solids, as the magnetization can be transferred more directly through the coherent action of heteronuclear and homonuclear dipolar couplings. As shown in Equation (2), the strength of the dipolar coupling between two nuclei is proportional to the inverse cube of the internuclear distance, which is the key to obtaining structural information. However, with the exception of couplings that involve protons (e.g., $^1H-^1H$ or $^1H-^{13}C$), the effects of homonuclear and heteronuclear dipolar coupling are often removed under MAS, since the spinning speed can routinely be made greater than the magnitude of the coupling constant. Thus, to measure dipolar couplings while retaining the high resolution afforded by MAS, the couplings must be selectively reintroduced.

4.1.1. Heteronuclear Recoupling: REDOR

The heteronuclear dipolar Hamiltonian introduced in Equation (2) contains the orientation-dependent term $(3\cos^2\theta - 1)$, and the spin-component-dependent term I_zS_z. In Section 3 we discussed how one can manipulate the spin component by CW and TPPM decoupling, or the spatial component by MAS. Both methods lead to the removal of the effects of this interaction. In the case of CW decoupling, it is easy to turn this interaction on and off by controlling the RF field. Recoupling a dipolar interaction that is removed by MAS is more complicated, as it is not practical to rapidly turn the spinning on and off.[110] By properly manipulating the spin component of the dipolar Hamiltonian in synchrony with the sample rotation, however, it is possible to partially undo the effect of MAS on the heteronuclear dipolar coupling.

For a single crystal that moves along a conical path under MAS, the value of the effective heteronuclear dipolar coupling interaction determined by H_{IS} changes both in intensity and sign (Figure 22a). Over a single rotation period,

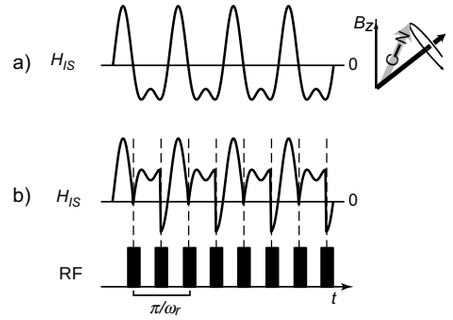

Figure 22. Time-dependent behavior of the heteronuclear dipolar coupling: a) The time-dependent evolution of H_{IS} with MAS; as the integral of the dipolar coupling over a single rotor cycle is zero, the dipolar coupling is effectively removed if the spinning speed is sufficiently high. Right: an internuclear vector between a carbon nucleus and a nitrogen nucleus traverses a conical path. b) The time-dependent evolution of H_{IS} with MAS with two π pulses on the S spin per rotor cycle. Each π pulse reverses the sign of the dipolar coupling Hamiltonian, thus creating a time evolution which no longer averages to zero. (Reproduced from ref. [43], with permission.)

the integrated magnitude of H_{IS} is zero, so the dipolar coupling is effectively removed under MAS. However, by applying RF pulses at proper intervals, it is possible to interfere with the trajectory of H_{IS} so that the value of H_{IS} is not zero over one rotation period. By applying π pulses, the S spin magnetization is flipped ($S_z \rightarrow -S_z$) and the sign of H_{IS} changes. Once again we point out that it is *not* the Hamiltonian that is directly manipulated but the spins. The equivalent picture of rotating the reference frame instead of the spins leads to the description of an effective Hamiltonian that changes sign. Indeed, by applying two π pulses per rotation period (Figure 22b), the evolution of H_{IS} can be altered in such a way that approximately 70% of the heteronuclear dipolar coupling is recoupled (i.e. the integrated magnitude of H_{IS} is 70% of its static value).

This two-π-pulse technique, known as rotational echo double resonance (REDOR),[111] is a powerful tool for determining dipolar couplings between two different nuclear species such as ^{13}C and ^{15}N. The pulse sequence for REDOR is shown in Figure 23. The ^{13}C nuclei are subjected to a $\pi/2$ pulse

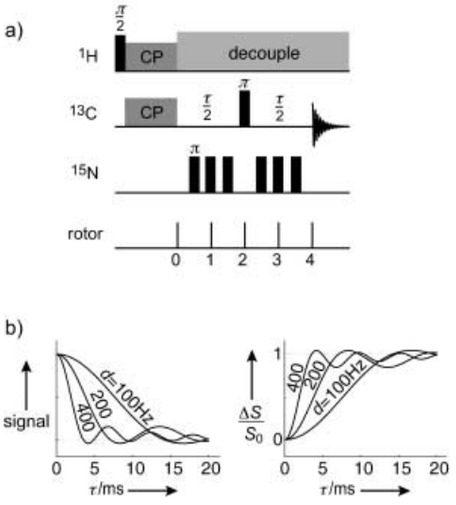

Figure 23. a) The REDOR pulse sequence: CP of the ^{13}C nuclei is followed by a period τ in which the ^{13}C magnetization is dephased by the application of a series of rotor-synchronized pulses on the ^{15}N magnetization, which recouple the $^{13}C-^{15}N$ dipolar coupling; the signal decays faster for larger coupling constants. b) Usually, the dephasing curves in the lower right hand corner are used, which show the amount of dephasing relative to the initial signal intensity ($\Delta S/S_0$). Apart from a scaling factor, these curves are mirror images of the actual dephasing curves on the left.

or are polarized through CP from the protons. During τ_m, two ^{15}N π pulses are applied per rotation period, so that the $^{13}C-^{15}N$ dipolar coupling is reintroduced. When a π pulse is applied at $t = \frac{1}{2}\tau_m$ in the ^{13}C channel instead of the ^{15}N channel, recoupling of heteronuclear coupling that involves a third nuclear species is avoided. The experiment is repeated in the absence of the ^{15}N pulses and the two spectra are compared. Under the influence of the (recoupled) $^{13}C-^{15}N$ dipolar coupling, the ^{13}C magnetization decays as a result of an averaging effect of the powder sample. By measuring the decay of the magnetization with increasing τ_m, and dividing the intensities by the signals of the "natural" decay measured without recoupling, a REDOR decay curve such as that shown in Figure 23b can be created. Figure 24 shows an experimental dephasing curve acquired for ^{13}C,^{15}N-labeled (10%) glycine. From the fitted line, a $^{13}C-^{15}N$ dipolar

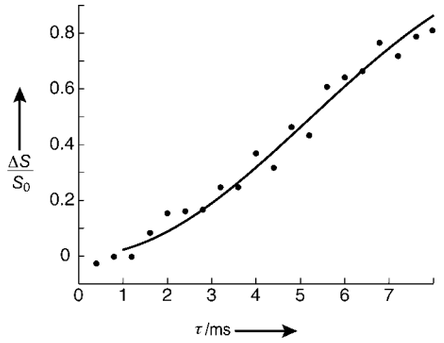

Figure 24. Dephasing curve: ^{13}C magnetization in ^{13}C- and ^{15}N-labeled glycine as a function of the length of the dephasing time τ. $\Delta S/S_0$ (the REDOR difference) is the normalized difference between the ^{13}C signal intensities with and without the ^{15}N pulses. By fitting the decay of the ^{13}C magnetization, the $^{13}C-^{15}N$ dipolar coupling was determined to be 195 Hz.

coupling constant of 195 Hz was obtained. From Equation (3), the $^{15}N-^{13}C$ internuclear distance was found to be 2.47 Å. As the strength of the heteronuclear dipolar coupling approaches $\sim$25 Hz, it becomes very difficult to determine distances by using REDOR. This corresponds to a $^{15}N-^{13}C$ distance of $\sim$5 Å and a $^{13}C-^{31}P$ distance of $\sim$7.5 Å. These distances exceed those typically studied in liquid-state NMR spectroscopy[46, 109] and they can provide useful constraints in structural studies of solids.

When the dephasing curve is a sum of the individual curves of several isolated spin pairs, a dipolar coupling constant spectrum can be obtained by using a so-called REDOR-transform.[112] Complications may arise when more than two spins are coupled. For this case, special techniques have been proposed for obtaining individual the coupling constants.[113, 114] A careful study of the viability of distance measurements in multiple-spin systems of unknown structures by REDOR-type recoupling techniques has been conducted by Fyfe and co-workers.[115, 116] F–Si distances in zeolites have been measured in this way.[117]

Frequency-selective heteronuclear recoupling can be achieved by using selective pulses on one of the channels, and has been employed, for example, to measure $^{13}C-^{15}N$ distances in uniformly labeled proteins.[118, 119] REDOR is not the only method to recouple heteronuclear dipolar interactions: other techniques are based on windowless frequency-, phase-, and amplitude-modulated sequences,[120, 121] and, strictly speaking, CP is a type of heteronuclear recoupling sequence.

4.1.2. Homonuclear Recoupling: DRAMA and RR

Homonuclear dipolar recoupling can be accomplished in much the same way as heteronuclear dipolar recoupling—manipulation of the spin component of the dipolar Hamiltonian influences the motional averaging produced by the spinning rotor. The main difference between heteronuclear

and homonuclear dipolar recoupling lies in the difficulty of individually addressing different homonuclear spins. In REDOR, one can repeatedly alternate the sign of H_{IS} by applying pulses to either the I or the S spin. In a homonuclear spin system I_1I_2 the two spins have very similar resonance frequencies, so any π pulse intended to change the sign of $\boldsymbol{I}_{1z}$, will also result in changing the sign of $\boldsymbol{I}_{2z}$. Thus, the application of a π pulse has little effect on the overall evolution frequencies determined by H_{II}.

One alternative to using π pulses is to use $\pi/2$ pulses, which change the orientation of the quantization axis of the dipolar coupling. In Figure 22a, we showed that over a single rotation period, the spatial evolution of the dipolar Hamiltonian is such that its average value is zero. However, by toggling between one or more of the Hamiltonians in Equations (10)—(12) during the rotation period by the application of $\pi/2$ pulses, the averaging produced by MAS can be interrupted. One such technique is DRAMA (dipolar recovery at the magic angle).[122] During this sequence, two $\pi/2$ pulses per rotation period toggle the reference frame from the z axis to the y axis and back again (Figure 25a). Under ideal conditions, the reference frame is directed along the z axis for half of the rotation period ($\tau = \tau_r/2$) and along the y axis for the other half. DRAMA recouples up to 45% of the homonuclear dipolar coupling. Because the two-pulse sequence also recouples the CSA under MAS, a better implementation of DRAMA also includes π pulses to refocus the CSA (Figure 25b).

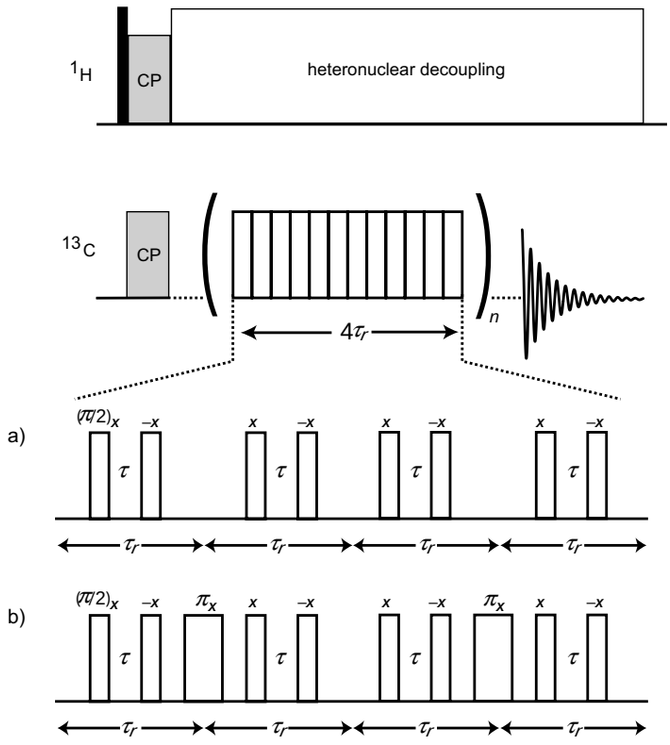

Figure 25. a) Pulse sequence for one cycle of the DRAMA homonuclear dipolar recoupling sequence consisting of $\pi/2$ pulses only. b) The partial recoupling of the CSA that occurs under the sequence in a) can be removed applying a π pulse at the end of each rotor cycle. τ_r = Rotor period.

Distance determination with DRAMA is carried out in generally the same way as with REDOR experiments. During the mixing period τ_m, the magnetization of the recoupled nuclei decays as a result of the dephasing effects of the homonuclear dipolar coupling. For example, Figure 26 shows solid-state NMR spectra of [carbonyl-^{13}C]polycarbonate obtained by using the pulse sequence in Figure 25b both with

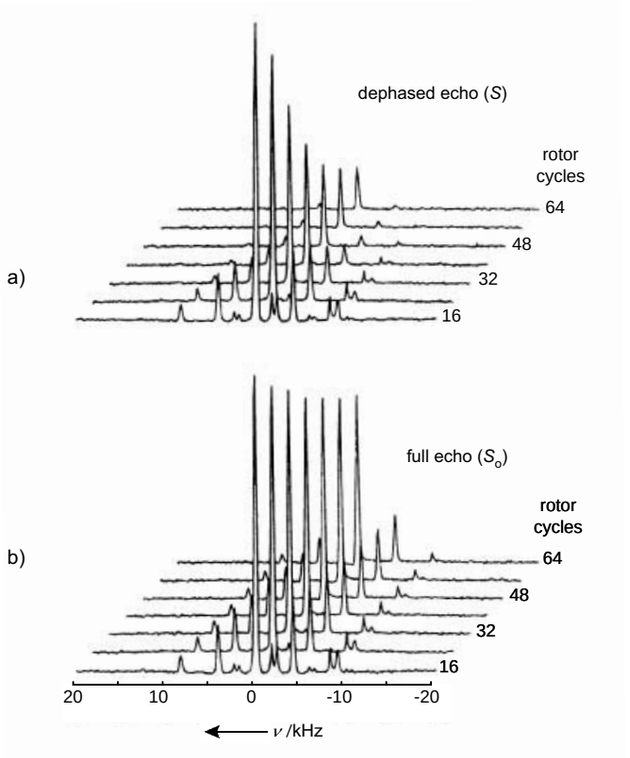

Figure 26. Solid-state ^{13}C NMR spectra of [^{13}C-carbonyl]polycarbonate, obtained by using the DRAMA sequence in Figure 25b. a) Decay of the ^{13}C carbonyl resonance as a function of the mixing time τ_m. As τ_m increases, the ^{13}C magnetization decays as a result of the reintroduction of homonuclear dipolar coupling between the chains. b) Experiment run without the DRAMA $\pi/2$ pulses. The observed decay is a result of the natural relaxation of the magnetization. The spinning speed was 4167 Hz, which corresponds to 64 rotor cycles with a 15.4-ms mixing time. (Reproduced from ref. [123], with permission.)

(Figure 26a) and without (Figure 26b) the recoupling pulses. As the mixing time increases, the intensities of all of the ^{13}C resonances decrease because of recoupled ^{13}C–^{13}C dipolar coupling (Figure 26a). This decay is substantially more pronounced than the natural decay of the magnetization when the DRAMA recoupling pulses are removed (Figure 26b). By measuring the decay of the ^{13}C magnetization as a function of τ_m, it is possible to determine the ^{13}C–^{13}C dipolar coupling constants and the corresponding internuclear distances. For the polycarbonate sample, the ^{13}C–^{13}C internuclear distances were used to help determine a model for polycarbonate chain packing in the solid state.[123]

Another example of a commonly used method for recoupling homonuclear dipolar couplings under MAS is rotational resonance or RR.[124] Unlike DRAMA, rotational resonance

does not require the application of pulses to interrupt the effect of the spinning rotor—in fact, rotational resonance utilizes the spinning rotor to recouple two spins. As shown in Section 2.5, the homonuclear dipolar coupling contains the "flip-flop" interaction terms, $I_1^+ I_2^- + I_1^- I_2^+$. When the chemical shifts of two nuclei differ by a frequency that is larger than the dipolar coupling constant, the flip-flop term is suppressed as it is no longer possible for the spins to undergo an energy-conserving transfer of spin angular momentum. However, when the frequency of the MAS rotor ω_r is set such that it is equal to an integer multiple of the difference in isotropic chemical shifts $\Delta\omega_{iso}$ of the two nuclear spins [Eq. (15)] then the homonuclear dipolar coupling is effectively recoupled.

$$\Delta\omega_{iso} = n\omega_r \tag{15}$$

Although the origin of this process is complex, it can generally be understood by considering the rotor to be an additional source of energy for the system to bridge the energy gap between the nuclear spin transitions. Only when the rotor spins at one of the rotational resonance conditions dictated by Equation (15) are the nuclei recoupled. Figure 27 shows a ^{13}C CPMAS spectrum of glycine taken at 12.0 and at 16.6 kHz, which corresponds to off and on rotational resonance conditions ($n=1$) in this case. The splitting in Figure 27 c at the rotational resonance condition is a result of the interaction between the nuclei, and is indicative of the coupling strength.

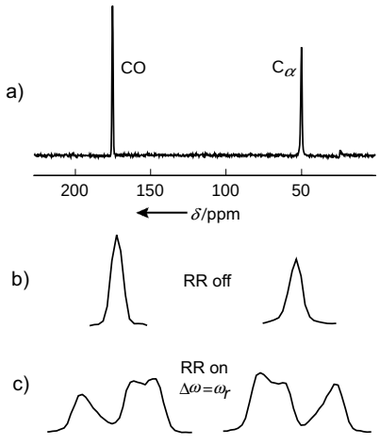

Figure 27. a) CP MAS NMR spectra (125 MHz) of uniformly ^{13}C-labeled (10%) glycine powder. The expansions show the two signals at rotor spinning speeds of 12 kHz (b; RR off) and of 16.6 kHz (c; RR on), which corresponds to the $n=1$ rotational resonance condition [Eq. (15)]. The signals are distorted as a result of the recoupling of H_{II}. (Courtesy of R. H. Havlin).

Distance measurements using RR are accomplished in a somewhat different manner than the recoupling techniques discussed so far. Figure 28 a shows a general pulse sequence for measuring $^{13}C-^{13}C$ homonuclear dipolar couplings by RR. The first step in RR is to set the spectrometer frequency to the resonance frequency of one of the two nuclei to be recoupled, and set the spinning speed so that it complies with the RR condition of Equation (15). Following the initial CP step, the

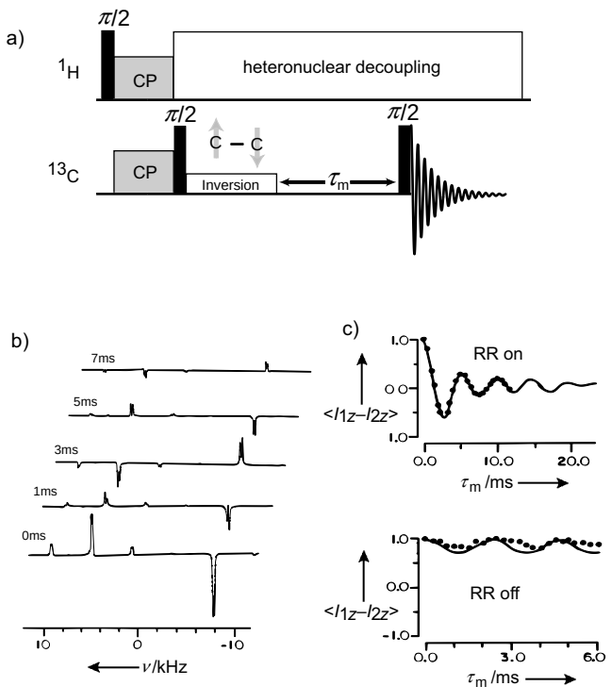

Figure 28. The RR experiment: a) Following ^1H CP, the ^{13}C magnetization is stored along the z axis and one of the resonances is inverted. The magnetization then decays for a period τ_m, before it is returned to the xy plane for detection. b) RR NMR spectra of doubly-^{13}C-labeled Zn acetate. As the mixing time τ_m increases, the ^{13}C nuclei have more time to exchange magnetization, to oscillate, and to decay back to equilibrium. C) The difference in the magnetization between the two peaks oscillates under RR conditions, but stays fairly constant just 100 Hz off the RR condition. (Adapted from ref. [124], with permission.)

^{13}C magnetization is returned to the z axis, at which point the magnetization of the on-resonance ^{13}C nuclei is inverted by using a long, low-power pulse. In the absence of any dipolar recoupling, the inverted ^{13}C nuclei slowly relax back to their equilibrium state. However, when the $^{13}C-^{13}C$ nuclei are recoupled by meeting the RR condition of Equation (15), they undergo energy-conserving flip-flop transitions, that is, the inverted spins flip up and the uninverted spins flop down. Often an oscillatory behavior of the magnetization is observed until the equilibrium is reached at which point the magnetization is equally distributed between the two spins. In Figure 28 b a series of ^{13}C RR spectra of a doubly ^{13}C-labeled Zn acetate is shown, acquired at different mixing times τ_m. By observing the oscillatory decay in the intensity of both peaks, it is possible to measure the magnitude of the dipolar coupling between the two ^{13}C sites and thereby determine the internuclear distance.

Especially in weakly enriched or unlabeled compounds with low natural abundance of the NMR-active isotopes (e.g. ^{13}C) it is difficult to observe the decaying signal that arises from a spin pair, as the bulk of the signal comes from isolated spins. To filter out these signals, a difference-spectroscopy technique can be employed.[125] Only the non-spin-pair magnetization survives long mixing times, and its spectrum can be subtracted from those acquired with shorter mixing times. An alternative and often cleaner approach is to employ

double-quantum filters to specifically select the signals from the spin pairs.[126, 127]

In addition to DRAMA and RR, a plethora of homonuclear recoupling sequences have been developed with acronyms such as HORROR,[128] DRAWS,[129] MELODRAMA,[130] BABA,[131] RFDR,[132] and C7.[133] Each of these sequences has certain strengths and weaknesses. The quality criteria for these sequences very much depend on the task at hand. They include broadband behavior, selectivity, robustness with respect to pulse errors, CSA dependence, sensitivity, scaling of the recoupled interaction, angular dependence of the recoupling in a powder, and the ability to filter spin pairs cleanly. A detailed evaluation of different homonuclear recoupling techniques is given by Baldus et al,[134] Dusold and Sebald,[135] as well as by Bennett, Griffin and Vega.[136] In this section, we have focused mainly on DRAMA and RR, merely because these were the first homonuclear recoupling techniques, and serve as instructive and illustrative examples (in much the same way as WAHUHA does for homonuclear decoupling). In practice, however, the most commonly used techniques seem to be RFDR,[132] C7,[133] and their variants. Continuous developments are underway in this field, and the advantages of a particular sequence over another is often difficult to rationalize theoretically. Recently, these sequences were classified according to certain symmetry principles, which helps to evaluate them and to choose the appropriate one for a particular application.[137] The value of these classification schemes cannot be underestimated, as they provide for the first time a uniform treatment of homo- and heteronuclear spin decoupling and recoupling under spinning conditions, ranging from simple CW decoupling and CP to more complicated experiments that involve RR as well as frequency-switched and phase-modulated sequences.[138]

4.2. Correlation Spectroscopy in the Solid State

We have discussed techniques that allow the reintroduction of the dipolar coupling for both homonuclear and heteronuclear systems and we have outlined how these techniques can be used to determine internuclear distances. In addition, the reintroduction of the dipolar coupling provides a magnetization exchange mechanism between spatially close nuclei that can be used for correlating their resonance frequencies in the same way as in liquid-state NMR techniques such as COSY, NOESY, or HMQC.[46, 55]

4.2.1. Heteronuclear Correlation Spectroscopy

The concept of heteronuclear correlation in solid-state NMR spectroscopy was introduced in Section 3 with a discussion of the $^{1}H-^{13}C$ HETCOR experiment. The relative simplicity of the HETCOR experiment is largely a consequence of the ability to transfer the polarization between nuclei using CP. When transferring the polarization between low-γ nuclei such as ^{13}C and ^{15}N, CP may become difficult to optimize as the $^{13}C-^{15}N$ dipolar coupling is effectively removed under MAS, even when the Hartmann–Hahn condition is specifically adjusted for rapid spinning.[139, 140] An alternative and often more robust means of producing heteronuclear dipolar correlation spectra is to utilize a REDOR-like recoupling (see Section 4.1) to exchange the magnetization between the ^{13}C and ^{15}N spins.[141]

Figure 29a shows a possible pulse sequence that produces a $^{13}C-^{15}N$ correlation spectrum in the solid state. The ^{13}C nuclei are first polarized through CP from the protons, after which a REDOR sequence is used to recouple the ^{13}C and ^{15}N nuclei. Following the REDOR sequence, the ^{15}N spins are allowed to evolve for a period t_1 (the indirect dimension), before a second REDOR sequence is used to return the magnetization to the ^{13}C spins for detection. Figures 29b, c show 2D $^{13}C-^{15}N$ correlation spectra of a solid sample of formyl-Met-Leu-Phe obtained with such a sequence (Figure 29a) by using different REDOR mixing times.[141] With short mixing times, the magnetization is transported over shorter distances, and the correlations are limited to neighboring atoms such as $N-C'$ and $N-C_\alpha$ (Figure 29b). However, when the spins are

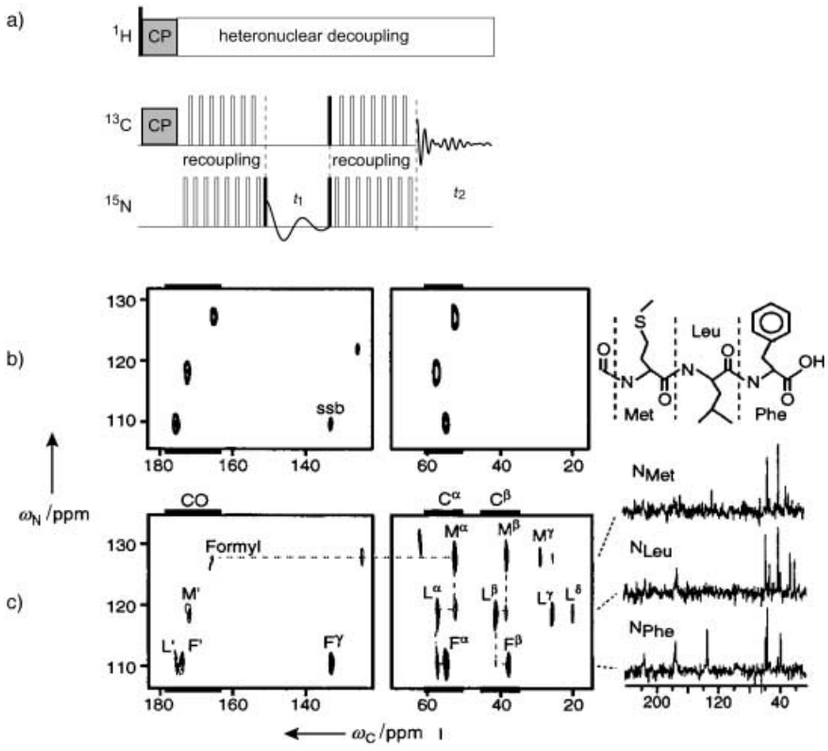

Figure 29. a) Heteronuclear correlation of ^{13}C and ^{15}N nuclei by dipolar recoupling. The modified REDOR pulse sequence incorporates pulses on the ^{13}C nuclei in addition to the standard pulses on the ^{15}N nuclei. b) 2D $^{13}C-^{15}N$ correlation spectrum of the tripeptide Formyl-Met-Leu-Phe obtained by using the pulse sequence in a). As a result of the short mixing time of 614.4 μs, the ^{13}C magnetization does not spread much further than one bond, giving rise only to $N-C'$ and $N-C_\alpha$ correlations. c) With a mixing time of 2.46 ms, the magnetization is transported further, thus permitting the observation of $N-C_\beta$ and $N-C_\gamma$ correlations. (Adapted from ref. [141], with permission.)

recoupled for longer periods (Figure 29c), the magnetization has more time to diffuse through the sample, thus leading to chemical shift correlations between more distant atoms (e.g. $N-C_\beta$ and $N-C_\gamma$). This REDOR-type technique has recently been shown to be very efficient in the heteronuclear magnetization transfer between ^1H and ^{13}C, and between ^1H and ^{15}N.[142, 143] In the latter case, even the reverse transfer from ^{15}N to ^1H has resulted in an improvement in sensitivity (analogous to inverse detection in liquid-state NMR spectroscopy.[46]

As indicated above, carefully optimized CP is another way of performing heteronuclear correlation experiments between low-γ nuclei and has been particularly effective with large magnetic fields. Remarkable $^{15}N-^{13}C$ correlation spectra have been collected to assign the resonances of uniformly labeled proteins and peptides in the solid state.[144–146]

4.2.2. Homonuclear Correlation Spectroscopy

Homonuclear 2D correlation spectra can be obtained in solids in a manner very similar to that used for heteronuclear correlations. Figure 30 outlines a general experimental procedure for a $^{13}C-^{13}C$ homonuclear dipolar coupling correlation experiment in the solid state. The sequence begins again with CP of the ^{13}C nuclei from the protons. The ^{13}C magnetization evolves during t_1, followed by a homonuclear recoupling sequence of the type introduced in Section 4.1 to recouple homonuclear dipolar coupling, thus allowing the transfer of magnetization between neighboring ^{13}C atoms. Finally, the ^{13}C magnetization is detected in the direct dimension t_2. Figure 31 shows a $^{13}C-^{13}C$ chemical shift correlation spectrum of uniformly-^{13}C-labeled erythromycin A obtained by using the sequence shown in Figure 30. In the experiment, the CMR7 method was used for ^{13}C homonuclear recoupling;[147] the method employs windowless rotor-synchronized π and 2π pulses. Resonance assignments become possible in uniformly and partially labeled proteins by using homonuclear correlation experiments of very high quality.[148–152] As in the heteronuclear correlation spectra of Figure 29b, c, the number of cross peaks in a homonuclear correlation spectrum can be controlled to some extent by the duration of the recoupling period. As the recoupling time increases, the magnetization diffuses further through the sample, thus leading to chemical shift correlations between an increasing number of spins. Many more variants of these experiments exist, including 3D correlation, double-quantum filtration, and double-quantum/single-quantum correlation experiments.[145, 153–155] This latter experiment has even been applied to protons for the investigation of the packing and dynamics of triphenylene and hexabenzocoronene derivatives.[156]

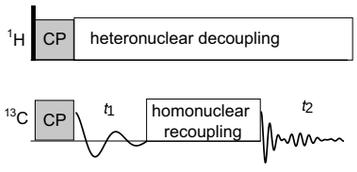

Figure 30. Typical pulse sequence for homonuclear correlation spectroscopy with dipolar recoupling. Once the ^{13}C magnetization has evolved in the indirect dimension, a homonuclear recoupling sequence is used to exchange magnetization between neighboring ^{13}C nuclear spins. The ^{13}C magnetization is then detected in the direct dimension.

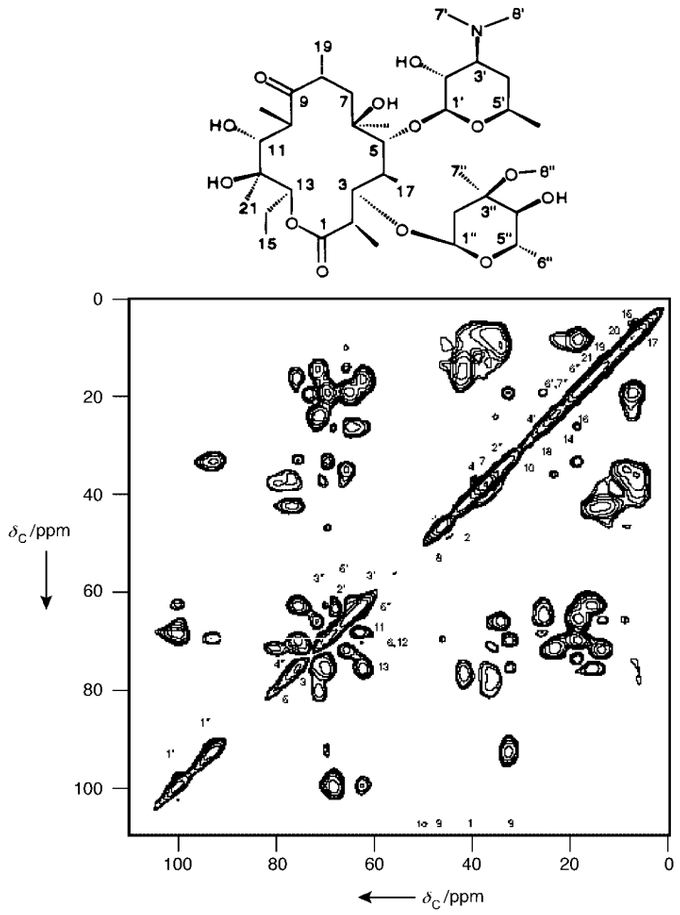

Figure 31. 2D $^{13}C-^{13}C$ correlation spectrum of uniformly ^{13}C-enriched erythromycin A. The spectrum was measured at a field of 9.4 T with a spinning speed of 8 kHz. A CMR-7 sequence was used to recouple the $^{13}C-^{13}C$ homonuclear dipolar coupling and create the $^{13}C-^{13}C$ correlations shown in the spectrum. (Reproduced from ref. [147], with permission.)

A pure recoupled double-quantum Hamiltonian can be used for spin-counting experiments under MAS (analogous to multiple-quantum spectroscopy in the static case discussed in Section 3.2.3).[157] In a related example, the time evolution of recoupled double-quantum coherences has been used to probe the torsion angles between different bonds.[158–160]

4.3. Recoupling away from the Magic Angle

Before leaving the topic of dipolar recoupling, we discuss a method to recouple H_{II} or H_{IS} effectively. As previously mentioned, it is not mechanically feasible to stop and restart the spinning sufficiently rapidly to reinstate the dipolar coupling under MAS. However, there is an alternative solution: as the dipolar coupling is fully removed only at the magic angle, if the axis of the spinning rotor is rotated at another angle (e.g., 0°, parallel to the external magnetic field)

the dipolar coupling emerges. The sample can then be returned to the magic angle for detection. This technique is known as switched-angle spinning or SAS.[161] Figure 32 shows a SAS spectrum of doubly ^{13}C-labeled zinc acetate in which

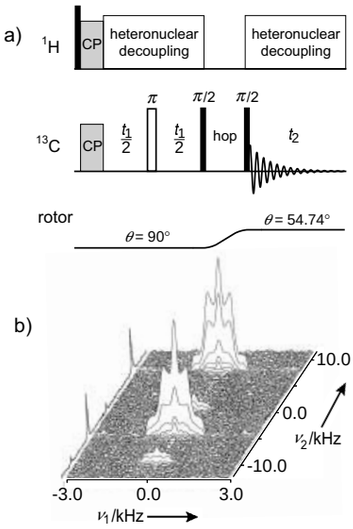

Figure 32. a) Pulse sequence for SAS. The experiment begins with the rotor oriented 90° relative to the external magnetic field. After the magnetization is excited by a CP sequence, the $^{13}C-^{13}C$ homonuclear dipolar coupling is detected in t_1 using a π pulse to refocus the CSA. A $\pi/2$ pulse stores the magnetization along the z axis while the rotor axis is reoriented at the magic angle, at which point a second $\pi/2$ pulse returns the magnetization to the xy plane for detection in t_2. b) 2D SAS NMR spectrum of uniformly 1,2-^{13}C labeled (10%) zinc acetate. The $^{13}C-^{13}C$ homonuclear dipolar coupling (displayed along the ν_1 axis) is attenuated by a factor of two because of the orientation of the rotor during t_1. ν_2 is the (isotropic) chemical shift dimension. (Reproduced from ref. [161], with permission.)

the $^{13}C-^{13}C$ homonuclear dipolar couplings are recoupled. If the rotor is oriented along B_0 during t_1, the recoupling efficiency is 100%. Mechanical difficulties with sudden changes in angle as well as difficulties in detecting the magnetization in this orientation make the perpendicular alignment of the rotor axis more practical. However, the efficiency in this case is only 50%. Spinning at different angles can also be used to reintroduce the CSA, and to perform isotropic/anisotropic correlation spectroscopy with quadrupolar nuclei. Although this approach requires the use of specialized probes and is mechanically very demanding, from a conceptual point of view these techniques offer significantly more degrees of freedom than spinning around a single axis.[162] This fact is the driving force behind many new hardware and application developments in this field.

4.4. Reintroduction of the Chemical-Shift Anisotropy

Figure 5 showed a ^{13}C static carbon spectrum of glycine obtained with heteronuclear spin decoupling. The spectrum has two broad lines that correspond to the CSA of the α- and carbonyl carbon atoms. The two signals are the direct result of the electronic structure around the nuclei, and thus contain a wealth of localized information about the structure, dynamics, and orientation of the nucleus with respect to its surrounding atoms. For example, the CSA for the α carbon atom of most amino acids in proteins and peptides depends on the secondary structure (α-helix versus β-sheet),[163, 164] as shown in Figure 33 for valine.

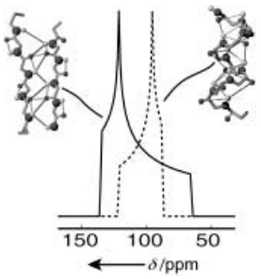

Figure 33. Simulated static spectra of the α-carbon atom of a L-valine residue in a peptide or protein. The shape of the α-carbon CSA depends strongly on whether the residue is located within an α-helix (- - - -) or a β-sheet (——).

Although the measurement of CSA signals from static solid-state NMR spectra is possible in singly and some doubly labeled samples, it is generally not feasible in multispin systems, which result in overlapping CSA powder patterns. Furthermore, static spectra typically require extensive signal averaging to obtain the signal intensity and resolution required to determine the CSA signal. In the following section we describe techniques that combine the high resolution of a MAS experiment with the anisotropic information content available from a static sample, and therefore represent powerful demonstrations of the potential of solid-state NMR spectroscopy.

4.4.1. Spinning-Sideband Analysis

Figure 8 showed a series of MAS spectra taken at different spinning speeds. With a decrease in the spinning speed, an increasing number of spinning sidebands appear in the spectrum as a result of incomplete motional averaging of the CSA by the rotation. As the spinning speed approaches zero, the envelope of the spinning sidebands takes on the shape of the static powder pattern shown in Figure 8e. Indeed, the intensities of the spinning sidebands contain information about the CSA, and through an appropriate analysis one can determine the three CSA parameters, δ_{11}, δ_{22}, and δ_{33}. The Herzfeld–Berger[45] method uses a series of precalculated surfaces to determine δ_{11}, δ_{22}, and δ_{33} from the integrated intensities of a number of spinning sidebands. The method is conceptually straightforward and not technically demanding, requiring only the acquisition of a 1D MAS spectrum. By taking spectra at different spinning speeds and averaging the values of δ_{11}, δ_{22}, and δ_{33} determined from the Herzfeld–Berger surfaces, the accuracy of the method can be further enhanced. Figure 34 shows a spectrum of ^{15}N-labeled adenosine monophosphate (AMP) acquired at a MAS speed of 1105 Hz. The spinning speed for the spectrum in Figure 34 was chosen specifically to minimize sideband overlap, thus allowing the determination of the CSAs of all five ^{15}N AMP sites by using the Herzfeld–Berger method.

Under circumstances in which the spectra are too crowded with sidebands to resolve the CSAs by this method, it is advantageous to use 2D NMR spectroscopy to spread the overlapping CSA patterns across a second dimension. A powerful technique for this is PASS (phase-adjusted spinning sidebands), which allows one to separate spinning-sideband

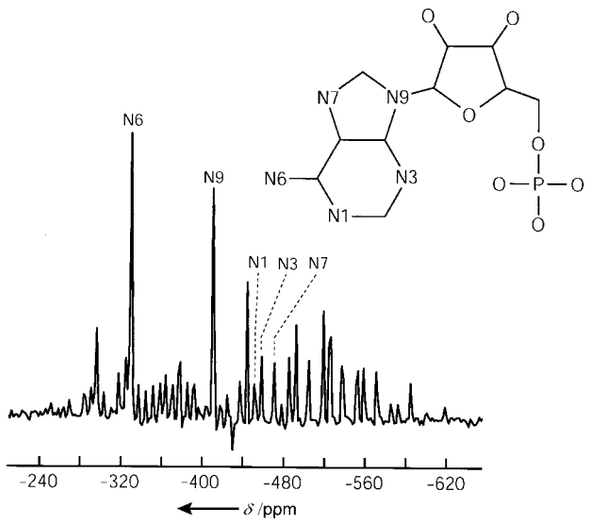

Figure 34. Slow-spinning CP MAS NMR spectrum of uniformly ^{15}N labeled adenosine monophosphate (AMP) obtained at a spinning speed of 1105 Hz. Because the sidebands are spaced at integer multiples of the spinning speed, the identity of each sideband can be ascertained based on its distance from any one of the five isotropic peaks (which are found by spinning at high speed). By fitting all of the sideband intensities (or integrals), the principal values of the CSA for each ^{15}N site were determined.

manifolds in a second dimension.[165, 166] A series of pulse sequences have been developed which allow one to manipulate sideband manifolds for various purposes, including the removal of spinning sidebands[167] and 3D experiments.[168] The many variants of these techniques are described in an excellent review article.[169] In the ODESSA experiment (one-dimensional exchange spectroscopy by sideband alternation), the magnetization associated with different spinning sidebands is polarized in alternate directions during the preparation period. Dynamic processes that redistribute the magnetization can be characterized by analyzing the sidebands from spectra acquired at different times after the preparation period. Exchange processes between chemically equivalent and non-equivalent nuclei have been determined in this way.[170, 171] Even regular 1D MAS in combination with a sideband analysis has been used to obtain evidence of otherwise invisible processes, such as bond rearrangements.[172]

4.4.2. Anisotropic-Isotropic Chemical Shift Correlation

Although slow-spinning MAS is an excellent way to determine the chemical shift anisotropy of a nucleus in the solid state, the method does not *really* reintroduce the CSA. Instead, this method takes advantage of the incomplete averaging of the CSA that occurs when the rotation frequency is smaller than the width of the CSA. It would be useful to observe a "static-like" powder pattern under fast MAS in a manner analogous to that used for dipolar recoupling. This would allow one to observe broad anisotropic peaks in one dimension and isotropic peaks in the directly detected dimension in a 2D NMR experiment.

The evolution of the CSA under MAS is very similar to that of the heteronuclear dipolar coupling. Therefore, a technique similar to REDOR, which applies two π pulses per rotor period effectively reintroduces the CSA under MAS. Although a two-pulse technique does work,[173] the resulting powder patterns tend to be distorted. An improved method by Tycko et al.[174] utilizes four π pulses per rotor period to reintroduce the CSA with very little distortion of the signal (Figure 35). By incorporating the 4-π-pulse sequence into the

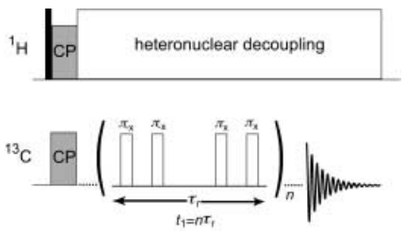

Figure 35. Pulse sequence for recoupling the CSA. τ_r = Rotor period.

indirect detection period of a 2D NMR experiment, it is possible to produce a spectrum that correlates the broad CSA signal in one dimension with the isotropic MAS spectrum in the other dimension. Figure 36 shows a series of CSA patterns from six of the seven ^{13}C sites in methyl-α-D-glucopyranoside. The spectrum was obtained by using the 4-π-pulse technique to reintroduce the CSA under MAS conditions. Below each experimentally obtained spectrum, a simulated best-fit CSA signal is shown.

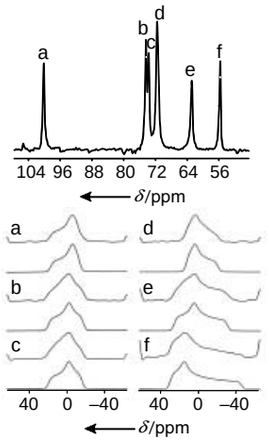

Figure 36. Isotropic ^{13}C NMR spectrum and CSA signals for six carbon atoms (a–f) in methyl-α-D-glucopyranoside obtained by using the 4-π-pulse technique. Best-fit simulations are shown below each experimentally obtained signal. (Reproduced from ref. [174], with permission.)

In addition to the 4-π-pulse method, a variety of other techniques that do not involve traditional pulsed recoupling have been developed to correlate the anisotropic and isotropic components of the chemical shift. Among these techniques are magic-angle hopping (MAH),[175] magic-angle turning (MAT),[176, 177] and variable-angle correlation spectroscopy (VACSY).[178, 179] The MAT experiment uses $\pi/2$ pulses to interrupt the chemical shift evolution during t_1 at 0, 120, and 270° of the MAS rotor position. The MAH pulse sequence is very similar, but uses rapid hops of the crystal axis around the magic-angle axis to align the former first with the x, then with the y, then with the z axis. After the magnetization has evolved in all three arrangements, the space appears isotropic (as is the case under MAS conditions), the CSA is removed, and a purely isotropic spectroscopic dimension is obtained.

The spinning speeds employed in MAT are usually low (< 1 kHz), and therefore the directly detected dimension

contains a wealth of spinning sidebands that form the anisotropic dimension. The recently improved MAT technique called FIREMAT achieves higher sensitivity; and an isotropic/anisotropic correlation spectrum is shown for erythromycin A in Figure 37.[180]

Figure 38 shows a 2D isotropic/anisotropic correlation spectrum of L-tyrosine · HCl produced with the VACSY method. In this experiment, the demands on hardware are lower than for the SAS experiment mentioned previously, as the spinning angle is only gradually changed between different 1D experiments (within seconds), rather than during the experiment (within a few milliseconds). Nevertheless, the same comment as at the end of Section 4.4 applies: although MAH, MAT, and VACSY all have definite advantages over slow-spinning MAS or the 4-π-pulse sequence, they are technologically more difficult to implement, and require specialized hardware. Since these methods are potentially more versatile, further developments in hardware can be expected.

4.5. *J* Coupling

As a final note in this section, we briefly introduce a Hamiltonian that has not yet played a role in this Review, the *J*-coupling Hamiltonian. In some instances, the signals in solid-state NMR specta can be made sufficiently narrow by MAS so that *J* coupling can be exploited for correlation spectroscopy (e.g. COSY and INADEQUATE) in much the same way as in liquid-state NMR spectroscopy.[117, 181–183] The *J* coupling exhibits no spatial orientation dependence, and is therefore not averaged out under MAS (we neglect here the anisotropic *J*-coupling contribution, which has a form similar to the dipolar coupling and is therefore removed by MAS).[184] In general, however, very strong dipolar coupling from abundant nuclei make the MAS approach impractical to reveal *J* coupling. Recent technological breakthroughs such as high-speed MAS and high-power proton homo- and heteronuclear decoupling has made it possible to observe and utilize *J* coupling in polycrystalline samples. Figure 39 shows an INADEQUATE spectrum[185] of a solid sample of L-tyrosine · HCl acquired under MAS with high-power homonuclear proton decoupling. This experiment has also been carried out on disordered solids.[186] High-power proton homodecoupling sequences have been described which use heteronuclear *J* couplings in solids, anal-

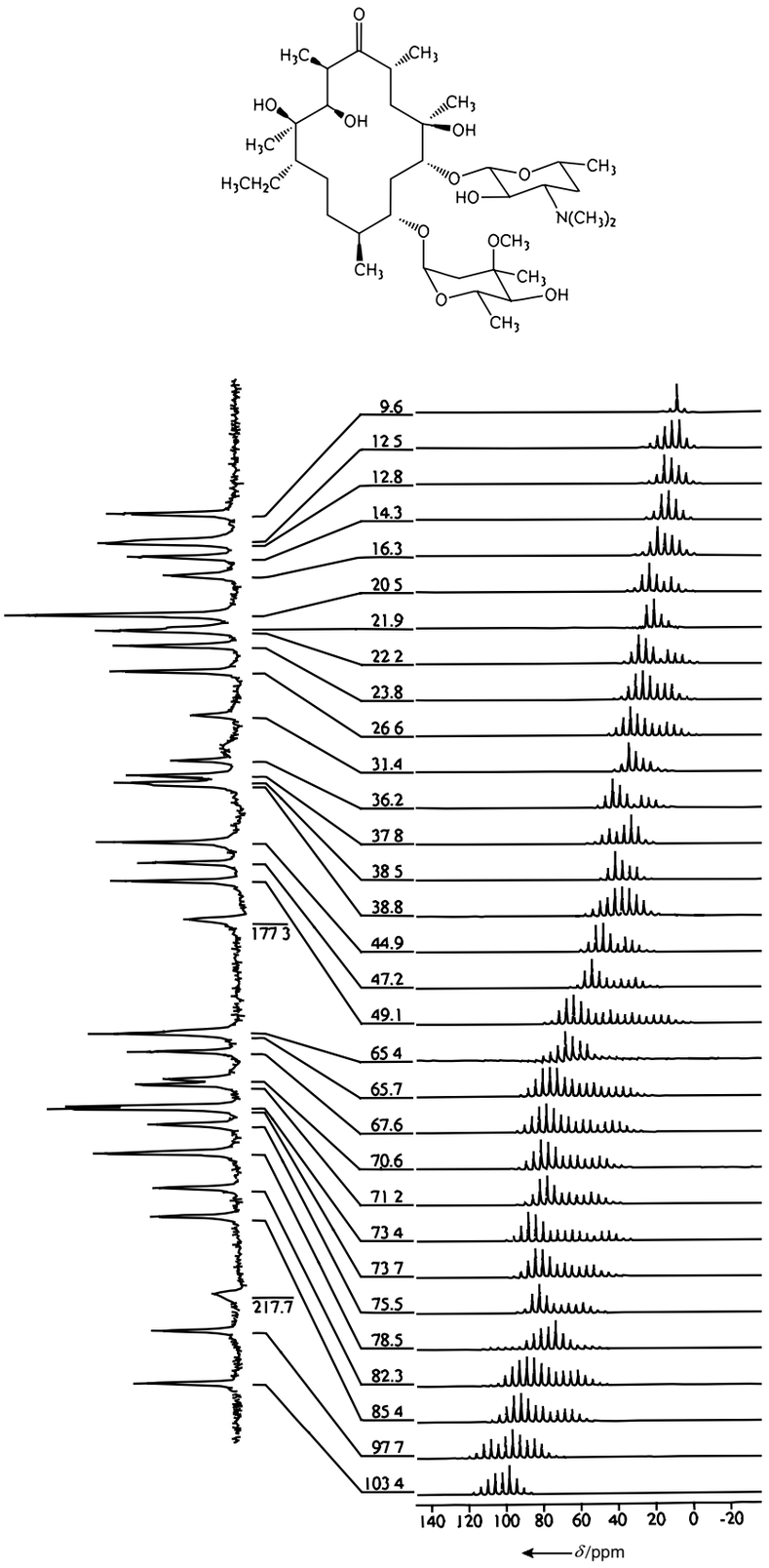

Figure 37. Isotropic chemical shift – CSA correlation spectrum of erythromycin A measured with the FIREMAT technique.[180] The slow MAS speed of 390 Hz produces a spinning-sideband pattern that closely resembles a CSA powder signal in the directly observed dimension. A multipulse sequence in the indirect dimension in combination with a special processing method produces isotropic lines.

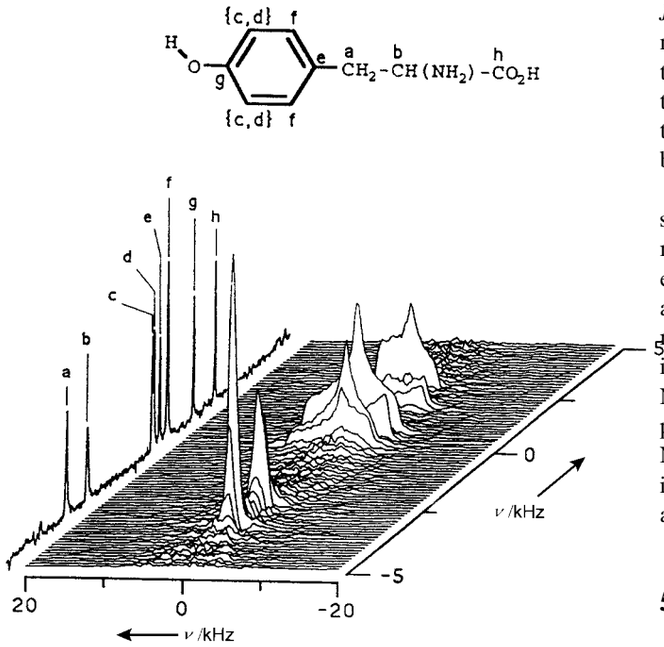

Figure 38. 2D NMR correlation spectrum of the isotropic/anisotropic chemical shifts of L-tyrosine measured with VACSY. The isotropic projection is shown with the assignment of the peaks. (Reproduced from ref. [178], with permission.)

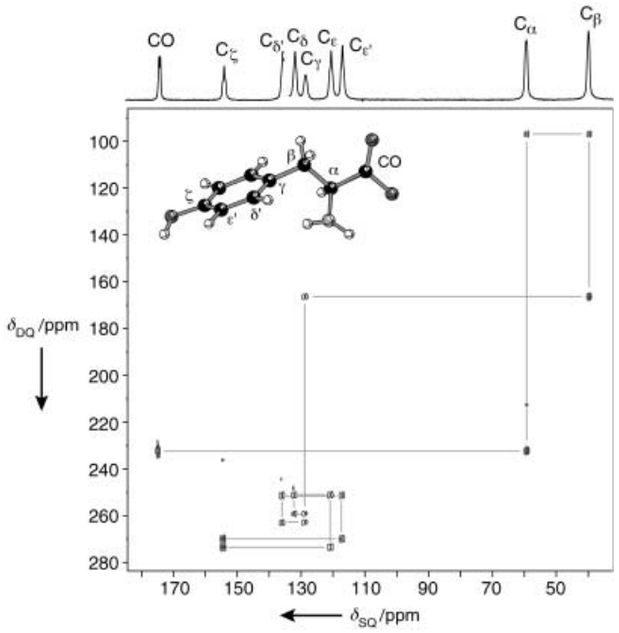

Figure 39. Solid-state 2D INADEQUATE NMR spectrum (125 MHz) of fully ^{13}C-labeled L-tyrosine · HCl. δ_{SQ} and δ_{DQ} are the single-quantum and the double-quantum frequencies, respectively, expressed in ppm. δ_{DQ} is the sum of the chemical shifts of the two correlated carbon atoms. The spinning speed was 22 kHz, and the ^{1}H decoupling field strength was 120 kHz. (Reproduced from ref. [43], with permission.)

ogous to the liquid-state HMQC experiment.[79, 187] In a different experiment, a specifically designed pulse sequence was used during the mixing period of the sequence of Figure 30 to eliminate all interactions except for the isotropic *J*-coupling interaction. In this way, 2D through-bond homonuclear correlation spectra have been obtained.[188–190] These techniques provide a convenient additional and complementary assignment tool, as they only indicate intramolecular through-bond coupling, as opposed to assignment strategies based on dipolar-coupling approaches.

In Sections 2 and 3, we discussed the interactions in solid-state NMR spectroscopy that prevent the acquisition of high-resolution NMR spectra as well as ways to counteract the effects of these interactions. Although dipolar coupling, CSA, and quadrupolar coupling (see Section 5) result in poorer resolution in the spectra, they contain useful structural information that is often difficult to obtain from liquid-state NMR spectroscopy. The techniques presented in this section provide a means to combine the advantages of high-resolution NMR spectroscopy with the ability to extract structural information contained in anisotropic interactions such as CSA and dipolar coupling.

5. Quadrupolar Nuclei

So far, our discussion of solid-state NMR spectroscopy has been restricted to spin ½ nuclei such as ^{1}H, ^{13}C, ^{15}N, ^{31}P, and ^{29}Si. We now extend our survey of solid-state NMR spectroscopy to include the majority of isotopes found in the periodic table, that is, those with spin $I > ½$. Although these quadrupolar nuclei possess the same set of basic interactions that were introduced in Section 2 (e.g. the CSA, dipolar coupling, etc.), there are two principal differences between spin ½ nuclei and those with spin $I > ½$: 1) For quadrupolar nuclei, the allowed values of the nuclear spin quantum number m_I are no longer simply $+½$ and $-½$. For a spin 1 nucleus (e.g. ^{2}H and ^{14}N), the allowed values for m_I are -1, 0, and $+1$; thus, in the presence of an external magnetic field, spin 1 nuclei have three energy levels and two transitions. Likewise, a spin ⅜ nucleus (e.g. ^{23}Na and ^{87}Rb) has four spins states with $m_I = -⅜, -½, ½$, and ⅜. In general, there are $2I+1$ spin states and $2I$ directly detectable transitions. 2) Quadrupolar nuclei possess a nonspherical charge distribution that can couple to electric-field gradients present in most solid-state materials.[191] This quadrupolar coupling has an enormous effect on the observed NMR spectrum (as seen below).

5.1. Spin 1 Nuclei

Although spin 1 nuclei are much more rare than half-integer quadrupolar nuclei, the literature on spin 1 nuclei is extensive, mainly because of the usefulness of deuterium (^{2}H) in NMR spectroscopy.[22, 192–194] Based on its small electron cloud and relatively low gyromagnetic ratio ($\sim$⅐ that of ^{1}H), and consequently a small chemical shift range of $\sim 3-4$ ppm and relatively weak dipolar couplings, one might expect static ^{2}H NMR line widths to be narrow. Thus, it may be somewhat surprising to learn that static ^{2}H NMR line widths routinely exceed 100 kHz, as shown in the spectrum of CDI_3 in Figure 40. Quadrupolar interactions are at the origin of this very broad line.

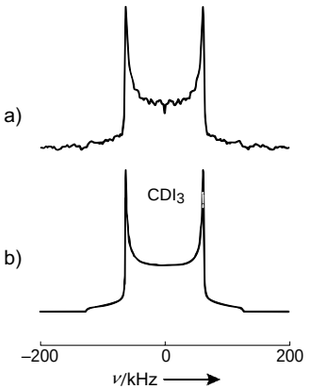

Figure 40. Static ^{2}H NMR spectrum of CDI_3: a) experimentally obtained spectrum; b) simulated spectrum based on the quadrupolar coupling constant derived from the spectrum in a); The qaudrupolar coupling frequency, ν_Q was determined to be 167.5 kHz, and the anisotropy η to be 0. (Adapted from ref. [257], with permission.)

To understand the ^{2}H quadrupolar signal displayed in Figure 40, it is helpful to examine the effect of the quadrupolar coupling on the ^{2}H Zeeman energy levels. In Figure 41 a, we show the energy levels of a spin 1 nucleus in an

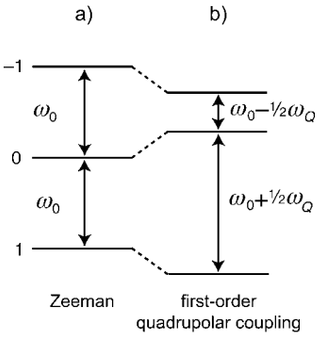

Figure 41. Energy-level diagram for spin 1 nuclei subject to a) the Zeeman interaction and b) to both the Zeeman and the first-order quadrupolar interactions. The splitting shown in b) is a result of the first-order quadrupolar coupling at one particular crystal orientation.

external magnetic field with no quadrupolar coupling present. Both the $-1 \rightarrow 0$ and $0 \rightarrow +1$ transitions have the same resonance frequency as the energy differences between the spin states are identical. Figure 41 b shows the same three energy levels under the influence of the first-order quadrupolar Hamiltonian $H_Q^{(1)}$ (the term "first order" is explained later). Whereas the $m_I = -1$ and the $m_I = +1$ spin states decrease in energy upon the addition of $H_Q^{(1)}$, the $m_I = 0$ spin state increases in energy. As a result, the $-1 \rightarrow 0$ and the $0 \rightarrow +1$ transitions differ in energy, and therefore resonate at two different frequencies. The difference between the frequencies is proportional to the first-order quadrupolar coupling constant ω_Q [Eq. (16)].

$$\omega_Q = \frac{3eq\,eQ}{2I\,(2I-1)\hbar} \tag{16}$$

In Equation (16), e is the electron charge, eq is the z component of the electric field gradient felt at the nucleus, and Q is the nuclear electric quadrupole moment. The constant Q is a nuclear property (like γ) that describes the strength with which a quadrupolar nucleus couples to an electric-field gradient at the nucleus. For example, deuterium has a relatively small nuclear electric quadrupole moment ($Q = 3 \times 10^{-31}$ m^2), and typically quadrupolar coupling constants are on the order of 100 – 300 kHz.[192] On the other hand, $Q = 2 \times 10^{-30}$ m^2 for ^{14}N (spin 1), and typical quadrupolar coupling constants are $\sim$10 times higher (1 – 5 MHz). The origin of the nuclear electric quadrupole moment (an asymmetric charge distribution) is simply the fact that a nucleus of uniform shape does not necessarily have a symmetric charge distribution, depending on the number of protons and neutrons. Under the influence of the electrostatic interaction, the nucleus arranges itself within an asymmetric electron cloud, which in turn influences the NMR-active energy transitions.

As is also seen in Figure 41 b, the effect of the first-order quadrupolar coupling is to produce a quadrupolar splitting whose magnitude is dictated by ω_Q. However, in Figure 40, we see not only a splitting, but rather a signal that strongly resembles the dipolar Pake pattern shown in Figure 4. This is because the splitting caused by the first-order quadrupolar coupling depends on the orientation of the molecule with respect to the magnetic field (in the same way as the CSA and, in the case of cylindrical symmetry, the dipolar coupling; for ^{2}H, this is very often a good approximation because of the axially symmetrical C–H bonds). Therefore, just as the width of the Pake pattern of Figure 4 was an exact measure of the dipolar coupling constant d, the width of the ^{2}H Pake pattern is a measure of the quadrupolar coupling constant ω_Q.

Since the orientational dependence of the first-order quadrupolar coupling is the same as for the CSA it comes as no surprise that this coupling can (in principle) be eliminated by MAS. This is exactly the case in Figure 42 a, which shows a static ^{2}H NMR spectrum of a mixture of deuterated hexamethylbenzene and deuterated ferrocene; the spectrum consists of two overlapping Pake patterns, which correspond to the two deuterium environments. MAS (Figure 42 b) results in the quadrupolar line width being reduced to a series of spinning sidebands; upon closer inspection of the residual isotropic signals, it is possible to discern the isotropic chemical shifts of the two ^{2}H sites. For completeness, we mention that the first high-resolution ^{2}H NMR spectrum of a solid was obtained by exciting the double-quantum transition between the $m_I = -1$ and $+1$ states and measuring it indirectly.[195] As seen in Figure 41 b the energy splitting between these two states is not affected by the first-order quadrupolar coupling, and is therefore independent of the orientation of the principal axes of the quadrupolar interaction. Incidentally, this transition was also successfully exploited for "double-quantum decoupling" of ^{2}H from ^{1}H nuclei. This method was used to acquire early high-resolution ^{1}H NMR spectra of partly deuterated solids.[196]

Although MAS can be quite effective in reducing the deuterium quadrupolar line width, ^{2}H NMR is often performed on static samples. The reasons for this choice are threefold: 1) In contrast to the vast amount of time necessary to acquire a static spectrum of a spin ½ nucleus, a static

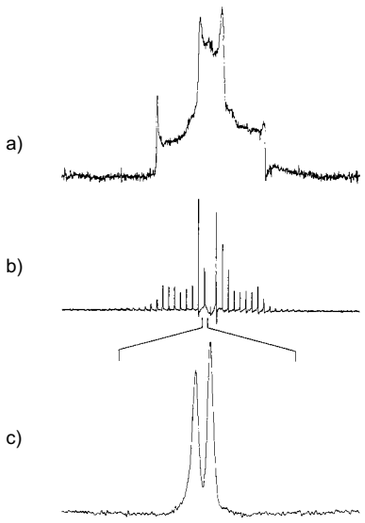

Figure 42. ^{2}H NMR spectra of a solid mixture of deuterated ferrocene and deuterated hexamethylbenzene, under: a) static conditions, b) magic-angle spinning. c) Expansion of the center band of b), which shows two resonances corresponding to the two deuterium sites. (Adapted from ref. [258], with permission.)

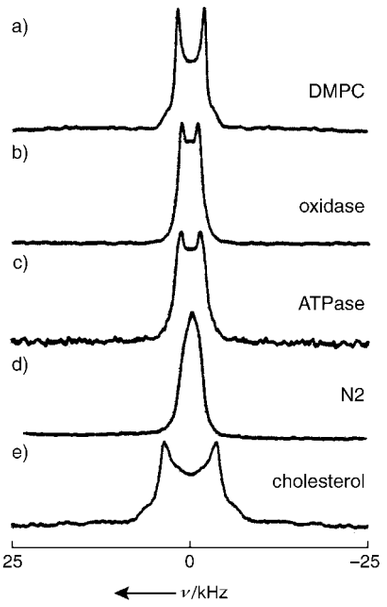

Figure 43. ^{2}H NMR spectra of [D_3]DMPC in the presence of various additives: a) excess water (30 °C); b) cytochrome c oxidase (67 wt %); c) sarcoplasmic reticulum adenosinetriphosphatase (67 wt %); d) beef brain myelin proteolipid apoprotein (N2; 67 wt %); e) cholesterol (33 wt %). [D_3]DMPC = 1-myristoyl-2(14,14,14-trideutero)myristoyl-*sn*-glycero-3-phosphocholine. (Adapted from ref. [197], with permission.)

quadrupolar spectrum can be obtained more rapidly because the quadrupolar coupling greatly facilitates the relaxation of quadrupolar nuclei, thus reducing the time required for the magnetization to relax back to thermal equilibrium. 2) The ^{2}H quadrupolar coupling is a sensitive measure of internal molecular motion.[193, 197] As the quadrupolar coupling depends on the molecular orientation with respect to the magnetic field, a reorientation of the molecule reduces the width and shape of a static ^{2}H resonance line. Figure 43 shows a series of ^{2}H NMR spectra of deuterated DMPC in a lipid bilayer. By adding different species to the bilayer (such as cholesterol or cytochrome c oxidase) it is possible to alter the mobility of the deuterated hydrophobic lipid tails. The narrow quadrupolar signals in Figure 43 b – d indicate that the added compounds increase the mobility of the lipid tails, whereas the addition of cholesterol to the bilayer (Figure 43 e) decreases the lipid mobility. 3) Static ^{2}H NMR spectroscopy is also a powerful tool for studying molecular orientation and order.[192, 198, 199] Solid-state ^{2}H NMR spectroscopy has also been shown to be an excellent probe for paramagnetic reaction centers in proteins.[200, 201]

Figure 44 a shows the sequence for a 2D exchange experiment. The spins are allowed to evolve with their characteristic resonance frequencies during t_1. Another $\pi/2$ pulse stores the magnetization along the z direction. During the mixing time τ_m, the nuclei may reorient or chemically exchange, and after the final $\pi/2$ pulse the spins evolve with either the same or—if exchange occurred—a different resonance frequency. In the absence of exchange, a 2D spectrum acquired in this way will display the quadrupolar Pake pattern along its diagonal (similar to that shown in Figure 40). If reorientation occurred during τ_m, the resonance frequency of a particular spin changes to some new location in the Pake pattern, and off-diagonal peaks start to appear (Figure 44 b). In this example,

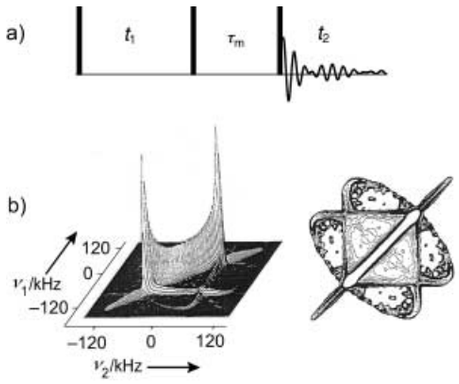

Figure 44. a) Pulse sequence for 2D exchange experiments, equally applicable to spin ½ and spin 1 nuclei. b) Left: 2D exchange spectrum of α-poly(vinylidene fluoride) at 370 K (τ_m = 200 ms); right: contour plot of the spectrum. (Adapted from ref. [202], with permission).

reorientation angle distributions were determined for the C – ^{2}H moieties in α-poly(vinylidene fluoride).[202]

Spin ½ nuclei have also been extensively studied by 2D exchange experiments: exchange and reorientation processes as well as local order have been investigated by correlating CSA and dipolar powder patterns with pulse sequences of the basic type shown in Figure 44 a.[54, 203, 204] Further modifications of these techniques include improved exchange experiments for spinning samples[205] and variable spinning-angle exchange experiments.[206]

Thus far, our discussion has been limited to ^{2}H NMR spectroscopy. The value of ω_Q for the deuterium nucleus is much smaller than that of other quadrupolar nuclei, and for this reason we have not alluded to the existence of a second,

more complex quadrupolar term—the second-order quadrupolar coupling. In every ^{2}H spectrum that was shown above, the second-order quadrupolar coupling was present, but relatively small in size. When the quadrupolar coupling is very large, as it is for ^{14}N, the second-order quadrupolar coupling can have a significant effect on the observed signal. Figure 45 shows the effect of the second-order quadrupolar coupling on the energy levels of spin 1 and spin ½ nuclei, which causes an additional asymmetric line broadening. As we will show in Section 5.2, even when the first-order quadrupolar coupling is completely removed, the second-order quadrupolar Hamiltonian can still be large enough to make the spectrum uninterpretable.

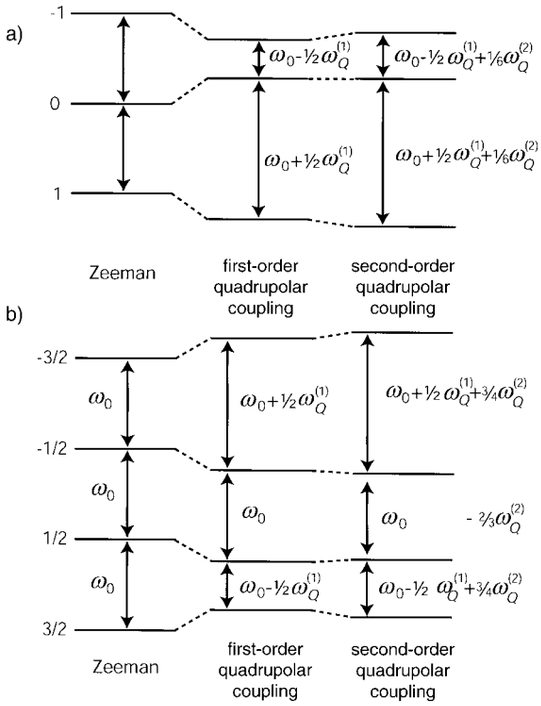

Figure 45. Effect of the Zeeman splitting and first- and second-order quadrupolar coupling on the energy levels of a) spin 1 and b) spin 3/2 nuclei.

5.2. Nuclei with Spin $I > 1$

With the exception of ^{10}B ($I = 3$), ^{50}V ($I = 6$), and ^{177}Lu ($I = 7$), all nuclei with spin $I > 1$ are half-integer quadrupolar nuclei. Nuclei with half-integer spins behave quite differently from nuclei with integer spins. The reason for this difference is made clear by examining the effect that the quadrupolar Hamiltonian has on the energy levels of a half-integer quadrupolar nucleus. Figure 45 b shows the energy levels for a spin ½ nucleus a) without any quadrupolar coupling, b) under the influence of the first order quadrupolar coupling, and c) including the second-order quadrupolar coupling. The first-order quadrupolar Hamiltonian shifts the $m_I = -½$ and the $m_I = ½$ energy levels by the same amount in the same direction. Thus, the resonance frequency of the $-½ \rightarrow +½$ transition, known as the central transition, is unchanged by the first-order quadrupolar Hamiltonian. In contrast, the resonance frequencies of the $-3/2 \rightarrow -½$ and $+½ \rightarrow 3/2$ transitions, known as the satellite transitions, are each shifted by an amount proportional to $\omega_Q^{(1)}$, the first-order quadrupolar coupling constant. The net result of $H_Q^{(1)}$ on a half-integer quadrupolar nucleus is to shift and broaden (in a powdered solid) the resonances that result from the satellite transitions substantially. Therefore, in a standard solid-state NMR experiment performed at the frequency of the central transition, the satellite transitions are seldom observed.[207] Yet, because the central transition is still broadened by the *second-order* quadrupolar coupling, the resulting line width can be quite large, as seen in the solid-state ^{23}Na NMR spectrum of sodium oxalate in Figure 46 b. In some cases, the second-order signal is impossible to detect by traditional methods.[208]

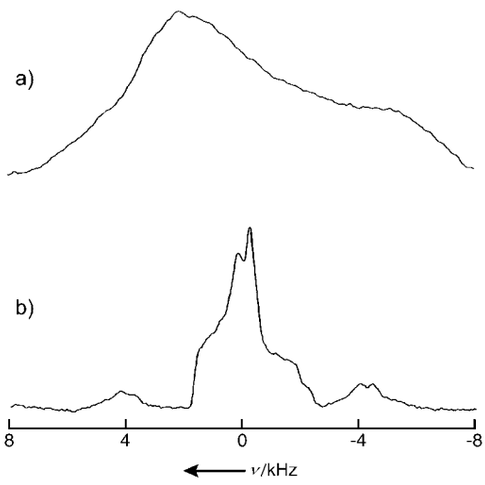

Figure 46. Solid-state ^{23}Na NMR spectrum (105 MHz) of sodium oxalate acquired a) without any sample spinning, and b) with spinning at 4 kHz at the magic angle. (Adapted from ref. [213], with permission.)

A full mathematical description of the second-order quadrupolar Hamiltonian $H_Q^{(2)}$ can be found in the literature.[207, 209, 210] Here, we just point out two important features of $H_Q^{(2)}$ that are relevant to the study of half-integer quadrupolar nuclei by solid-state NMR spectroscopy. First, $H_Q^{(2)}$ has associated with it a coupling constant $\omega_Q^{(2)}$ [Eq. (17), ω_0 = Larmor frequency].

$$\omega_Q^{(2)} = \frac{(\omega_Q^{(1)})^2}{2\omega_0} \tag{17}$$

From Equation (17) it becomes clear why the effects of the second-order quadrupolar coupling are rarely observed in ^{2}H NMR spectroscopy. Even if $\omega_Q^{(1)}$ is as large as 300 kHz, the magnitude of $\omega_Q^{(2)}$ in a 2.3-T magnetic field is only $\sim$3 kHz. Equation (17) also provides a major motivation for studying quadrupolar nuclei at high fields: the size of $\omega_Q^{(2)}$ can always be decreased by increasing B_0.

Another important feature of the second-order quadrupolar Hamiltonian $H_Q^{(2)}$ is its orientation dependence, which is more complicated than that of the first-order Hamiltonians $H_Q^{(1)}$ addressed thus far. There are three orientational terms associated with $H_Q^{(2)}$; these terms correspond mathematically

to the zeroth- [Eq. (18)], second- [Eq. (19)], and fourth-order [Eq. (20)] Legendre polynomials:[162, 211]

$$P_0(\cos\theta) = 1 \quad (18)$$

$$P_2(\cos\theta) = -\tfrac{1}{2}(3\cos^2\theta - 1) \quad (19)$$

$$P_4(\cos\theta) = \tfrac{1}{8}(3 - 30\cos^2\theta + 35\cos^4\theta) \quad (20)$$

Although these equations are appropriate only for axially symmetric quadrupolar couplings, the following qualitative discussion is equally applicable to the general case. The zeroeth-order term is a scalar, and just like the isotropic component of the chemical shift, is not dependent on θ. Indeed, one of the effects of the second-order quadrupolar coupling is to produce an isotropic quadrupolar shift that cannot be removed. This shift is also observed in liquids in which molecular reorientation is not too rapid.[212] The second-order term of $H_Q^{(2)}$ is dependent on $(3\cos^2\theta - 1)$ and can therefore be removed by MAS. Figure 46 shows ^{23}Na NMR spectra of solid polycrystalline sodium oxalate; the spectra were obtained with (Figure 46b) and without MAS (Figure 46a). Although there is some narrowing, the effect is not nearly as dramatic as that of spin ½ nuclei. The primary reason that the line broadening does not disappear with rotation at the magic angle is that the terms $P_2(\cos\theta)$ and $P_4(\cos\theta)$ equal zero at different values of θ (Figure 47). Therefore, to remove the second-order quadrupolar coupling and produce a narrow line, a technique other than MAS must be employed. For many years, research in high-resolution solid-state NMR spectroscopy was focused on this challenge.

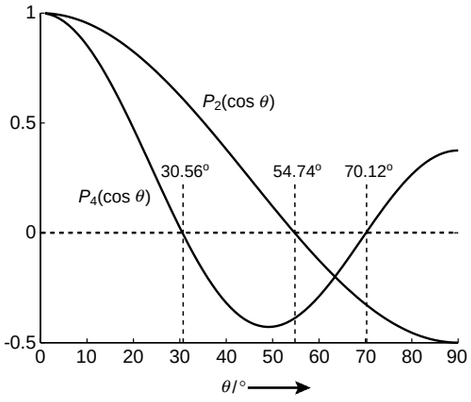

Figure 47. Plot of the second- and fourth-order Legendre polynomials $P_2(\cos\theta)$ and $P_4(\cos\theta)$, respectively, as a function of θ. $P_2(\cos\theta) = 0$ at the magic angle of 54.74°; $P_4(\cos\theta) = 0$ at angles of 30.56° and 70.12°.

5.2.2. Double Rotation

A number of techniques have been developed to counter the effects of the second-order quadrupolar Hamiltonian in order to produce sharp NMR spectra of quadrupolar nuclei. The first technique that we discuss is conceptually simple but challenging to implement experimentally: to eliminate the CSA in a powdered sample, it is common practice to spin the sample at an angle of 54.74° relative to the magnetic field to average the $P_2(\cos\theta)$ spatial term of the CSA Hamiltonian to zero. Similarly, double rotation (DOR)[213–215] eliminates the second-order quadrupolar coupling by spinning at the angles of 54.74° and 30.56° *simultaneously* to remove the $P_2(\cos\theta)$ *and* $P_4(\cos\theta)$ spatial terms of $H_Q^{(2)}$. This is accomplished by using the "rotor in a rotor" design shown in Figure 48, which

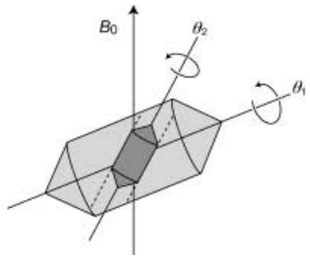

Figure 48. "Rotor-in-a-rotor" design for an NMR probe for DOR experiments. The outer rotor spins about an axis oriented at the magic angle, while the inner rotor spins about an axis oriented at 30.56° with respect to the outer axis.

allows the simultaneous rotation of the sample about two different axes. Under DOR conditions, all the second-order quadrupolar coupling is removed, except for its isotropic component, thus leaving a sharp isotropic peak flanked by a series of sidebands spaced at integer multiples of the outer rotor frequency. Figure 49 shows ^{23}Na DOR NMR spectra

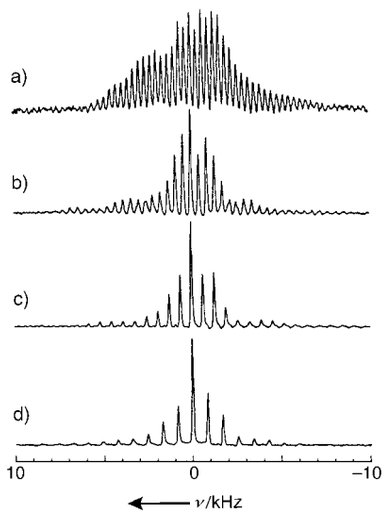

Figure 49. ^{23}Na DOR NMR spectra (105 MHz) of sodium oxalate acquired at outer-rotor spinning speeds of a) 320 Hz, b) 440 Hz, c) 640 Hz, and d) 850 Hz. (Adapted from ref. [259], with permission.)

of sodium oxalate obtained at various outer rotor speeds. When compared to the ^{23}Na NMR spectra of sodium oxalate in Figures 46a, b, the high resolution that is made possible through DOR is quite dramatic, and these experiments were the first to open the door to truly high-resolution NMR spectroscopy of quadrupolar nuclei in the solid state.[216, 217] In a method similar to the sideband analysis introduced by Herzfeld and Berger (see Section 4.4.1) one can obtain information about the strength of the quadrupolar coupling and asymmetry parameters from the sidebands.[218]

5.2.3. Dynamic-Angle Spinning

Dynamic-angle spinning (DAS) is an alternative technique for removing the second-order quadrupolar coupling.[219, 220] Like DOR, DAS seeks to remove the second-order quadrupolar coupling by spinning the sample at multiple angles. However, DAS spins *sequentially* at two different angles rather than simultaneously.

As an example, let us assume that a powdered sample of a sodium salt is spun about an axis inclined at an angle of 37.38° with respect to the static magnetic field. As the central transition magnetization of the ^{23}Na nuclei evolves following a π/2 pulse, the nuclei in different crystal orientations precess at different frequencies, depending on the value of $H_Q^{(2)}$. As a result, one can expect quadrupolar signals similar to those shown in Figure 50a. When the same sample is spun at an

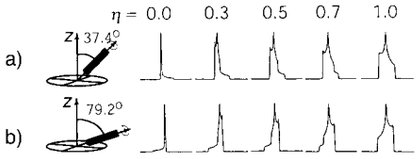

Figure 50. Simulated second-order quadrupolar powder patterns for the central transition of a spin I = 3/2 nucleus spinning at an angle of 37.38° (a) and 79.19° (b). η is the anisotropy of the quadrupolar coupling. (Adapted from ref. [218], with permission.)

angle of 79.19°, the second-order quadrupolar signals look like those shown in Figure 50b. It is interesting to see that these two sets of simulated spectra are exact mirror images of each other. This means that $H_Q^{(2)}$ for a crystal spinning at 37.38° has the opposite sign of that for a crystal spinning at 79.19°. Therefore, whatever the contribution of the quadrupolar coupling to the resonance frequencies, its effect can be removed by sequentially spinning the sample at these two angles. In fact, there are an infinite number of so-called DAS angle pairs.[162, 219, 221] It is no coincidence that the angles 37.38° and 79.19° correspond to the symmetry of an icosahedron (dodecahedron). Just as MAS corresponds to the dynamic implementation of cubic symmetry (see Section 2), DAS is the dynamic realization of icosahedral symmetry.[162, 222]

Figure 51a, b shows two possible pulse sequences for the implementation of DAS experiments. For magnetization to evolve at two different angles, one must use a NMR probe that allows the spinning rotor axis to change orientation. As it is impractical to move a spinning rotor while actively acquiring a signal, DAS is incorporated into a two-dimensional experiment in which the second-order quadrupolar coupling is removed in the indirect dimension t_1 but not in the direct dimension t_2. First, the magnetization is excited with a π/2 pulse and is allowed to evolve while spinning at 37.38° for a period of time $t_{1a} = \frac{1}{2}t_1$. The magnetization is then rotated back along the z axis (so that the evolution is interrupted) and the rotor axis is reoriented at an angle of 79.19°. The magnetization is then returned to the x,y plane by means of another π/2 pulse. The magnetization then evolves over a period of time t_{1b}. At the end of the t_1 period, the magnetization is detected in the direct dimension t_2. By incrementing the

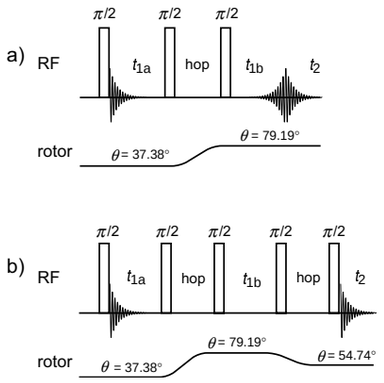

Figure 51. Pulse sequences for 2D DAS NMR experiments. a) Conventional sequence to obtain an isotropic/anisotropic correlation with powder patterns in the direct dimension characteristic of the second spinning angle. b) Sequence with a second hop to allow detection at the magic angle. With the chosen angles, t_{1a} has to be equal to t_{1b}, as the residual powder spectra at both spinning angles are the exact mirror images of each other as shown in Figure 50.

evolution time of the indirect dimension, it is possible to produce a two-dimensional spectrum that correlates the narrow isotropic lines with the broad second-order quadrupolar signal. Figure 52 shows a 2D ^{87}Rb DAS NMR spectrum

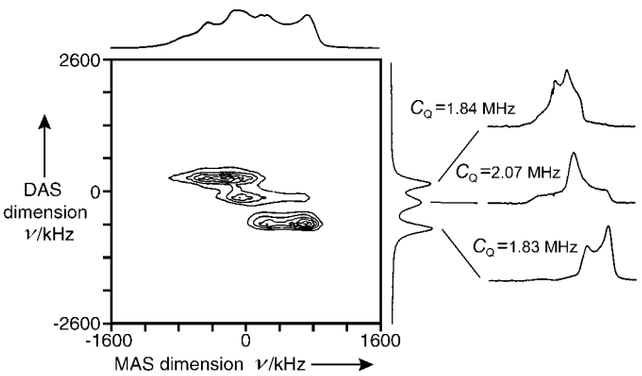

Figure 52. A 2D DAS NMR spectrum of the central transitions of ^{87}Rb in $RbNO_3$. The spectrum was obtained by using the pulse sequence in Figure 51b. By taking slices in the isotropic (indirect) dimension at the different isotropic frequencies, powder patterns can be obtained which are characteristic of the different sites and from which the quadrupolar coupling constants and asymmetry parameters can be determined. The quadrupolar coupling is often given as the so-called quadrupolar coupling constant parameter $C_Q = e^2qQ/h$ (in MHz). (Figure courtesy of P. J. Grandinetti.)

of $RbNO_3$, which has three non-equivalent rubidium sites. Although the Rb resonances overlap heavily in the projection of the anisotropic dimension, they are resolved in the isotropic dimension. By fitting the second-order quadrupolar signals obtained by taking slices at the positions of the three isotropic peaks, it is possible to determine the magnitude and anisotropy of the quadrupolar coupling at each site. In recent years, the structural analysis of glasses has relied much on the application of this technique (for examples, see refs. [223, 224]).

5.2.4. Multiple-Quantum MAS

Both DAS and DOR are very good techniques for removing the effects of the second-order quadrupolar coupling in half-integer-spin quadrupolar nuclei. A technically simpler approach, known as multiple-quantum MAS (MQMAS)[225, 226] capitalizes ingeniously on multiple-quantum coherence and coherence transfer with a standard MAS probe to remove $H_Q^{(2)}$.

Although the mathematical description of MQMAS is beyond the scope of this review, we can provide a conceptual description of the experiment. As shown in the energy-level diagram in Figure 45b for spin ½ nuclei, the frequency of the central transition was decreased by an amount proportional to $\omega_Q^{(2)}$, whereas the frequency of the triple-quantum transition $-\frac{1}{2} \rightarrow \frac{3}{2}$ was increased by an amount proportional to $\omega_Q^{(2)}$. The first-order quadrupolar coupling is removed for central transitions, and the term for the second-order interaction is removed by MAS, as mentioned above. If one were first to excite the triple-quantum transition, let the magnetization evolve for a period t_{1a}, and then transfer the magnetization into the central (single-quantum) transition and evolve for a period t_{1b}, at the end of the two periods the effects of the second-order quadrupolar coupling could be removed by adjusting the ratio t_{1a}/t_{1b} appropriately, as the resonance-frequency shifts induced by the second-order quadrupolar coupling are proportional to each other for both transitions. This method is analogous to the cancellation of $H_Q^{(2)}$ by the evolution of the magnetization at two different angles in DAS techniques, except that in MQMAS the rotor angle remains fixed and the magnetization evolves under two different coherences.

The similarity between MQMAS and DAS can be further illustrated by examining the MQMAS pulse sequence in Figure 53. First, the triple-quantum transition is excited by using an appropriate RF irradiation pulse. The magnetization then evolves for a period t_{1a}, after which it is transferred to the single-quantum $-\frac{1}{2} \rightarrow \frac{1}{2}$ transition by means of a second pulse. The magnetization then evolves for a period t_{1b}, after which it is detected during t_2. Similar to the case of the DAS technique, a 2D spectrum is obtained by varying the time $t_1 = t_{1a} + t_{1b}$ of the indirect dimension (but keeping the t_{1a}/t_{1b} ratio constant). Figure 54 shows an ^{27}Al MQMAS NMR spectrum of kyanite (Al_2SiO_5). With the high resolution obtained in the isotropic dimension (ω_1), it is possible to resolve three aluminum sites in the sample. By fitting the second-order quadrupolar signals obtained from slices through the three isotropic peaks, the quadrupolar couplings and anisotropy parameters of all aluminum sites are determined. From this information, it is possible to obtain the magnitude and asymmetry parameters of the electric-field gradients present at each site. A variety of extensions and enhancements of the basic sequence of Figure 53 have been proposed recently, some of which achieve either higher sensitivity, a more convenient quantitative characterization, or a higher resolution of the signals.[227–232] The MQMAS technique has proved to be very successful for the structure elucidation of minerals,[233, 234] glasses,[235–238] cement pastes,[239] zeolites and molecular sieves,[240–242] and biological solids.[31, 243–247]

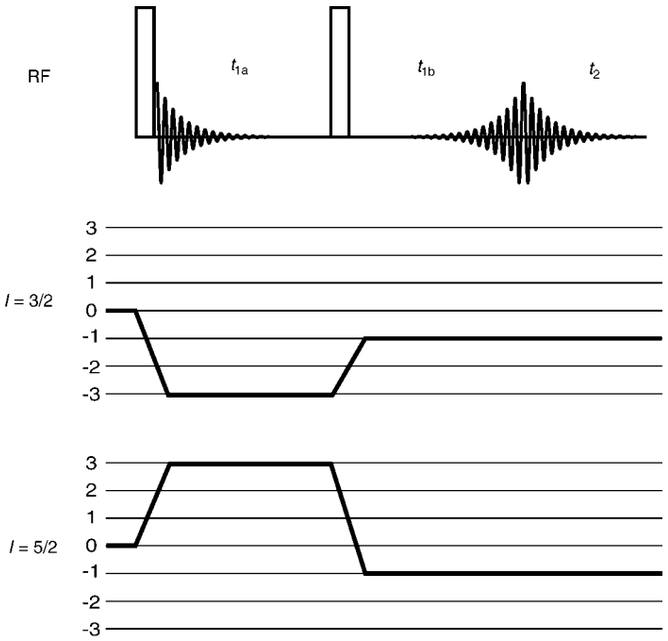

Figure 53. MQMAS pulse sequence and coherence pathway. In the time interval $t_{1a} + t_{1b}$, the second-order quadrupolar coupling is averaged to zero, leaving a scaled isotropic spectrum in the indirect dimension. For spin 3/2 nuclei, the $0 \rightarrow -3 \rightarrow -1$ coherence pathway is selected. For spin 5/2 nuclei, the $0 \rightarrow 3 \rightarrow -1$ coherence pathway is selected. (Figure courtesy of S. H. Wang.)

When compared to other solid-state NMR interactions, the quadrupolar coupling appears to be more complex. Nevertheless, we hope that this section has provided some insight into the behavior and spectroscopy of quadrupolar nuclei. For nuclei with small quadrupolar couplings (e.g. ^{2}H), information on dynamics and orientation is both simple to acquire and relatively easy to interpret. High-resolution spectra of nuclei such as ^{23}Na, ^{43}Mn, or ^{27}Al require more complex experiments such as DAS or MQMAS. The latter techniques have significantly contributed to the recent boom in the study of quadrupolar nuclei for everyday research in chemistry and materials science.[21] Only recently hetero- and homonuclear correlation experiments based on cross-polarization and recoupling have been developed for quadrupolar nuclei in the solid state.[248–252] In combination with recent sensitivity-boosting techniques,[253–256] and satellite-transition correlation experiments,[262–264] this field holds great promise for facilitating novel methods of spectral assignment and structure elucidation.

We are grateful to Professor Alex Pines for his continued inspiration and guidance. We also thank Professor Angelika Sebald for her extensive comments and Dr. Dimitris Sakellariou, Dr. Sungsool Wi, and Dr. Henrike Heise for their comments and suggestions on the manuscript. D.D.L. gratefully acknowledges the Howard Hughes Medical Institute for a predoctoral fellowship, A.J. thanks the Austrian Science Foundation for an Erwin Schrödinger fellowship. The work at Berkeley is supported by the U.S. Department of Energy (contract no. DE-AC03-76SF00098).

Received: July 2, 2001 [A 482]

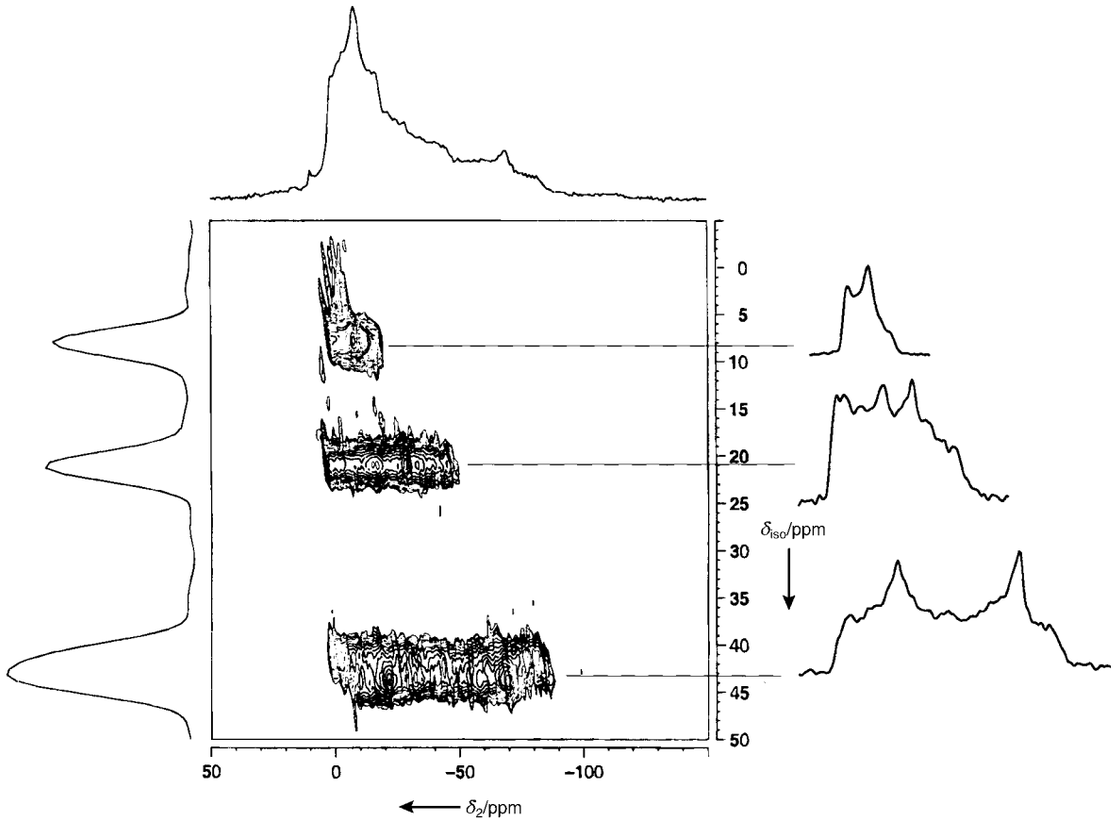

Figure 54. ^{27}Al MQ MAS NMR spectrum (104.217 MHz) of kyanite (Al_2SiO_5) at a MAS spinning speed of 22978 Hz. This spectrum was taken with a variant of the basic pulse sequence shown in Figure 53 with an additional z filter.[260] 1D spectra for each of the sites were obtained by taking slices through the peaks in the isotropic (δ_{iso}) dimension. (Adapted from ref. [261], with permission.)

[1] A. Pines, M. G. Gibby, J. S. Waugh, *J. Chem. Phys.* **1973**, *59*, 569.
[2] M. Auger, *Curr. Issues Mol. Biol.* **2000**, *2*, 119.
[3] B. Bechinger, R. Kinder, M. Helmle, T. C. Vogt, U. Harzer, S. Schinzel, *Biopolymers* **1999**, *51*, 174.
[4] B. Bechinger, *Mol. Membr. Biol.* **2000**, *17*, 135.
[5] B. Bechinger, *FEBS Lett.* **2001**, *504*, 161.
[6] T. A. Cross, *Methods Enzymol.* **1997**, *289*, 672.
[7] H. J. de Groot, *Curr. Opin. Struct. Biol.* **2000**, *10*, 593.
[8] C. Dybowski, S. Bai, *Anal. Chem.* **2000**, *72*, 1R.
[9] L. Frydman, *Annu. Rev. Phys. Chem.* **2001**, *52*, 463.
[10] R. Fu, T. A. Cross, *Annu. Rev. Biophys. Biomol. Struct.* **1999**, *28*, 235.
[11] R. G. Griffin, *Nat. Struct. Biol.* **1998**, *5* (Suppl.), 508.
[12] S. Hafner, D. E. Demco, R. Kimmich, *Solid State Nucl. Magn. Reson.* **1996**, *6*, 275.
[13] M. Hunger, *Solid State Nucl. Magn. Reson.* **1996**, *6*, 1.
[14] D. G. Lynn, S. C. Meredith, *J. Struct. Biol.* **2000**, *130*, 153.
[15] F. M. Marassi, S. J. Opella, *Curr. Opin. Struct. Biol.* **1998**, *8*, 640.
[16] L. M. McDowell, J. Schaefer, *Curr. Opin. Struct. Biol.* **1996**, *6*, 624.
[17] S. J. Opella, *Nat. Struct. Biol.* **1997**, *4* (Suppl.), 845.
[18] I. Schnell, H. W. Spiess, *J. Magn. Reson.* **2001**, *151*, 153.
[19] H. Schwalbe, A. Bielecki, *Angew. Chem.* **2001**, *113*, 2100; *Angew. Chem. Int. Ed.* **2001**, *40*, 2045.
[20] G. Siegal, J. van Duynhoven, M. Baldus, *Curr. Opin. Chem. Biol.* **1999**, *3*, 530.
[21] M. E. Smith, E. R. H. Van Eck, *Prog. Nucl. Magn. Reson. Spectrosc.* **1999**, *34*, 159.
[22] D. J. Siminovitch, *Biochem. Cell. Biol.* **1998**, *76*, 411.
[23] Y. Tong, E. Oldfield, A. Wieckowski, *Anal. Chem.* **1998**, *70*, 518A.
[24] R. Tycko, *Solid State Nucl. Magn. Reson.* **1994**, *3*, 303.
[25] R. Tycko, *Curr. Opin. Chem. Biol.* **2000**, *4*, 500.
[26] R. Tycko, *Methods Enzymol.* **2001**, *339*, 390.
[27] R. Tycko, *Annu. Rev. Phys. Chem.* **2001**, *52*, 575.
[28] A. Watts, *Biochim. Biophys. Acta* **1998**, *1376*, 297.
[29] A. Watts, I. J. Burnett, C. Glaubitz, G. Grobner, D. A. Middleton, P. J. Spooner, J. A. Watts, P. T. Williamson, *Nat. Prod. Rep.* **1999**, *16*, 419.
[30] A. Watts, *Curr. Opin. Biotechnol.* **1999**, *10*, 48.
[31] G. Wu, *Biochem. Cell. Biol.* **1998**, *76*, 429.
[32] G. E. Pake, *J. Chem. Phys.* **1948**, *16*, 327.
[33] F. Bloch, *Phys. Rev.* **1956**, *102*, 104.
[34] F. Bloch, *Phys. Rev.* **1958**, *111*, 841.
[35] A. J. Shaka, J. Keeler, *Prog. Nucl. Magn. Reson. Spectrosc.* **1987**, *19*, 47.
[36] M. H. Levitt, *Prog. Nucl. Magn. Reson. Spectrosc.* **1986**, *18*, 61.
[37] A. R. Edmonds, *Angular Momentum in Quantum Mechanics*, Princeton University Press, **1960**.
[38] "High Resolution NMR in Solids: Selective Averaging": U. Haeberlen, *Adv. Magn. Reson.* **1976**, Suppl. 1.
[39] M. Mehring, *High Resolution NMR in Solids*, Springer, New York, **1983**.
[40] E. R. Andrew, A. Bradbury, R. G. Eades, *Nature* **1958**, *182*, 1659.
[41] I. J. Lowe, *Phys. Rev. Lett.* **1959**, *2*, 285.
[42] M. M. Maricq, J. S. Waugh, *J. Chem. Phys.* **1979**, *70*, 3300.
[43] L. Emsley, D. D. Laws, A. Pines, *Proc. Int. Sch. Phys. "Enrico Fermi"* **1999**, *129*, 45.
[44] M. H. Levitt, *J. Magn. Reson.* **1989**, *82*, 427.
[45] J. Herzfeld, A. E. Berger, *J. Chem. Phys.* **1980**, *73*, 6021.
[46] J. Cavanagh, A. G. Palmer, W. Fairbrother, N. Skelton, *Protein NMR spectroscopy: Principles and practice*, Academic Press, San Diego, **1996**.
[47] A. E. Derome, *Modern NMR Techniques for Chemistry Research*, Pergamon, Oxford, **1987**.
[48] S. R. Hartmann, E. L. Hahn, *Phys. Rev.* **1962**, *128*, 2042.
[49] A. Pines, M. G. Gibby, J. S. Waugh, *J. Chem. Phys.* **1972**, *56*, 1776.

[50] E. O. Stejskal, J. Schaefer, J. S. Waugh, *J. Magn. Reson.* **1977**, *28*, 105.
[51] J. Schaefer, E. O. Stejskal, *J. Am. Chem. Soc.* **1976**, *98*, 1031.
[52] R. K. Harris, P. Jackson, *Chem. Rev.* **1991**, *91*, 1427.
[53] A. Jurkiewicz, C. E. Bronniman, G. E. Maciel, *Fuel* **1990**, *69*, 804.
[54] K. Schmidt-Rohr, H. W. Spiess, *Multidimensional Solid-State NMR and Polymers*, Academic Press, San Diego, **1994**.
[55] R. R. Ernst, G. Bodenhausen, A. Wokaun, *Principles of Nuclear Magnetic Resonance in One and Two Dimensions*, Clarendon Press, Oxford, **1987**.
[56] H. Kessler, M. Gehrke, C. Griesinger, *Angew. Chem.* **1988**, *100*, 507; *Angew. Chem. Int. Ed. Engl.* **1988**, *27*, 490.
[57] K. Schmidt-Rohr, J. Clauss, H. W. Spiess, *Macromolecules* **1992**, *25*, 3273.
[58] I. Quijada-Garrido, M. Wilhelm, H. W. Spiess, J. M. Barrales-Rienda, *Macromol. Chem. Phys.* **1998**, *199*, 985.
[59] L. M. Bronstein, C. Joo, R. Karlinsey, A. Ryder, J. W. Zwanziger, *Chem. Mater.* **2001**, *13*, 3678.
[60] S. M. de Paul, J. W. Zwanziger, R. Ulrich, U. Wiesner, H. W. Spiess, *J. Am. Chem. Soc.* **1999**, *121*, 5727.
[61] J. S. Waugh, L. M. Huber, U. Haeberlen, *Phys. Rev. Lett.* **1968**, *20*, 180. The acronyms WAHUHA and WHH-4 are derived from the author names.
[62] M. Lee, W. I. Goldburg, *Phys. Rev. A* **1965**, *140*, 1261.
[63] U. Haeberlen, J. S. Waugh, *Phys. Rev.* **1968**, *175*, 453.
[64] P. Mansfield, *Phys. Lett. A* **1970**, *32*, 485.
[65] P. Mansfield, *J. Phys. C* **1971**, *4*, 1444.
[66] W. K. Rhim, D. D. Elleman, R. W. Vaughan, *J. Chem. Phys.* **1972**, *58*, 1772.
[67] D. P. Burum, W. K. Rhim, *J. Chem. Phys.* **1979**, *71*, 944.
[68] D. P. Burum, M. Linder, R. R. Ernst, *J. Magn. Reson.* **1981**, *44*, 173.
[69] D. G. Cory, *J. Magn. Reson.* **1991**, *94*, 526.
[70] K. Takegoshi, C. A. McDowell, *Chem. Phys. Lett.* **1985**, *116*, 100.
[71] M. Hohwy, P. V. Bower, H. J. Jakobsen, N. C. Nielsen, *Chem. Phys. Lett.* **1997**, *273*, 297.
[72] A. Bielecki, A. C. Kolbert, M. H. Levitt, *Chem. Phys. Lett.* **1989**, *155*, 341.
[73] A. Bielecki, A. C. Kolbert, H. J. M. de Groot, R. G. Griffin, M. H. Levitt, *Adv. Magn. Reson.* **1990**, *14*, 111.
[74] M. H. Levitt, A. C. Kolbert, A. Bielecki, D. J. Ruben, *Solid State Nucl. Magn. Reson.* **1993**, *2*, 151.
[75] B.-J. van Rossum, H. Förster, H. J. M. de Groot, *J. Magn. Reson.* **1997**, *124*, 516.
[76] J. D. Cross, P. R. Costa, R. G. Griffin, *J. Chem. Phys.* **1998**, *108*, 7286.
[77] M. Baldus, B. H. Meier, *J. Magn. Reson.* **1997**, *128*, 172.
[78] A. Ramamoorthy, F. M. Marassi, M. Zasloff, S. J. Opella, *J. Biomol. NMR* **1995**, *6*, 329.
[79] A. Lesage, D. Sakellariou, S. Steuernagel, L. Emsley, *J. Am. Chem. Soc.* **1998**, *120*, 13194.
[80] V. Ladizhansky, S. Vega, *J. Chem. Phys.* **2000**, *112*, 7158.
[81] B.-J. van Rossum, C. P. de Groot, V. Ladizhansky, S. Vega, H. J. M. de Groot, *J. Am. Chem. Soc.* **2000**, *122*, 3465.
[82] P. K. Madhu, X. Zhao, M. H. Levitt, *Chem. Phys. Lett.* **2001**, *346*, 142.
[83] J. Baum, M. Munowitz, A. N. Garroway, A. Pines, *J. Chem. Phys.* **1985**, *83*, 2015.
[84] M. Munowitz, M. Mehring, A. Pines, *J. Chem. Phys.* **1987**, *86*, 3172.
[85] J. Baum, A. Pines, *J. Am. Chem. Soc.* **1986**, *108*, 7447.
[86] M. Munowitz, A. Pines, *Science* **1986**, *233*, 525.
[87] W. S. Warren, D. P. Weitekamp, A. Pines, *J. Chem. Phys.* **1980**, *73*, 2084.
[88] M. Carravetta, F. Castiglione, G. De Luca, M. Edgar, J. W. Emsley, R. D. Farrant, E. K. Foord, J. C. Lindon, M. Longeri, W. E. Palke, D. L. Turner, *J. Magn. Reson.* **1998**, *135*, 298.
[89] O. N. Antzutkin, J. J. Balbach, R. D. Leapman, N. W. Rizzo, J. Reed, R. Tycko, *Proc. Natl. Acad. Sci. USA* **2000**, *97*, 13045.
[90] P. Carvatti, G. Bodenhausen, R. R. Ernst, *Chem. Phys. Lett.* **1982**, *89*, 363.
[91] P. Carvatti, L. Braunschweiler, R. R. Ernst, *Chem. Phys. Lett.* **1983**, *100*, 305.
[92] B.-J. van Rossum, E. A. M. Schulten, J. Raap, H. Oschkinat, H. J. M. de Groot, *J. Magn. Reson.* **2002**, *155*, 1.
[93] K. Hester, J. L. Ackerman, V. R. Cross, J. S. Waugh, *Phys. Rev. Lett.* **1976**, *36*, 1081.
[94] K. Schmidt-Rohr, D. Nanz, L. Emsley, A. Pines, *J. Phys. Chem.* **1994**, *98*, 6668.
[95] S. Caldarelli, M. Hong, L. Emsley, A. Pines, *J. Phys. Chem.* **1996**, *100*, 18696.
[96] C. H. Wu, A. Ramamoorthy, S. J. Opella, *J. Magn. Reson., Ser. A* **1994**, *109*, 270.
[97] F. M. Marassi, S. J. Opella, *J. Magn. Reson.* **2000**, *144*, 150.
[98] J. K. Denny, J. F. Wang, T. A. Cross, J. R. Quine, *J. Magn. Reson.* **2002**, *154*, 80.
[99] M. H. Levitt, R. Freeman, T. Frenkiel, *J. Magn. Reson.* **1982**, *47*, 328.
[100] M. H. Levitt, R. Freeman, T. Frenkiel, *Adv. Magn. Reson.* **1983**, *12*, 47.
[101] A. J. Shaka, J. Keeler, T. Frenkiel, R. Freeman, *J. Magn. Reson.* **1983**, *52*, 335.
[102] A. E. Bennett, C. M. Rienstra, M. Auger, K. V. Lakshmi, R. G. Griffin, *J. Chem. Phys.* **1995**, *103*, 6951.
[103] M. Mehring, G. Sinning, A. Pines, *Z. Phys. B* **1976**, *24*, 73.
[104] G. Sinning, M. Mehring, A. Pines, *Chem. Phys. Lett.* **1976**, *43*, 382.
[105] M. Mehring, G. Sinning, *Phys. Rev. B* **1977**, *15*, 2519.
[106] M. Ernst, H. Zimmerman, B. H. Meier, *Chem. Phys. Lett.* **2000**, *317*, 581.
[107] Z. H. Gan, R. R. Ernst, *Solid State Nucl. Magn. Reson.* **1997**, *8*, 153.
[108] M. Eden, M. H. Levitt, *Chem. Phys. Lett.* **1999**, *111*, 1511.
[109] K. Wüthrich in *Encyclopedia of NMR*, *Vol. 2* (Eds.: D. M. Grant, R. K. Harris), Wiley, Chichester, **1996**, S. 932.
[110] Mechanically demanding experiments have been performed in which the MAS rotor was stopped briefly to recouple the chemical shift anisotropy and then restarted to detect the NMR signal in t_2 (R. C. Zeigler, R. A. Wind, G. E. Maciel, *J. Magn. Reson.* **1988**, *79*, 299).
[111] T. Gullion, J. Schaefer, *J. Magn. Reson.* **1989**, *81*, 196.
[112] K. T. Mueller, T. P. Jarvie, D. J. Aurentz, B. W. Roberts, *Chem. Phys. Lett.* **1995**, *242*, 535.
[113] T. Gullion, C. H. Pennington, *Chem. Phys. Lett.* **1998**, *290*, 88.
[114] O. Liivak, D. B. Zax, *J. Chem. Phys.* **2000**, *113*, 1088.
[115] C. A. Fyfe, A. R. Lewis, J. M. Chezeau, *Can. J. Chem.* **1999**, *77*, 1984.
[116] C. A. Fyfe, A. R. Lewis, *J. Phys. Chem. B* **2000**, *104*, 48.
[117] C. A. Fyfe, D. H. Brouwer, A. R. Lewis, J. M. Chezeau, *J. Am. Chem. Soc.* **2001**, *123*, 6882.
[118] C. P. Jaroniec, B. A. Tounge, J. Herzfeld, R. G. Griffin, *J. Am. Chem. Soc.* **2001**, *123*, 3507.
[119] C. P. Jaroniec, B. A. Tounge, C. M. Rienstra, J. Herzfeld, R. G. Griffin, *J. Am. Chem. Soc.* **1999**, *121*, 10237.
[120] R. Fu, S. A. Smith, G. Bodenhausen, *Chem. Phys. Lett.* **1997**, *272*, 361.
[121] Y. Ishii, T. Terao, *J. Chem. Phys.* **1998**, *109*, 1366.
[122] R. Tycko, G. Dabbagh, *Chem. Phys. Lett.* **1990**, *173*, 461.
[123] C. A. Klug, W. Zhu, K. Tasaki, J. Schaefer, *Macromolecules* **1997**, *30*, 1734.
[124] D. P. Raleigh, M. H. Levitt, R. G. Griffin, *Chem. Phys. Lett.* **1988**, *146*, 71.
[125] T. Nakai, C. A. McDowell, *J. Magn. Reson. Ser. A* **1995**, *140*, 199.
[126] T. Karlsson, M. Edén, H. Luthman, M. H. Levitt, *J. Magn. Reson. Ser. A* **2000**, *145*, 95.
[127] S. Dusold, A. Sebald, *J. Magn. Reson.* **2000**, *145*, 340.
[128] N. C. Nielsen, H. Bildsoe, H. J. Jakobsen, M. H. Levitt, *J. Chem. Phys.* **1994**, *101*, 1805.
[129] S. Kiihne, M. A. Mehta, J. A. Stringer, D. M. Gregory, J. C. Shiels, G. P. Drobny, *J. Phys. Chem.* **1998**, *102*, 2274.
[130] B.-Q. Sun, P. R. Costa, D. Kocisko, P. T. Lansbury, R. G. Griffin, *J. Chem. Phys.* **1995**, *102*, 702.
[131] M. Feike, D. E. Demco, R. Graf, J. Gottwald, S. Hafner, H. W. Spiess, *J. Magn. Reson. Ser. A* **1996**, *122*, 214.
[132] A. E. Bennett, J. H. Ok, R. G. Griffin, S. Vega, *J. Chem. Phys.* **1992**, *96*, 8624.
[133] M. Hohwy, H. J. Jakobsen, M. Edén, M. H. Levitt, N. C. Nielsen, *J. Chem. Phys.* **1998**, *108*, 2686.
[134] M. Baldus, D. G. Geurts, B. H. Meier, *Solid State Nucl. Magn. Reson.* **1998**, *11*, 157.
[135] S. Dusold, A. Sebald, *Annu. Rep. NMR Spectrosc.* **2000**, *41*, 185.
[136] A. E. Bennett, R. G. Griffin, S. Vega, *NMR* **1994**, *33*, 3.
[137] M. Carravetta, M. Edén, X. Zhao, A. Brinkmann, M. H. Levitt, *Chem. Phys. Lett.* **2000**, *321*, 205.

[138] M. H. Levitt in *Encyclopedia of NMR, Supplement* (Eds.: D. M. Grant, R. K. Harris), Wiley, Chichester, in press.
[139] G. Metz, X. Wu, S. O. Smith, *J. Magn. Reson. Ser. A* **1994**, *110*, 219.
[140] M. Baldus, D. G. Geurts, S. Hediger, B. H. Meier, *J. Magn. Reson. Ser. A* **1996**, *118*, 140.
[141] M. Hong, R. G. Griffin, *J. Am. Chem. Soc.* **1998**, *120*, 7113.
[142] I. Schnell, B. Langer, S. H. M. Söntjens, M. H. P. van Gebderen, R. P. Sijbesma, H. W. Spiess, *J. Magn. Reson.* **2001**, *150*, 57.
[143] K. Saalwächter, R. Graf, H. W. Spiess, *J. Magn. Reson.* **2001**, *148*, 398.
[144] T. A. Egorova-Zachernyuk, J. Hollander, N. Fraser, P. Gast, A. J. Hoff, R. Cogdell, H. J. M. de Groot, M. Baldus, *J. Biomol. NMR* **2001**, *19*, 243.
[145] C. M. Rienstra, M. Hohwy, M. Hong, R. G. Griffin, *J. Am. Chem. Soc.* **2000**, *122*, 10979.
[146] J. Pauli, M. Baldus, B. van Rossum, H. de Groot, H. Oschkinat, *ChemBioChem* **2001**, *2*, 272.
[147] C. M. Rienstra, M. E. Hatcher, L. J. Mueller, B. Sun, S. W. Fesik, R. G. Griffin, *J. Am. Chem. Soc.* **1998**, *120*, 10602.
[148] J. M. Griffiths, A. E. Bennett, M. Engelhard, F. Siebert, J. Raap, J. Lugtenburg, J. Herzfeld, R. G. Griffin, *Biochemistry* **2000**, *39*, 362.
[149] T. A. Egorova-Zachernyuk, B. van Rossum, G. J. Boender, E. Franken, J. Ashurst, J. Raap, P. Gast, A. J. Hoff, H. Oschkinat, H. J. M. de Groot, *Biochemistry* **1997**, *36*, 7513.
[150] A. McDermott, T. Polenova, A. Bockmann, K. W. Zilm, E. K. Paulsen, R. W. Martin, G. T. Montelione, *J. Biomol. NMR* **2000**, *16*, 209.
[151] Alia, J. Matysik, C. Soede-Huijbregts, M. Baldus, J. Raap, J. Lugtenburg, P. Gast, H. J. van Gorkom, A. J. Hoff, H. J. M. de Groot, *J. Am. Chem. Soc.* **2001**, *123*, 4803.
[152] J. Pauli, B. van Rossum, H. Förster, H. J. M. de Groot, H. Oschkinat, *J. Magn. Reson.* **2000**, *143*, 411.
[153] B.-Q. Sun, C. M. Rienstra, P. R. Costa, J. R. Williamson, R. G. Griffin, *J. Am. Chem. Soc.* **1997**, *119*, 8540.
[154] H. Geen, J. Gottwald, R. Graf, I. Schnell, H. W. Spiess, J. J. Titman, *J. Magn. Reson.* **1997**, *125*, 224.
[155] A. S. D. Heindrichs, H. Geen, J. J. Titman, *J. Magn. Reson.* **2000**, *147*, 68.
[156] S. P. Brown, I. Schnell, J. D. Brand, K. Müllen, H. W. Spiess, *J. Mol. Struct.* **2000**, *521*, 179.
[157] H. Geen, R. Graf, A. S. D. Heindrichs, B. S. Hickman, I. Schnell, H. W. Spiess, J. J. Titman, *J. Magn. Reson.* **1999**, *138*, 167.
[158] S. Ravindranathan, X. Feng, T. Karlsson, G. Widmalm, M. H. Levitt, *J. Am. Chem. Soc.* **2000**, *122*, 1102.
[159] X. Feng, P. J. E. Verdegem, Y. K. Lee, D. Sandström, M. Edén, P. Bovee-Geurts, W. J. de Grip, J. Lugtenburg, H. J. M. de Groot, M. H. Levitt, *J. Am. Chem. Soc.* **1997**, *119*, 6853.
[160] F. J. Blanco, R. Tycko, *J. Magn. Reson.* **2001**, *149*, 131.
[161] A. C. Kolbert, P. J. Grandinetti, M. Baldwin, S. B. Prusiner, A. Pines, *J. Phys. Chem.* **1994**, *98*, 7936.
[162] A. Samoson, B. Q. Sun, A. Pines in *Pulsed Magnetic Resonance: NMR, ESR, and Optics* (Ed.: D. M. S. Bagguley), Clarendon, Oxford, **1992**.
[163] J. Heller, D. D. Laws, M. Tomaselli, D. S. King, D. E. Wemmer, A. Pines, R. H. Havlin, E. Oldfield, *J. Am. Chem. Soc.* **1997**, *119*, 7827.
[164] R. H. Havlin, H. Le, D. D. Laws, A. C. deDios, E. Oldfield, *J. Am. Chem. Soc.* **1997**, *119*, 11951.
[165] W. T. Dixon, *J. Chem. Phys.* **1982**, *77*, 1800.
[166] S. Féaux de Lacroix, J. J. Titman, A. Hagemeyer, H. W. Spiess, *J. Magn. Reson.* **1992**, *97*, 435.
[167] O. N. Antzukin, Z. Song, X. Feng, M. H. Levitt, *J. Chem. Phys.* **1994**, *100*, 130.
[168] J. J. Titman, S. Féaux de Lacroix, H. W. Spiess, *J. Chem. Phys.* **1993**, *98*, 3816.
[169] O. N. Antzutkin, *Prog. Nucl. Magn. Reson. Spectrosc.* **1999**, *35*, 203.
[170] V. Gérardy-Montouillout, C. Malveau, P. Tekely, Z. Olender, Z. Luz, *J. Magn. Reson. Ser. A* **1996**, *123*, 7.
[171] P. Tekely, D. Reichert, H. Zimmermann, Z. Luz, *J. Magn. Reson.* **2000**, *145*, 173.
[172] C. Jäger, D. Reichert, H. Zimmermann, T. Sen, R. Poupko, Z. Luz, *J. Magn. Reson.* **2001**, *153*, 227.
[173] M. Alla, E. I. Kundla, E. Lippmaa, *JETP Lett.* **1978**, *27*, 194.
[174] R. Tycko, G. Dabbagh, P. A. Mirau, *J. Magn. Reson.* **1989**, *85*, 265.
[175] A. Bax, N. M. Szeverenyi, G. Maciel, *J. Magn. Reson.* **1983**, *55*, 494.
[176] Z. H. Gan, *J. Am. Chem. Soc.* **1992**, *114*, 8307.
[177] J. Z. Hu, A. M. Orendt, D. W. Alderman, R. J. Pugmire, C. Ye, D. M. Grant, *Solid State Nucl. Magn. Reson.* **1994**, *3*, 181.
[178] L. Frydman, G. C. Chingas, Y. K. Lee, P. J. Grandinetti, E. A. Eastman, G. A. Barall, A. Pines, *Isr. J. Chem.* **1992**, *32*, 161.
[179] L. Frydman, G. C. Chingas, Y. K. Lee, P. J. Grandinetti, M. A. Eastman, G. A. Barrall, A. Pines, *J. Chem. Phys.* **1992**, *97*, 4800.
[180] D. W. Alderman, G. McGeorge, J. Z. Hu, R. J. Pugmire, D. M. Grant, *Mol. Phys.* **1998**, *95*, 1113.
[181] C. A. Fyfe, H. Grondey, Y. Feng, G. T. Kokotailo, *Chem. Phys. Lett.* **1990**, *173*, 211.
[182] C. A. Fyfe, H. Grondey, Y. Feng, G. T. Kokotailo, S. Ernst, J. Weitkamp, *Zeolites* **1992**, *12*, 50.
[183] C. A. Fyfe, Y. Feng, H. Grondey, G. T. Kokotailo, A. Mar, *J. Phys. Chem.* **1991**, *95*, 3747.
[184] R. E. Wasylishen in *Encyclopedia of NMR*, *Vol. 3* (Ed.: D. M. Grant, R. K. Harris), Wiley, Chichester, **1996**, S. 1685.
[185] A. Lesage, C. Auger, S. Caldarelli, L. Emsley, *J. Am. Chem. Soc.* **1997**, *119*, 7867.
[186] A. Lesage, M. Bardet, L. Emsley, *J. Am. Chem. Soc.* **1999**, *121*, 10987.
[187] A. Lesage, P. Charmont, S. Steuernagel, L. Emsley, *J. Am. Chem. Soc.* **2000**, *122*, 9739.
[188] E. H. Hardy, R. Verel, B. H. Meier, *J. Magn. Reson.* **2001**, *148*, 459.
[189] M. Baldus, R. J. Iuliucci, B. H. Meier, *J. Am. Chem. Soc.* **1997**, *119*, 1121.
[190] A. S. D. Heindrichs, H. Geen, C. Giordani, J. J. Titman, *Chem. Phys. Lett.* **2001**, *335*, 89.
[191] Quadrupolar nuclei located within a cubic crystal will not experience a quadrupolar coupling as a consequence of the symmetry of the lattice. Evidence for this can be seen in the ^{14}N NMR spectrum of NH_4Cl or in the ^{23}Na NMR spectrum of NaCl, which have very narrow signals.
[192] H. H. Mantsch, H. Saitó, I. C. P. Smith, *Prog. Nucl. Magn. Reson. Spectrosc.* **1977**, *11*, 211.
[193] L. W. Jelinski, *Annu. Rev. Mater. Sci.* **1985**, *15*, 359.
[194] N. Chandrakumar, *Spin-1 NMR*, *Vol. 34*, Springer, Berlin, **1996**.
[195] S. Vega, T. W. Shattuck, A. Pines, *Phys. Rev. Lett.* **1976**, *37*, 43.
[196] A. Pines, S. Vega, M. Mehring, *Phys. Rev. B* **1978**, *18*, 112.
[197] R. L. Smith, E. Oldfield, *Science* **1984**, *225*, 280.
[198] P. Diehl, C. L. Khetrapal, *NMR* **1969**, *1*, 1.
[199] "Nuclear Magnetic Resonance of Liquid Crystals": Z. Luz, *NATO ASI Ser. Ser. C* 1983, *141*, 315.
[200] H. Lee, P. R. Ortiz de Montellano, A. E. McDermott, *Biochemistry* **1999**, *38*, 10808.
[201] H. Lee, T. Polenova, R. H. Beer, A. E. McDermott, *J. Am. Chem. Soc.* **1999**, *121*, 6884.
[202] J. Hirschinger, D. Schaefer, H. W. Spiess, *Macromolecules* **1991**, *24*, 2428.
[203] G. Dabbagh, D. P. Weliky, R. Tycko, *Macromolecules* **1994**, *27*, 6183.
[204] R. H. Lewis, H. W. Long, K. Schmidt-Rohr, H. W. Spiess, *J. Magn. Reson. Ser. A* **1995**, *115*, 26.
[205] E. R. deAzevedo, T. J. Bonagamba, K. Schmidt-Rohr, *J. Magn. Reson.* **2000**, *142*, 86.
[206] L. Frydman, Y. K. Lee, L. Emsley, G. C. Chingas, A. Pines, *J. Am. Chem. Soc.* **1993**, *115*, 4825.
[207] A. Abragam, *Principles of Nuclear Magnetism*, Clarendon, Oxford, **1961**.
[208] A. Medek, V. Frydman, L. Frydman, *J. Phys. Chem. A* **1999**, *103*, 4830.
[209] C. P. Slichter, *Principles of Nuclear Magnetic Resonance*, 3rd ed., Springer, New York, **1990**.
[210] A. J. Vega in *Encyclopedia of NMR* (Eds.: D. M. Grant, R. K. Harris), Wiley, Chichester, **1995**.
[211] A. Samoson, E. I. Kundla, E. Lippmaa, *J. Magn. Reson.* **1982**, *49*, 350.
[212] L. Werbelow, R. E. London, *Concepts Magn. Reson.* **1995**, *8*, 325.
[213] A. Samoson, E. Lippmaa, A. Pines, *Mol. Phys.* **1988**, *65*, 1013.
[214] A. Samoson, A. Pines, *Rev. Sci. Instrum.* **1989**, *60*, 3239.
[215] A. Llor, J. Virlet, *Chem. Phys. Lett.* **1988**, *152*, 248.
[216] B. F. Chmelka, K. T. Mueller, A. Pines, J. Stebbins, Y. Wu, J. W. Zwanziger, *Nature* **1989**, *339*, 42.

[217] Y. Wu, B. F. Chmelka, A. Pines, M. E. Davis, P. J. Grobet, P. A. Jacobs, *Nature* **1990**, *346*, 6284.
[218] B. Q. Sun, J. H. Baltisberger, Y. Wu, A. Samoson, A. Pines, *Solid State Nucl. Magn. Reson.* **1992**, *1*, 267.
[219] K. T. Mueller, B. Q. Sun, G. C. Chingas, J. W. Zwanziger, T. Terao, A. Pines, *J. Magn. Reson.* **1990**, *86*, 470.
[220] J. H. Baltisberger, S. L. Gann, E. W. Wooten, T. H. Chang, K. T. Mueller, A. Pines, *J. Am. Chem. Soc.* **1992**, *114*, 7489.
[221] K. T. Mueller, Y. Wu, B. F. Chmelka, J. Stebbins, A. Pines, *J. Am. Chem. Soc.* **1991**, *113*, 32.
[222] E. W. Wooten, K. T. Mueller, A. Pines, *Acc. Chem. Res.* **1992**, *25*, 209.
[223] R. E. Youngman, J. W. Zwanziger, *J. Phys. Chem.* **1996**, *100*, 16720.
[224] J. W. Zwanziger, *Solid State Nucl. Magn. Reson.* **1994**, *3*, 219.
[225] A. Medek, J. S. Harwood, L. Frydman, *J. Am. Chem. Soc.* **1995**, *117*, 12779.
[226] L. Frydman, J. S. Harwood, *J. Am. Chem. Soc.* **1995**, *117*, 5367.
[227] P. K. Madhu, A. Goldbourt, L. Frydman, S. Vega, *Chem. Phys. Lett.* **1999**, *307*, 41.
[228] S. P. Brown, S. Wimperis, *J. Magn. Reson.* **1997**, *128*, 42.
[229] D. Iuga, H. Schäfer, R. Verhagen, A. P. M. Kentgens, *J. Magn. Reson.* **2000**, *147*, 192.
[230] T. Vosegaard, D. Massiot, P. J. Grandinetti, *Chem. Phys. Lett.* **2000**, *326*, 454.
[231] G. Wu, D. Rovnyak, R. G. Griffin, *J. Am. Chem. Soc.* **1996**, *118*, 9326.
[232] A. Jerschow, J. W. Logan, A. Pines, *J. Magn. Reson.* **2001**, *149*, 268.
[233] S. E. Ashbrook, A. J. Berry, S. Wimperis, *Am. Mineral.* **1999**, *84*, 1191.
[234] S. E. Ashbrook, H. McManus, K. J. D. MacKenzie, S. Wimperis, *J. Phys. Chem. B* **2000**, *104*, 6408.
[235] J. F. Stebbins, J. V. Oglesby, S. K. Lee, *Chem. Geol.* **2001**, *174*, 63.
[236] J. F. Stebbins, P. D. Zhao, S. K. Lee, J. V. Oglesby, *J. Non-Cryst. Solids* **2001**, *293*, 67.
[237] Z. Xu, J. F. Stebbins, *Solid State Nucl. Magn. Reson.* **1998**, *11*, 243.
[238] F. Angeli, T. Charpentier, S. Gin, J. C. Petit, *Chem. Phys. Lett.* **2001**, *341*, 23.
[239] P. Faucon, T. Charpentier, D. Bertrandie, A. Nonat, J. Virlet, J. C. Petit, *Inorg. Chem.* **1998**, *37*, 3726.
[240] J.-P. Amoureux, F. Bauer, H. Ernst, C. Fernandez, D. Freude, D. Michel, U.-T. Pingel, *Chem. Phys. Lett.* **1998**, *285*, 10.
[241] U.-T. Pingel, J.-P. Amoureux, T. Anupold, F. Bauer, H. Ernst, C. Fernandez, D. Freude, A. Samoson, *Chem. Phys. Lett.* **1998**, *294*, 345.
[242] A. Tuel, S. Caldarelli, A. Meden, L. B. McCusker, C. Baerlocher, A. Ristic, N. Rajic, G. Mali, V. Kaucic, *J. Phys. Chem. B* **2000**, *104*, 5697.
[243] S. Sham, G. Wu, *Inorg. Chem.* **2000**, *39*, 4.
[244] S. Ding, C. A. McDowell, *Chem. Phys. Lett.* **2000**, *320*, 316.
[245] D. Rovnyak, M. Baldus, G. Wu, N. V. Hud, J. Feigon, R. G. Griffin, *J. Am. Chem. Soc.* **2000**, *122*, 11423.
[246] C. V. Grant, V. Frydman, L. Frydman, *J. Am. Chem. Soc.* **2000**, *122*, 11743.
[247] C. V. Grant, V. Frydman, J. S. Harwood, L. Frydman, *J. Am. Chem. Soc.* **2002**, *124*, 4458.
[248] J. C. C. Chan, *J. Magn. Reson.* **1999**, *140*, 487.
[249] S. H. Wang, S. M. de Paul, L. M. Bull, *J. Magn. Reson.* **1997**, *125*, 364.
[250] M. Baldus, D. Rovnyak, R. G. Griffin, *J. Chem. Phys.* **2000**, *112*, 5902.
[251] M. Nijman, M. Ernst, A. P. M. Kentgens, B. H. Meier, *Mol. Phys.* **2000**, *98*, 161.
[252] S. Wi, L. Frydman, *J. Am. Chem. Soc.* **2001**, *123*, 10354.
[253] F. H. Larsen, J. Skibsted, H. J. Jakobsen, N. C. Nielsen, *J. Am. Chem. Soc.* **2000**, *122*, 7080.
[254] F. H. Larsen, A. S. Lipton, H. J. Jakobsen, N. C. Nielsen, P. D. Ellis, *J. Am. Chem. Soc.* **1999**, *121*, 3783.
[255] A. S. Lipton, J. A. Sears, P. D. Ellis, *J. Magn. Reson.* **2001**, *151*, 48.
[256] A. S. Lipton, G. W. Buchko, J. A. Sears, M. A. Kennedy, P. D. Ellis, *J. Am. Chem. Soc.* **2001**, *123*, 992.
[257] A. C. Kunwar, H. S. Gutowsky, E. Oldfield, *J. Magn. Reson.* **1985**, *62*, 521.
[258] J. Ackerman, R. Eckman, A. Pines, *Chem. Phys.* **1979**, *42*, 423.
[259] Y. Wu, B. Q. Sun, A. Pines, A. Samoson, E. Lipmaa, *J. Magn. Reson.* **1990**, *89*, 297.
[260] J.-P. Amoureux, C. Fernandez, S. Steuernagel, *J. Magn. Reson. Ser. A* **1996**, *123*, 116.
[261] L. B. Alemany, S. Steuernagel, J.-P. Amoureux, R. L. Callender, A. R. Barron, *Solid State Nucl. Magn. Reson.* **1999**, *14*, 1.
[262] Z. H. Gan, *J. Am. Chem. Soc.* **2000**, *122*, 3242.
[263] C. Huguenard, F. Taulelle, B. Knott, Z. Gan, *J. Magn. Reson.* **2002**, *156*, 131.
[264] S. E. Ashbrook, S. Wimperis, *J. Magn. Reson.* **2002**, in press.